# Hypervelocity Impact Detection:

# An Investigation into Piezoelectric Response of PVDF Films
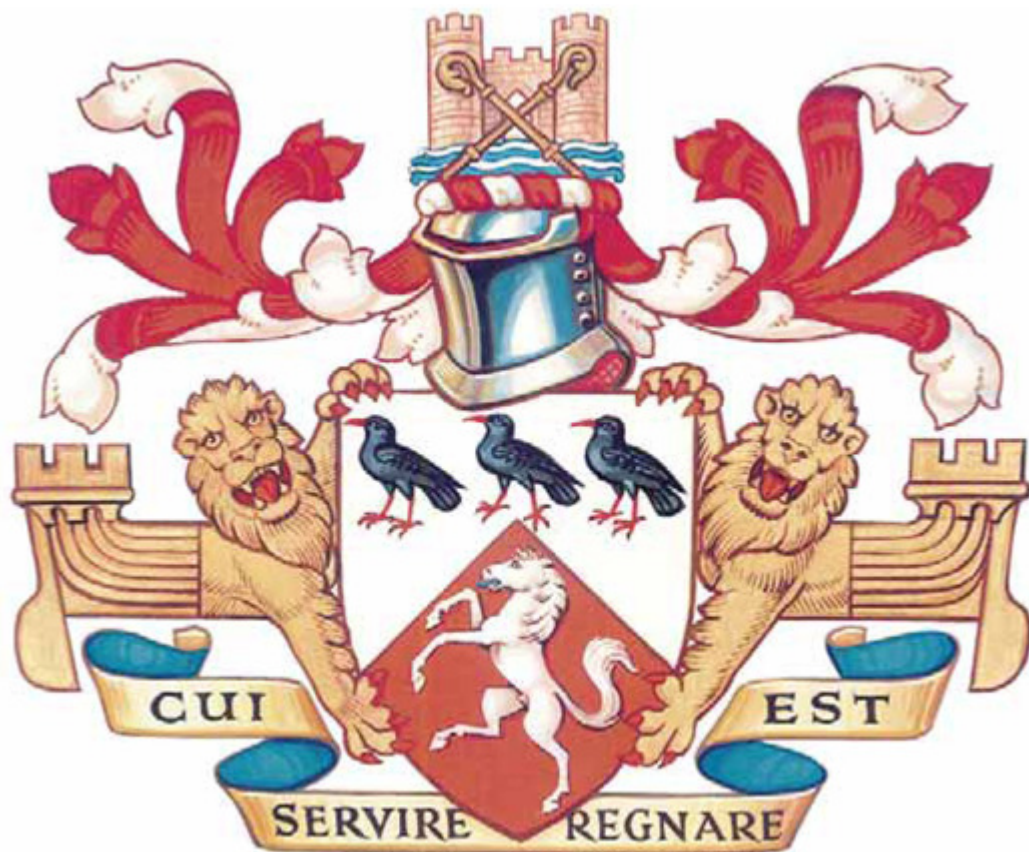
by

Samuel Perkins

*To my Parents and Family,*
*whom I love.*

# − ABSTRACT −

It is proposed in this thesis that an experimental method may be successfully employed with the purpose of discerning the differences in the resultant strain of thin aluminium plates due to impacts of projectiles with varying composition and speed. It also proposes a method for discerning the relative energy imparted to a plate initially hit by a projectile, compared with a plate positioned behind the initial plate, for the purpose of speculating why a relatively energetic projectile may yield less strain of the initial plate when compared with the results of the use of lower energy projectiles of a different composition.

Poly(vinylidene fluoride) films are used to measure the strain of the plates, by observing the induced voltage given by the films as they are strained along with the plate. The voltage induced by the sensors, for any impact in question within the project, is recorded over a specific time period, and from this data a peak voltage amplitude is ascertained and is associated with the energy transferred to the plate by the relevant projectile.

This thesis finds that differences in the response of PVDF sensors are observed as projectiles with different characteristics are used, and that further study should be undertaken to allow for a proper understanding of the relation between projectile properties, and the amount of strain detected by impact sensors. The decay time of the acoustic signal trace given by impact sensors is shown to increase exponentially as projectile density is increased. It has been shown that for a range of projectiles used to produce penetrative impacts with thin aluminium plates, most of the kinetic energy of the projectile is retained by the projectile after penetration, and that relatively higher density projectiles retain more than those with a lower density.

# Acknowledgements

> O, if this were seen,
> The happiest youth, viewing his progress through,
> What perils past, what crosses to ensue,
> Would shut the book, and sit him down and die.[1]

It is through others that we ourselves advance. It is through those who choose to associate with us that we are given encouragement, reassurance, affection, censure, guidance, and trust, and without whom we would be alone. It is others who act in such a way that brings out the best in us that I am referring to; those who would drive us to excellence, and who truly have our best interests at heart. Such are the people who I would wish to mention here, without whom, I would not have been able to achieve many accomplishments, including the writing of this thesis. I am in debt to these people, and I am thoroughly unable to portray their kindness, or how much they have given to me, with these words alone.

At the School of Physical Sciences, University of Kent, I would like to thank my supervisor, Mark Burchell, who has been of great support. He has been vigilant in making sure that my progress continued, and gave me the opportunity to express and use my own ideas within this work. I would like to thank Mike Cole, who has been a

---

[1] William Shakespeare, *King Henry the Fourth*

Without my family, none of this would have been possible. I would like to thank my mother and my father, for everything that they have given to me. Thank you. I love you both very much, and I could not have hoped to achieve anything that I have without you.

~

*Postscript:* I would also like to thank Professor Michael Smith, from the University of Kent, and Doctor Paul Hazell, from Cranfield University, for taking the time to read and assess my work. Their suggested additions have been included within this thesis.

# CONTENTS

# CHAPTER ONE: INTRODUCTION

This chapter will provide an introduction to the project. This will include background information with regard to the context in which this work has relevance, and it will provide reasons for the importance of study within this area.

## 1.1 Impacts and Spacecraft

Whenever a spacecraft enters space, there is some likelihood that over a given time period that it remains there, that it will be struck by another object. There are three main contributing factors to the predictability of such an occurrence. The first would be the total surface area of the spacecraft, the second is the duration of time that the spacecraft is expected to remain in some particular region of space, and the third is related to the radius that the spacecraft is expected to be travelling from the earth (whether it would be orbiting or otherwise). If the flux of debris (both natural and man-made) is known, this provides a fixed value to allow for a prediction of the number of potential impacts, despite there being some components of this flux that are sporadic. However, because some potentially damaging impact may be sporadic, does not mean that it cannot be accounted and prepared for in the majority of cases. For example, the likelihood that a spacecraft is struck anywhere in space by an

enormous object is far less likely that it is of being struck by a much smaller, more abundantly sized object.

Some preparation shall be made in most cases to protect against the possible impact damage from objects travelling at a particular velocity and of a particular size and composition. Of course, such protection must be made so that there is an assumption in place, which is that the design of such a preventative against damage is tailored to whatever characteristic of impact is going to be most likely or abundant during the intended space mission. This will provide the greatest potential for protection of the spacecraft. However, it then requires some base knowledge of which impacts are going to be most likely to occur during the mission, for example, which kind of object, and what its velocity is likely to be. Due to the large degree of uncertainty in such factors, the degree of effectiveness of suitable protection is limited. This is why spacecraft systems are designed so that for a given mission the operational effectiveness and crew safety (for manned missions) is fully maintained for the time period required; this can be seen as being the condition for which the exists the greatest probability of no harmful damage occurring to the craft, over the given time period. In figure 1.1, we can see that a probability prediction of a potentially damaging impact can be made for a specific orbit within a specific time period, given data from modelling and observation of the orbital debris flux.
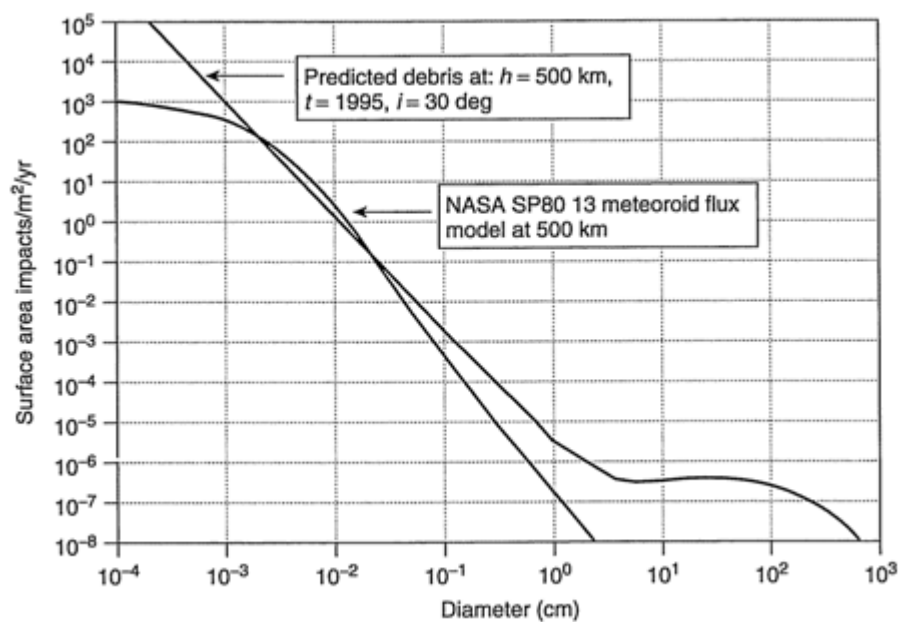


Figure 1 .1: The flux is shown as the cumulative number of impacts per metre squared per year, of objects above or equal to the given diameter. [1]

Modelling of the orbital debris flux [2, 3] allows for a prediction to be made of the most likely number of impacts, of the most likely sizes and velocities, over a given time period. This allows for the design of spacecraft shielding to be considered on the basis of the level of protection that it will need to offer.

One example of this method is given now. The model that has been used is the ORDEM2000 model [4], implemented by the ORDEM software package, provided by the NASA Orbital Debris Program Office, courtesy of Dr. Nicholas L. Johnson, Chief Scientist for Orbital Debris. The parameters given for the calculation were the orbital characteristics of the International Space Station, so that context could be given to the example. When this specific orbit was used as a basis for the modelling parameters, the values for the predictability of impacts was given in table 1.1.

Table 1.1: This table shows the calculated orbital material flux at the orbit of the international space station.

--> Average flux ($/m^2$/yr):

| Objects | $> 10\ \mu m$ | $> 100\ \mu m$ | $> 1\ mm$ | $> 1\ cm$ | $> 10\ cm$ | $> 1\ m$ |
|---|---|---|---|---|---|---|
| | 4.55E+02 | 1.56E+01 | 2.98E-02 | 2.48E-06 | 1.50E-07 | 9.94E-08 |

--> Average relative velocity (km/s):

| Objects | $> 10\ \mu m$ | $> 100\ \mu m$ | $> 1\ mm$ | $> 1\ cm$ | $> 10\ cm$ | $> 1\ m$ |
|---|---|---|---|---|---|---|
| | 7.35 | 7.31 | 7.18 | 7.04 | 6.40 | 6.36 |

It can be seen that in Table 1.1, for the range of projectile sizes given, the average velocity is only calculated to vary by 0.99 km s$^{-1}$, between the smallest and the largest objects. However, the likelihood of impact varies significantly for differently sized objects. A flux of 1 m$^{-2}$ yr$^{-1}$ is one impact of that size taking place, over a mission lasting one year, for a spacecraft with a surface area of 1m$^2$. Therefore, for any projectile of a particular size, if the calculated flux per year, per metre squared, is less than 1, then it is unlikely that such an impact would take place unless either the time frame were increased, or the size of the spacecraft were increased. At the orbit given, it has been shown that, theoretically, of the order of 455 objects with a diameter equal to or greater than 10μm will impact during one year, for a spacecraft with a surface area of 1m. However, it is unlikely for projectiles of larger sizes (eg.

cm scale) to impact with this spacecraft during one year. It must be taken into account, however, that for the specific example of the international space station, the surface area of the craft is larger than 1m, and the duration of its stay in orbit is longer than one year (being of the order of 10 − 20 years). In this case, the area is measured in hundreds of metres squared, so a 1mm (or larger) objects hits in the order of once per year. Therefore, once the flux has been multiplied by the appropriate factors relating to the size of the craft, and the duration of its stay, then it would be known which projectiles were most likely to impact, and at what average speed. This would allow for consideration of what impact protection should be used to be given[†].

## 1.2 Some Reasons for the Study of Impact Sensors

Many impacts may occur that, due to their small size, remain of negligible effect upon the space mission individually, but may become detrimental cumulatively over time, i.e., may degrade the performance of solar panels over time [5]. However, there is also some probability that larger and potentially more damaging impacts will take place. Given that this is the case, it can be seen to be beneficial to implement some method of detection of impact damage and location upon spacecraft. These were considerations for (now cancelled) NASA's Constellation program; this featured a large human element on board spacecraft. This has emphasised the need for some new impact detection method to be developed. One current method is based on visually (and manually) searching for impact damage e.g. astronauts look at the exterior of the ISS as they undertake space walks. Some impact damage is so small that it may go undetected by human observation, either in person or through some form of observation such as a camera. This would also hold the requirement that the field of view of the observer, by whatever means, could inspect the entire surface of the spacecraft. This is obviously an impractical method of impact detection. Impact damage has also been assessed by retrieving the spacecraft, or panels from them, and then inspecting them in the lab.

---

† The speeds given are mean speeds, which means that caution should be taken when considering impact probability. The speed of particles for a given size will have a width as well as a mean. Contributions to the flux that have an interplanetary component will have high speeds than those that are an orbital debris component.

There are many reasons that necessitate the improved design and study of impact sensing, mainly because there are many practical (and necessary) uses that they have. For instance, one such use is the direct, in situ, detection of impacts in low earth orbit. This would serve to provide a catalogue of data that provides more information on the quantity and nature of material in close proximity to earth [6]. Other such uses would include the detection of potentially detrimental impacts. The listed uses include the necessity to be able to identify properties of the impactor. With regard to the original purpose, which is to use impact sensing as an in-situ method of cataloguing impact probability in low earth orbit, physical properties of the impactor can be found with the retrieval of the sensor device, as direct analysis of the impact damage may be performed. However, in other cases this is not possible or useful. For example, detecting harmful damage during a space mission may require "real time" data about the impact and its location. With the example of spacecraft damage, it could prove necessary to know the size and composition of the impactor, as well as a location of impact and possible damage that may have been caused by it [7, 8].

## 1.3 Defining a Hypervelocity Impact

A hypervelocity impact is the impact of an object into a target at a speed that greatly exceeds the speed of sound in both the target body and the projectile [9]. This kind of impact features a shock pressure which far exceeds the strength of the target material. This has the effect of causing the constituent material within the vicinity of the target area to flow, and behave like a liquid instead of a solid, for a particular duration of time during the impact event. The 'liquid' motion of the target's constituent particles produces a bowl shaped crater around the impact of the object, and as the shockwave disperses through the material, its energy will disperse also. As the pressure of the shockwave in any given region falls below the strength of the given target material, the liquid-like motion ceases and the structure behaves like a solid once more, which solidifies the crater in place as though suddenly frozen still. Deformation of the impactor also occurs during the impact, and the deformation of both the target and impactor are influenced by the following factors: the velocity of the impactor, the size of the impactor, the composition of the impactor and the composition of the target material [10].

When the target of a hypervelocity impact is a plate, of finite thickness, the main consideration when predicting the final deformation of the material, is the relative diameter of the impactor. It can be seen in fig 1.2, that when the impactor diameter is much smaller than the thickness of the plate, then a crater will form upon the incident surface. The ballistic limit is the point at which the diameter of the impactor is large enough to ensure that penetration will occur. This is when the impactor just manages to penetrate the plate, leaving a hole in the bottom of the formed crater (second example from the top in fig 1.2) [11].
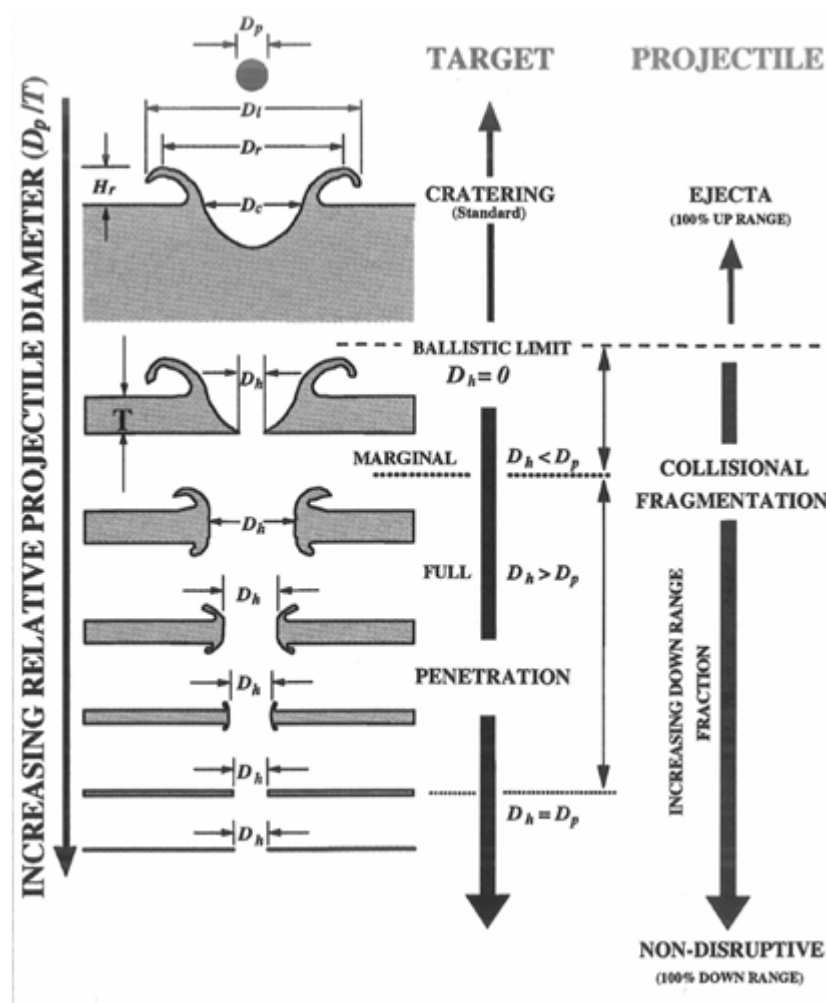


Figure 1.2: An illustration of the variation in crater profile with plate thickness. [11]

## 1.4 Spacecraft Design Considerations

Weight and cost restraints upon the design of a spacecraft mean that the design of any shielding must be well considered. This means that it must be as light as possible, while still providing suitable protection. For this to be possible, the

shielding must be designed specifically to protect against the type of impacts that will most likely be encountered within the mission environment. This is to ensure that the shielding is not heavier than necessary by offering protection against larger impacts than are likely occur, whilst also making sure that the shielding is effective enough to protect against those impacts that do possess some possibility of posing a threat. In simple terms: If there is too much shielding, then its design will be heavier than necessary, and if there is not enough armour then the spacecraft is at an intolerable risk. As has been mentioned previously, the method allowing for the design of the most suitable amount of protection is to be able to predict the properties of the most likely impacts that may occur. For this to happen we must have some method of measuring the flux of material in space, so that we understand the size and speed of objects present within environments of interest. When this is known, the specifications of shielding can be tailored to accommodate protection against such objects. One such method of measuring the flux of impacts in space is to utilize impact sensors. Other methods include radar (for small cm scale objects in LEO), or laboratory analysis of cratering on retrievable spacecraft surfaces.

Some typical designs of spacecraft impact protection designs can be seen in figure 1.5. Each design begins with a "bumper" shield as the outer surface, usually made of a thin plate of aluminium. This is used to shock the impactor, causing it to break apart. Spacing is present between the bumper and the back-up wall or intermediate layer, to allow the cloud of debris from the impactor to spread over a larger area. The back-up wall is typically made of a thicker plate of aluminium. Various intermediate layers of material can be used to change the effectiveness of the overall design. Thin layers of multilayer insulation (mli) can also be added to the outside of a shield, mainly for thermal control, but this design also offers some protection against small impactors. Where the first layer of protection would disrupt the projectile, forming a debris cloud, the second layer of protection would vaporise the remaining debris. This form of protection is known as a 'Whipple' bumper shield, named after its developer, Fred Lawrence Whipple.

## 1.5 The Moon and the local Space Environment

It was originally proposed that there would be a long duration mission to the moon, for which spacecraft shielding would be required. The moon is a satellite in orbit

around the Earth with a period of around 27.3 days at a distance of around 384440km. It is an almost spherical body of rock with a mean radius of 1737.1 km and an approximate difference between the polar and equatorial radii of around 2 km. It has an approximate mass of around $7.35\times10^{22}$ kg and a volume of approximately $2.1958 \times10^{10}$ m$^3$, giving the moon an approximate mean density of 3350 kg m$^{-3}$. From this we can asses that, on average, the moon is composed of a lower density rocky material than that of the Earth,
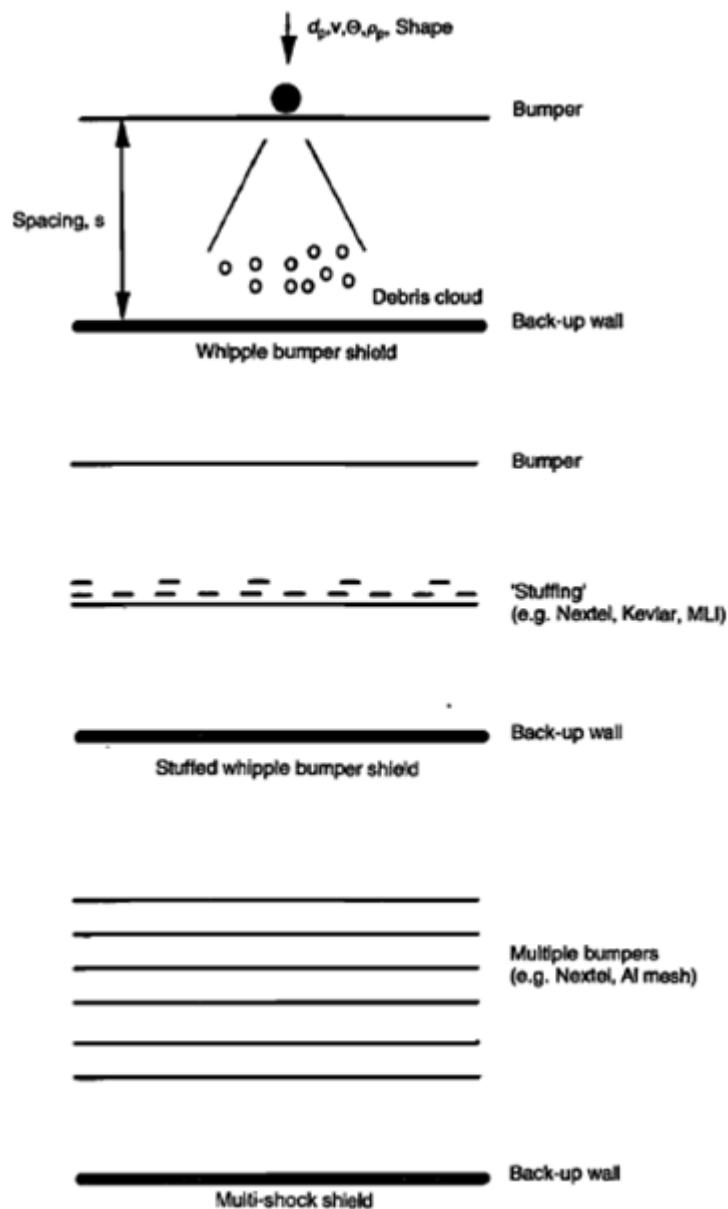


Figure 1.3: A diagram showing three typical designs for impact protection. The uppermost example is a basic Whipple shield, the centre is a 'Stuffed' Whipple shield, and the third is a multi-layer bumper shield. [1]

considering that the moon has a volume that is roughly the equivalent to 2% of that of the Earth, which has an approximate density of around 5515 kg m$^{-3}$. The mass of the moon is approximately equivalent to around 1.2% of that of the Earth [12].

Most of the knowledge that has been gained from the moon has been gathered purely from observation. The surface of the moon provides an abundant wealth of information, and is an aid to understanding geological processes on satellites and planetary bodies. The moon, being the nearest body to Earth within the Solar system, has provided a benchmark for understanding a wide variety of problems when considering other planetary bodies. This is because of the relative ease of gathering data compared to other locations within the solar system. Similarities between the Moon and other such bodies allow for a comparison to be made when data is collected from the Moon, and so far the Moon has been subjected to many different types of scrutiny, including the following: Earth-based and orbital remote sensing, manned reconnaissance, *in situ* geographical stations, and sample return. [12]

Early volcanic and tectonic activity on the Moon produced high land and lava flows we see today, but that theory was subsequently modified. There are many factors contributing to how the observable surface of the Moon has been formed. However, one major difference compared to the earth is the lack of an appreciable atmosphere that could cause any significant weathering or erosion effects. There are two main causes for the lack of any possibility of there being an atmosphere about the Moon. The first is that the gravitational field strength of the Moon is too small, and the second is that the Moon has no significant magnetic field. The first reason indicates that the escape velocity of the Moon is not high enough to prevent gas particles from dissipating. The escape velocity may be represented as follows:

$$v = \sqrt{\frac{2GM}{r}},$$  (1)

where '$v$' is the escape velocity, '$r$' is the radius between the centre of gravity and the escaping object (the surface of the Moon, in this case), '$M$' is the mass of the Moon, and '$G$' is the universal gravitational constant. Assuming a Boltzmann type type distribution of a gas a temperature '$T$', the root mean squared velocity of an ideal gas particle can be expressed as:

$$v_{rms} = \sqrt{\frac{3kT}{m}},$$

<div align="right">(2)</div>

where '$v_{rms}$' is the root mean squared velocity, '$m$' is the molecular mass, '$T$' is the temperature, and '$k$' is the Boltzmann constant. The value of the ratio of the root mean square velocity of an ideal gas particle, divided by the escape velocity, provides a basis to assume whether or not the gravitational field strength of the planetary body is strong enough to retain an atmosphere.

If the ratio is greater than 0.3, then the atmosphere will have dissipated very quickly: within the order of weeks. If the ratio is greater than 0.2, then half of the gas would have dissipated within one billion years. If the ratio is less than 0.1, then the atmospheric gasses would remain present for billions of years. A second reason for the Moon having no appreciable atmosphere is that ionized molecules and subatomic particles from solar winds would not encounter any perturbating forces from a magnetic field. Here on Earth, such particles are deflected by the magnetic field and are channelled into the polar regions to create the Aurora Borealis. However, the effect of no such shielding of the Moon is that any atmosphere present would be abated by such high velocity collisions with the particles of the solar winds. The Apollo landing missions measured a low ambient pressure on the lunar surface of $10^{-7}$ Pa by day, and $10^{-10}$ Pa by night.

A second major cause for the current surface features of the Moon to be present is the abundance of impact events throughout the Moon's history. As can be seen in figures 1.5 and 1.6, the moon is covered with the effects of these events, and their study scientifically fruitful, for example the relative ages of surface regions of the Moon and other planetary bodies can be obtained. This is done by comparing craters, to give one simplistic example: When a small crater is observed within another larger one, it can be stated that the smaller impact event happened after the larger one and thus indicates that this surface region is relatively young. The number of craters covering the surface is counted, and then plotted per $km^2$ versus crater size. For example, a region with many large craters per $km^2$ can be described as an old region.

This is of course another simplistic example, but it serves to illustrate how the surface regions of the Moon and even surfaces of other bodies can be compared in terms of their relative age.



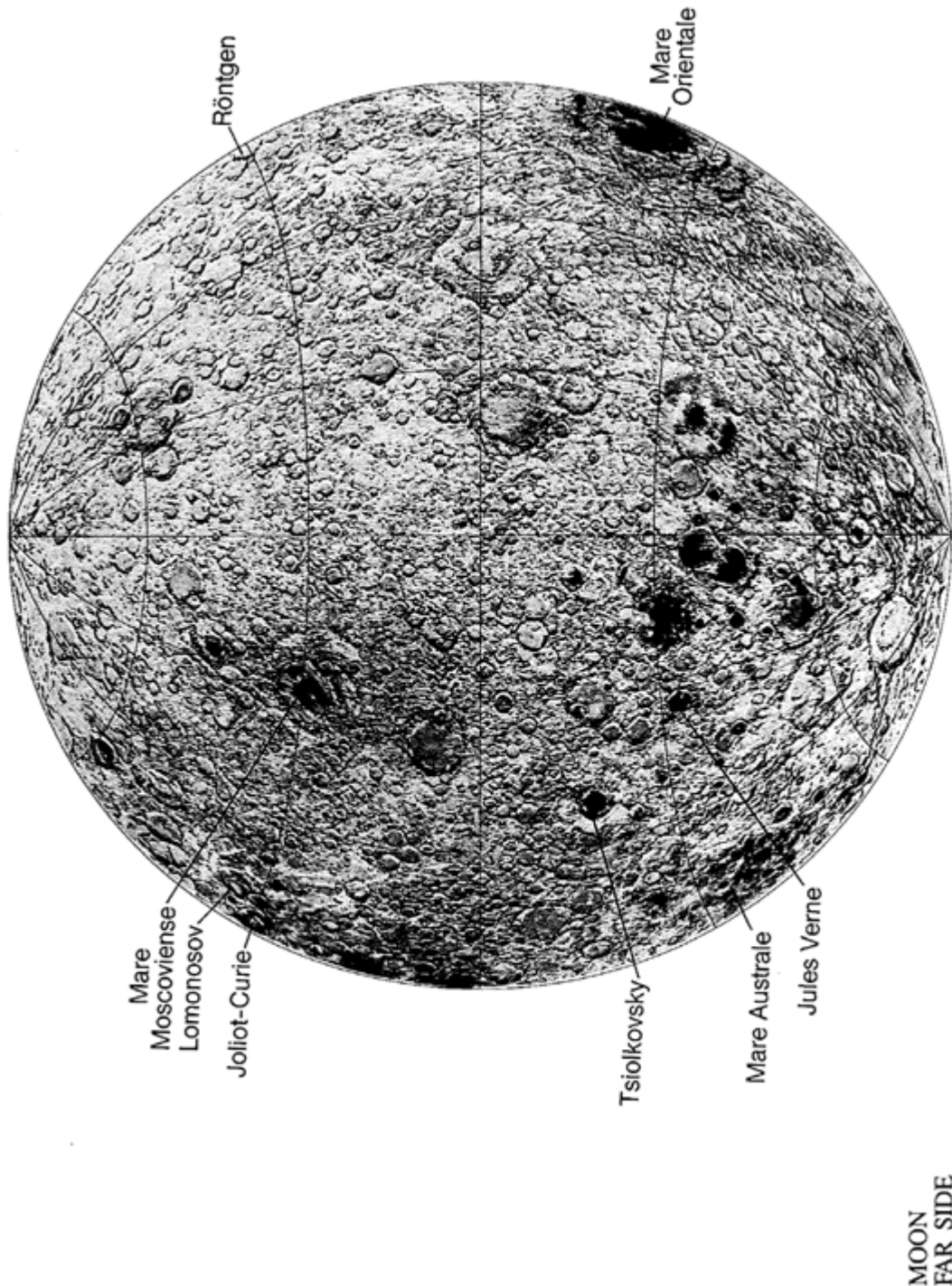Figure 1.4: This is an image of the side of the moon that faces away from the Earth [12].
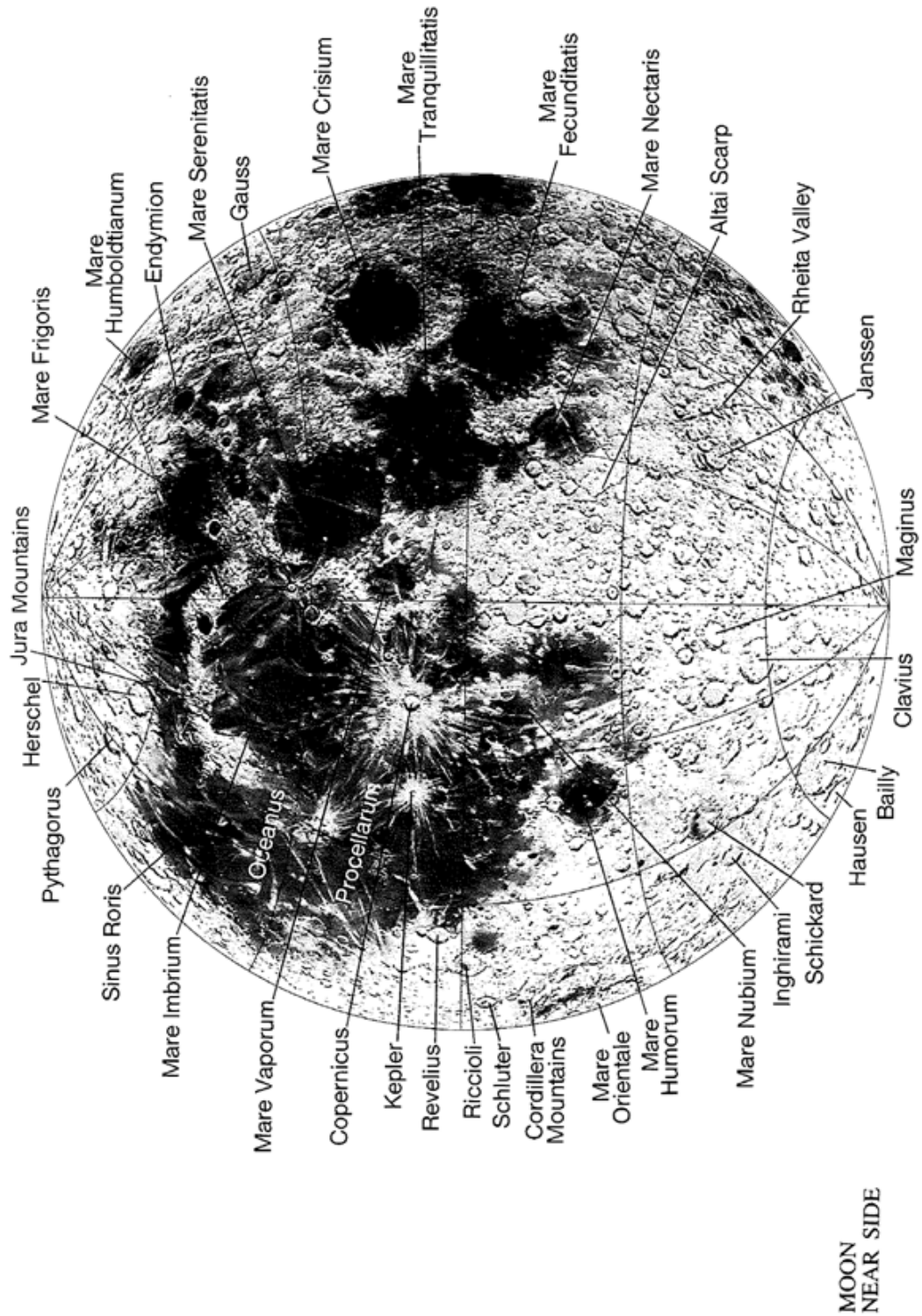
Figure 1.5: This is an image of the Earth-facing side of the moon [12].

The lack of an atmosphere leaves impact craters intact and free from erosion effects. The lack of tectonic or volcanic activity since early in the Moon's history preserves the surface. Volcanic activity, early in the Moon's history (~ 1 billion years ago), is

another major contributor to the features of the Moon's surface. In fact, extrusive volcanism deposits cover approximately 17% [12] of the Moons' entire surface, mainly upon the Earth facing side of the Moon. A large quantity of these deposits exist within the same region as impact craters, which is most likely due to the penetrative effect of the impactor striking the Moons' crust. A diagram showing the distribution of lunar mare deposits is shown in figure 1.7.

The moon possesses a regolith, which is a layer of loose, heterogeneous particulate matter. The Lunar regolith is primarily composed of fine, granular rock and glassy agglutinate materials. Geochemical analysis shows that less than or approximately 1% of the Lunar regolith is comprised of meteoritic material [6]. This is due to the fact that impact events will prevent a localized build up of exogenic material, as the soils present at the surface are vaporized or possibly ejected from the impact site at high velocity. As the impact strikes the lunar crust, the immediate transference of an enormous amount of kinetic energy causes much of the endogenous material to melt, and production of the opaque, dark, agglutinated glasses occurs, which is how the dark soils covering the majority of the surface are produced. The lunar regolith is vertically inhomogeneous and possesses layers; the outermost layer of the Moon is composed primarily of particles with a diameter of less than $100\mu m$, being a constituent of a surface that has the consistency of a very fine powder. The surface is also very porous and the average density of the uppermost 1cm is in the order of $1.4gcm^{-3}$ [12].

It is currently unknown whether or not the Moon possesses a metallic core, composed of Iron. However, if such a core exists, it has been estimated that it's maximum radius is approximately 400km; deduced from data collected by seismic and electromagnetic experiments [12]. The Earth-facing side of the Moon possesses a crust around 60km thick, detected by seismic experimentation left behind by the Apollo mission [12]. Topographic and gravitational data on the Moon suggest that far side of the Moon possesses a thicker crust than the near-side. Directly recovered samples, as well as remote measurements of the surface, have both indicated that the lunar crust is composed dominantly of an anorthositic gabbro. [12]

Other than the presence of impact cratering upon the surface of the Moon, there is other evidence that meteoroids collide with the lunar surface. Light flares have been

observed to originate from the Moon[13,14]. These are actually impact flashes, caused when a meteoroid strikes the lunar surface, and some of the kinetic energy of the projectile is converted to electromagnetic radiation in the visible and IR parts of the EM spectrum. This has been verified by simultaneously observing the Moon with more than one telescope. Similarly, causing a controlled impact with the lunar surface (the Smart 1 satellite) [15], which have also produced impact flashes.

## 1.6 Considerations for the Possibility of a Lunar Base

The lunar surface is, on average, subject to a number of impacts equalling a flux of approximately 300 events/$m^2$/yr./2πsr for 10μm impactors, and 30,000 events/$m^2$/yr./2πsr for 0.1μm sized objects [16]. These, and larger impacts, all strike the lunar surface with a velocity greater than escape velocity (>2.38kms$^{-1}$), and are unperturbed by any atmosphere [16]. They strike the surface of the Moon with their total kinetic energy, giving them the potential to cause damage to man-made structures on the surface. The consequences of damage sustained to human facilities on the Moon could vary greatly. However, whether the result of damage was merely a minor detrimental influence on the operational function[†] of a piece of equipment or a lethal destruction of the facility's environmental integrity, the initial necessary response to the impact may remain the same.

Let us assume that there is a requirement to know when an impact has significantly damaged a man-made construct upon the Moon [17, 18]. First the response might well be to implement a suitable method of impact detection. Determining when

---

† It is worth noting that the function of an object might be construed as the use to which the object is put, or as the process which the object performs (assuming it does). Thus, for example, the function of a map – that is, the use to which it is put – might be to guide movement. The function of an assembly robot, on the other hand, might be to perform the process of assembling a product. This distinction is of relevance because in order to predict whether or not an impact would affect the function of a construct when 'function' is construed as the use to which the construct is put (eg the use of a structural set of walls to contain an atmosphere on the surface of the Moon), one has to take into account different considerations from those which apply when determining whether an impact would affect the undertaking of some process by the construct. This is because an impact will definitely change the form of the construct upon collision (even if in a very minor way which does not prove to cause "significant" damage), which may affect the use to which it is put, but an impact may not necessarily have any effect upon how a construct that has the purpose of performing some process actually performs that process.

damage becomes significant, rather than superficial or negligible, depends upon both the object that is impacted upon, and upon the physical properties of the impactor.

We make three assumptions: firstly, that the physical characteristics of the man-made construct are well known; secondly, that damage becomes "significant" when it has a detrimental effect upon the function of a construct, with respect to its specific purpose; thirdly, that the function of a construct is known sufficiently well to be able to determine what physical changes in the construct's structure would be detrimental to the performance of its function. The study of hypervelocity impacts is required to understand the response of a given structure to impact. This is achieved through modelling and hypervelocity impact experimentation [19, 20]. With this in mind, it seems reasonable to suggest that if the impactor properties for an impact event upon a known construct could be ascertained from sensor signal data, then the effected changes to the construct could immediately be approximated; since the changes to the construct would be known (after extensive modelling and experimentation), it would also be known whether or not the damage to the construct was significant.

Consider the following simplified example, to clarify the discussion. An external wall of a lunar base is subjected to a hypervelocity impact. It is known that due to the wall's testing, combined with data from modelling, any object travelling at greater than the Moon's escape velocity, and possessing a greater mass than 2g, will surpass the wall's ballistic limit, and will puncture the wall fully. An impact does occur, and the acoustic sensors mounted within the wall transmit signal data about the impact to a computer. The computer determines that the object that has impacted upon the wall has a mass of 4g. Therefore, it has punctured the wall, as the latter's ballistic limit has been surpassed. The wall's purpose was to form a solid barrier, containing the internal environment of the lunar habitat, and it no longer fulfils this purpose. Therefore, the wall has suffered significant damage.

Consider also this second imaginary event, for the same imaginary wall: an impact event occurs, and the acoustic sensors within the wall transmit signal data from the impact to a computer. The computer calculates that the mass of the impactor was 0.2g. Therefore, the wall will undoubtedly have suffered change in some way (in the form of an impact crater), but this erosive damage would not have penetrated the wall. Therefore, the wall does still fulfil its purpose, as it still remains solid barrier,

and it contains an atmosphere within the lunar habitat. However, this erosion could prove troublesome, as the location of the impact may now provide less resistance to impacts, compared with the rest of the unscathed wall. Therefore, the sensor signal data is still valuable. Thus we see that there exists a basis for the "real time" application of impact sensors, in terms of providing damage alerts. This shows that, on the aforementioned assumptions, impact sensors with accompanying analysis software could provide an immediate alarm for cases where an impact has caused a risk to life, or to mission objectives (see figure 1.6). This is useful, because it means that if alerts are provided in real-time, then action could perhaps be taken to limit the detrimental consequences of the damage.

This chapter has provided background information pertaining to the possible uses of impact sensors in space. It has highlighted the importance of the development of sensors with regard to the specific aims of the experiments included within this project. The next chapter will provide details of the experimental method, along with the reasons for why those methods are being used. If the sensor can find where the impact occurred, this will help with any follow up inspection, and damage assessment.
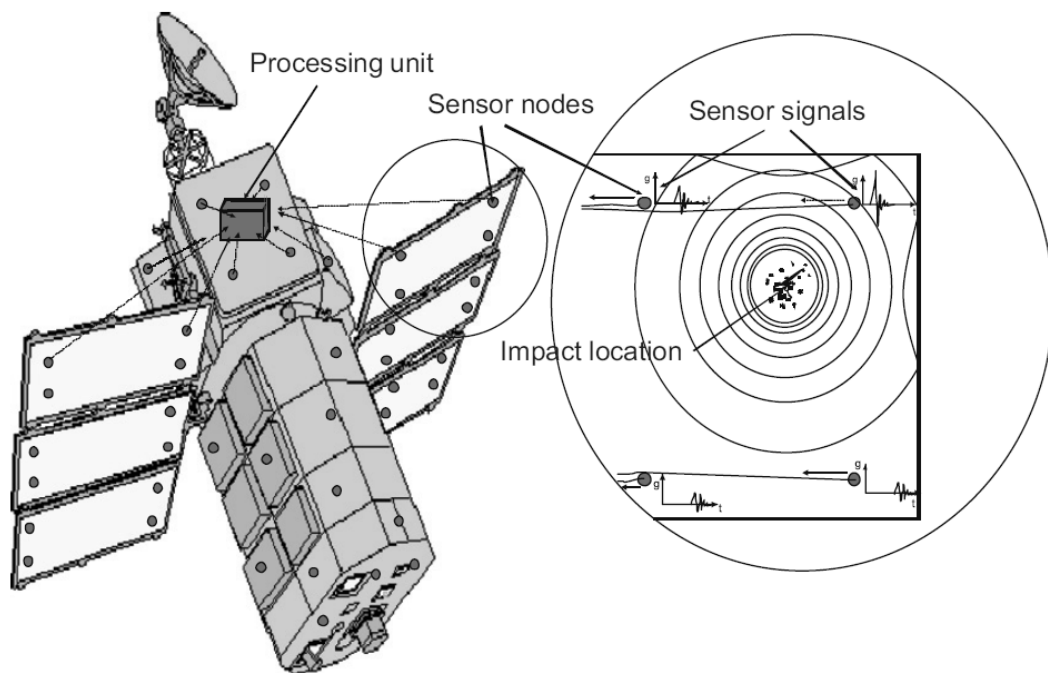


Figure 1.6: An example of a structure in a space environment (a typical satellite) making use of acoustic sensors as a method of real time impact detection. [7]
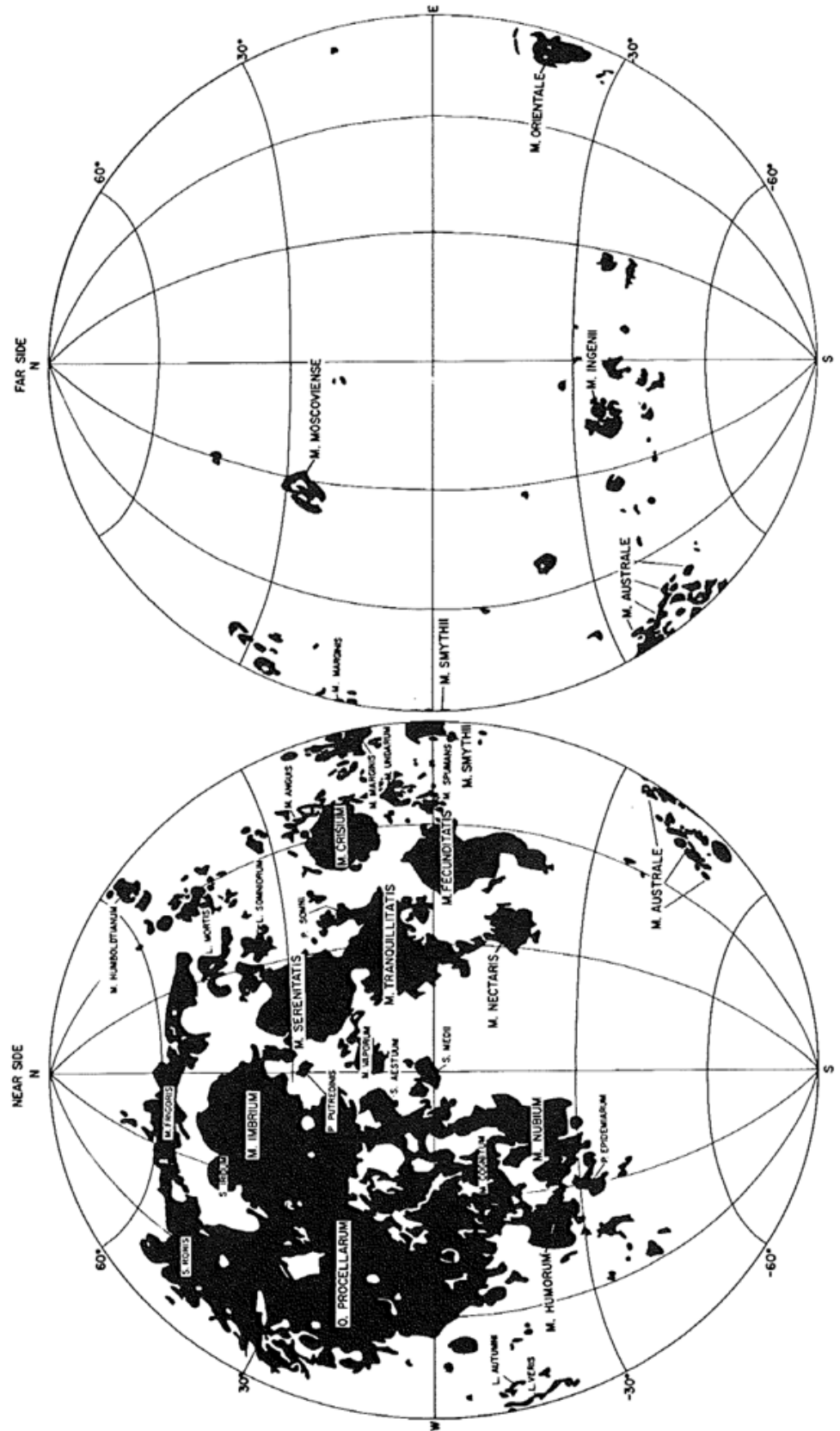
Figure 1.7: Spatial distribution of mare deposits upon the Moon [12].

# CHAPTER TWO: METHODOLOGY

The purpose of this chapter is to describe the equipment used during this project, and to detail how the experiments included within it were carried out. Attention has mainly been given to a description of the two-stage light gas gun, located at the University of Kent in Canterbury, which is where the project was undertaken. The FOMIS (Fibre Optic Micrometeoroid Impact Sensor) target [21], fibre-optical sensors, and their signal pre-amplifier were all supplied Robert D. Corsaro (United States Naval Research Laboratory). Aluminium plates were provided by the University of Kent workshop. The computer program used to record signal data was *National Instruments LabVIEW SignalExpress.* The digitizer used within this project was a National Instruments model NI6132, with a maximum sample rate of $3x10^6$ samples per second. Glass projectiles used within this project were supplied by *Whitehouse Scientific Ltd* [22].

**2.1 The Light Gas Gun:**

In this project, the light gas gun [23] at the University of Kent was used to propel projectiles, as a means of producing controlled hypervelocity impacts [24]. The

purpose of this was to simulate impacts in space, incident upon man-made materials. The gun may be used to fire individual objects between sizes of 0.8mm and 3mm, but may also be used to fire objects as small as 0.001mm upwards, in a 'buckshot' fashion. Those particles fired in the latter manner are too small to be fired individually due to them being easily perturbed from the intended flight path (larger objects have a larger mass, and are thus less affected by similar perturbing forces). Perturbation is undesirable, as it can lead to the projectile failing to reach the target.

The gun uses a powder filled shotgun cartridge as a means of providing the explosive charge to initiate propulsion. This method allows for a controlled variation of charge, as the amount of powder, and the powder's burning speed can be selected based on the desired result. By way of example, consider that if a larger quantity of powder with high burn speed was used in place of a relatively smaller quantity of powder, or powder with a low burn speed, then the explosive force would be different and would alter the resultant projectile velocity, as the amount of energy that the charge imparts is altered. The explosive force of the charge is used to propel a piston along a pump tube, which is first evacuated of air, and then filled with a chosen gas. The movement of the piston causes the gas within the chamber to become highly compressed.

The gas, which is used to propel the selected projectile, encased in a sabot, is chosen based on the desired projectile velocity; a lighter gas may yield a higher velocity, and a heavier gas may yield a lower velocity. Examples of gases which may typically be used are hydrogen, helium, and nitrogen, however, there are others. The gas may initially be pressurized to varying magnitudes of pressure within the pump tube, which is a factor that may be selectively altered as desired for each shot. The variation of initial gas pressure within the tube is another method for altering the projectile speed to acquire the desired value. A lower gas pressure will result in an increase in projectile velocity, and a higher gas pressure (i.e., a larger mass of total gas within the chamber) will result in a decrease in projectile velocity.

The rear end of the pump tube is sealed by the piston, and the opposite end is sealed with a 'burst disk", which is a thin circular aluminium cap that is designed to literally burst open as the pressure of the gas within the tube reaches some critical magnitude as it is compressed by the piston. This burst disk may be altered to allow

for it to be ruptured earlier, or rather, when a lower critical gas pressure is achieved. This is done by 'scoring' grooves into the surface of the disk to weaken it, allowing it to receive less stress before it ruptures. If the burst disk ruptures earlier, the affect of this is that there is less energy transfer between the light gas and the sabot.

A sabot is a casing that is equipped to a projectile with the intention of making it effectively wider, with respect to the barrel of the gun that will be used to shoot it. The term 'sabot' is French for 'clog', and is named as such because the device is used to fill the space around the projectile, between its surface and the edge of the barrel. To successfully propel the projectile, a seal must be formed between the projectile and the barrel, so that gas is trapped behind it within the barrel. When the gas expands, this forces the projectile along the barrel. If a projectile with a smaller diameter than the barrel is to be used, then a sabot is required to form a casing around the projectile to make it wide enough to propel (i.e., providing a sufficient diameter to form a seal with the barrel).

As the burst disk ruptures, the sabot is propelled through the 'launch tube' of the light gas gun. In the work here, this is a rifled barrel section of the gun, which will allow the light gas to expand as the sabot is pushed through it. The rifling of the launch tube will cause any sabot propelled through it to rotate around an axis normal to its direction of movement. This is to provide the projectile with an angular momentum bias, to reduce any perturbing forces that may cause it to be deviated from its desired trajectory. The mathematical description of this is as follows [1, 25]:

Considering an object with centre of mass, C, with an angular momentum, L:

$$\frac{d\boldsymbol{L}}{dt} = \boldsymbol{T},\tag{2.1}$$

where: 'T' is an external force that has a moment about the centre of mass of the object. This is known as an 'external torque'[†]. The component of 'T' that lies along the same path as the angular momentum will only alter the magnitude of the angular momentum. The component of 'T' that is perpendicular to the angular momentum,

---

† It is necessary to mention that this case is in reference to an 'external' torque only, because 'internal' torques, which are torques between constituent components within the body of the object, have no resultant affect upon the overall angular momentum of the body.

labelled 'T$_N$', will cause the angular momentum to change direction towards the torque, 'T' (this is called precession).
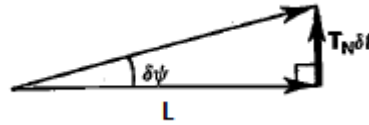


Figure 2.1

The rate of precession can be written as:

$$\frac{d\Psi}{dt} = \frac{T_N}{L}.$$

(2.2)

When 'L' is made to be very large, then the rate of precession due to a given torque is reduced. Therefore, if the given object has a very high angular momentum, then the effect of a torque impulse is made very small. A torque impulse may be written as:

$$I_T = \int_0^t T \, dt.$$

(2.3)

The rifling of the launch tube causes the sabot, and consequently the projectile, to spin rapidly. Depending on the launch tube used, this may be clockwise or anti-clockwise. While the projectile has a rate of spin, about an axis normal to the direction in which it is travelling, it also possesses angular momentum about this axis. The consequence of this is that any perturbing forces acting upon the projectile, with any component perpendicular to its horizontal trajectory, will have much less of an effect than if the projectile was not spinning (it did not possess a large angular momentum normal to its direction of travel).

As the projectile exits the narrow launch tube and enters the wider blast tank, the sabot discards (interlocking teeth holding two halves of the sabot together 'unlock',), which means that it falls apart and allows the projectile to continue its flight unaffected. The segments of the sabot will collide with the stop plate, and not continue past this point (unless some malfunction has occurred). The projectile continues to travel until it leaves the blast tank, and passes through two light-curtains. These light curtains are created by a pair of lasers. They are focussed onto

sensors, which are light sensitive devices (photodiodes). The intensity of the signal from each sensor will decrease during the time that the projectile passes through the beam from each laser, as it obscures each laser's path to the optical sensor momentarily. This will happen to the first laser, closest to the pump tube, before it happens to the furthest laser. The change in signal amplitude (which is related to the intensity of light received by the optical sensors) is recorded by the oscilloscope for both of the lasers (see Fig 2.1), and the time delay between the two events can be shown by comparing the two signals. The distance between the two lasers is known,

and when the time delay between each signal distortion is also known, this allows the projectile velocity to be calculated. The separation between the two lasers is 0.499m ± 1mm.
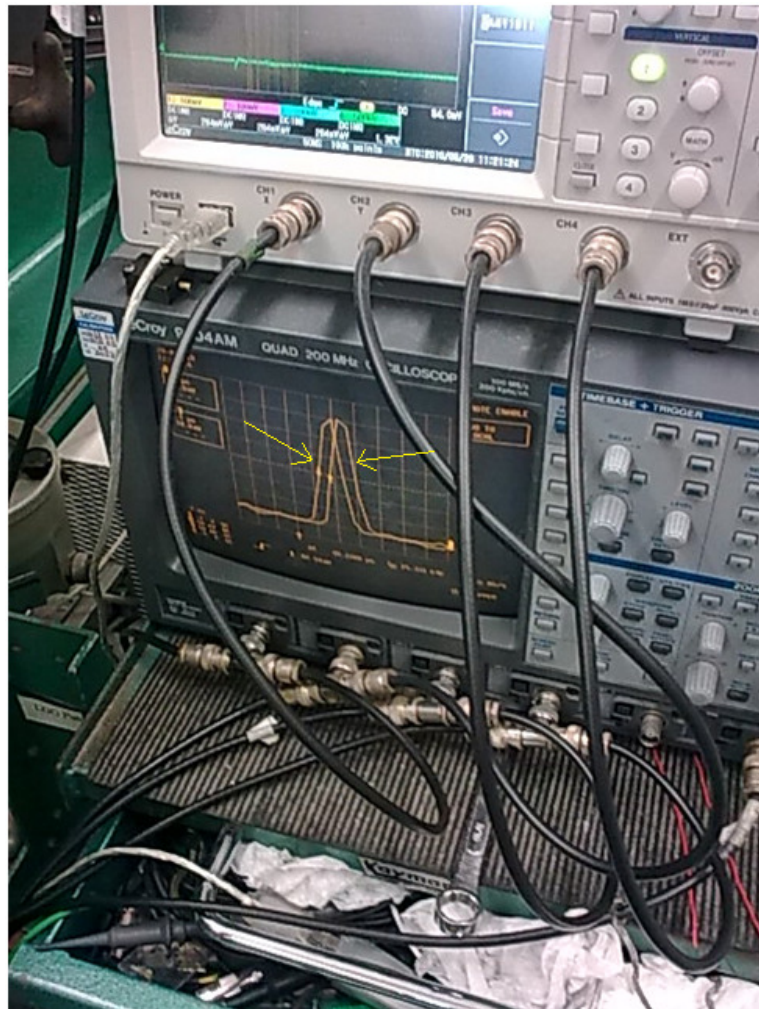


Figure 2.2: An image of the oscilloscope trace post shot. The two signal changes caused by the transit of the projectile can clearly be seen (arrowed), as can the time delay between the two events.
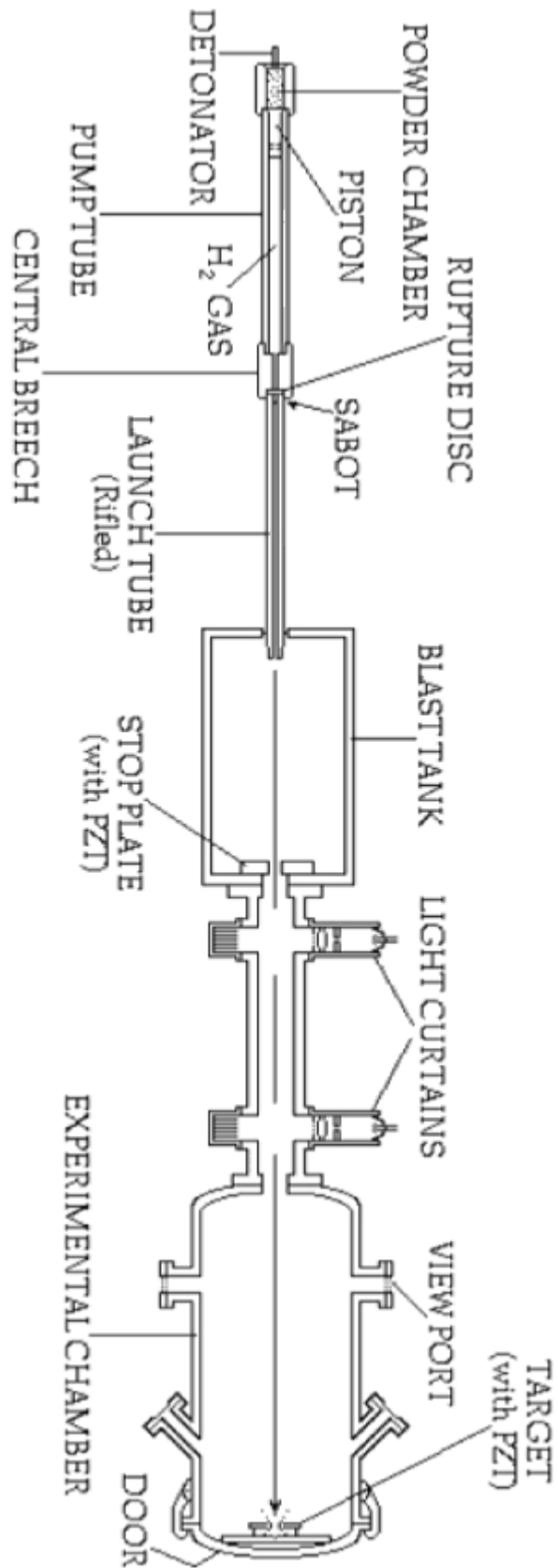
Figure 2.3: A diagram of the light gas gun, taken from: http://astro.kent.ac.uk/facilities/lgg.htm

Typically, the time between the two signals shown on the oscilloscope can be measured to better than 1%, and hence the accuracy of the calculated speed is better than within 1%.

The final stage of the projectile's flight through the gun is when it enters the target chamber, which is usually evacuated to a pressure of <1mbar during a shot. After passing through the light curtains, the projectile enters the target chamber, where it will impact into a target of choice, usually mounted onto the inside of the door to the target chamber at the rear of the gun. After the shot, the gun is then ventilated by allowing air to enter from the lab whilst drawing it through a vent mounted within the door of the test chamber, and through a filter, before it is allowed to flow to the fume extraction system. This ventilation period lasts for ten minutes, and is necessary for both safety, and as a measure to help to keep the gun clean and free from unnecessary build-up of residue left behind by the combustion of gunpowder. After each shot, the pump tube and launch tube are both cleaned.
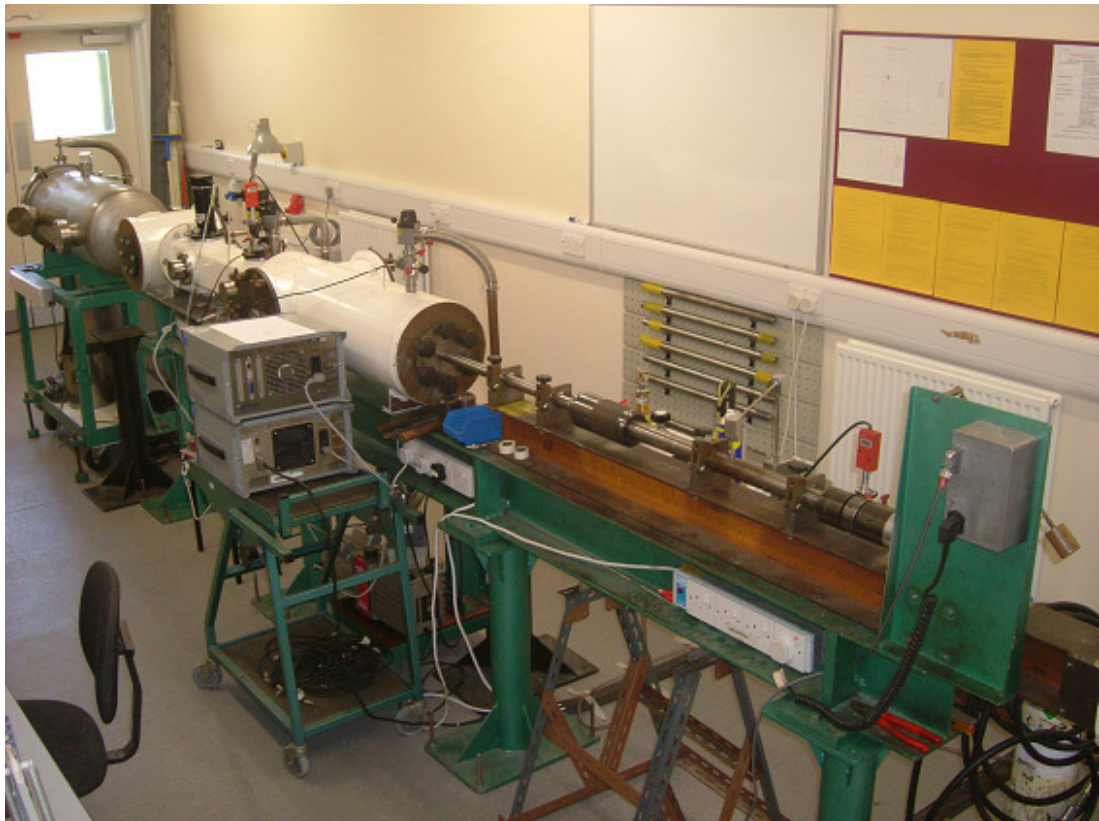


Figure 2.4: The light gas gun at the University of Kent.

## 2.2 PVDF Sensors:

PVDF is an acronym for the term polyvinylidene-fluoride, which is the name of a piezoelectric material. The chemical structure of the repeating unit of PVDF is: $-CH_2 - CF_2 -$. PVDF is a polymer, which due to it having a relatively large piezoelectric property, may be used effectively to detect small variations in stress over the area of the material. Some materials, such as PVDF, containing polar molecules, which are subjected to an application of stress, may experience a polarization of their constituent molecules. This polarization can cause a potential difference to be induced across the body of material, which may be caused to induce an electric current. Alternatively, applying an electric field to the body of the material will cause a strain to be produced. The description of the behaviour of a piezoelectric effect is given by the Equations 2.4 and 2.5, providing the strain, *e*, and polarization, *P*, produced by an applied stress, σ, and an electric field, *E*, assuming that they are simultaneously applied [26]:

$$P = -d\sigma + \varepsilon_0 \chi E, \tag{2.4}$$

$$e = -s\sigma + dE, \tag{2.5}$$

where, 'χ', and 's', are both constants.

Experimentally, stress will be applied to the PVDF, and the charge displaced between two electrodes, which are shorted together and are bonded to the PVDF sample, is measured. The electrodes are made from evaporated metal, and are formed into a thin film that can be deformed with the PVDF sample without distorting the applied stress. The measured charge is thus [27]:

$$\frac{\partial Q}{\partial \sigma} = A \frac{\partial P}{\partial \sigma} + P \frac{\partial A}{\partial \sigma}, \tag{2.6}$$

where, '$Q$', is the measured charge, and '$A$' is the area of the electrodes. This makes the change in polarization:

$$\frac{\partial P}{\partial \sigma} = \frac{1}{A} \frac{\partial Q}{\partial \sigma} - \frac{P}{A} \frac{\partial A}{\partial \sigma}. \tag{2.7}$$

PVDF sensors were used, and were adhered to aluminium plate targets.

## 2.3 FOMIS:

The FOMIS apparatus (fig 2.5), or the Fibre Optic Micrometeoroid Impact Sensor, is a purpose built piece of equipment, designed to receive impacts while in space, or while positioned on the surface of the Moon [21].
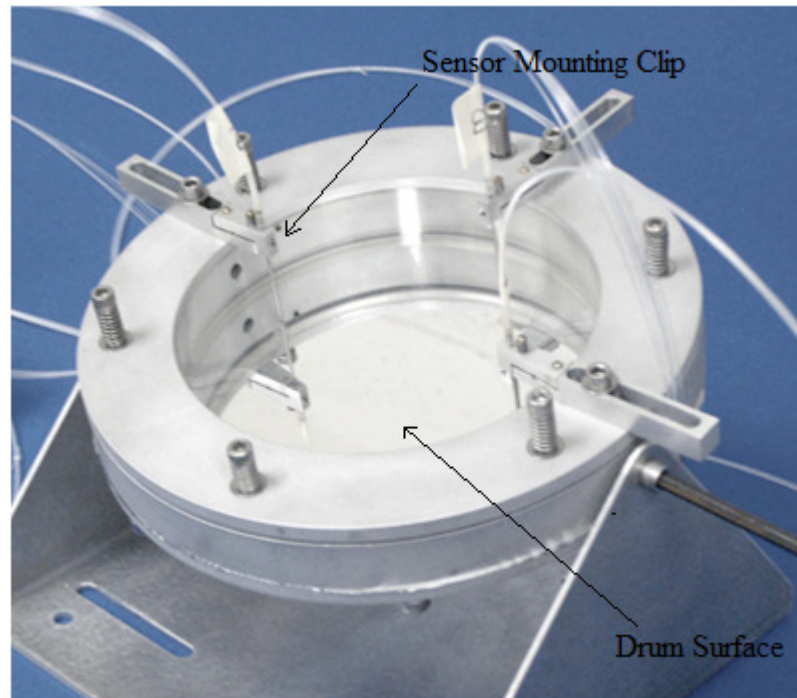


Figure 2.5: This is an image of the rear side of the FOMIS apparatus. Three clamps can be seen, positioned around the diameter of the drum, holding the fibre optical sensors directed towards the surface of the drum (Corsaro et al. 2010).

The FOMIS is comprised of a mounting stand, there as a supporting frame, and also to allow a change in the orientation of the sensor. There is a drum frame, attached to the mounting stand, which is there to hold the drum 'skin' in place. The drum skin is a thin mylar film (but it can be aluminium foil, or even fabric), stretched tight by being clamped into place within the frame, while a spring applies tension across the surface from around the circumference of the film. There are screw threads positioned around the drum frame to allow for the attachment of clamps, which can be used to hold fibre optic sensors in place. These sensors are suspended near to the rear surface of the drum (this is adjustable, but is of the order of 1-2 mm), pointing directly at it, perpendicular to it. The sensors detect optical intensity, and can measure slight variations in the vertical displacement of the drum surface, during

oscillations caused by acoustic vibration. The principle for its operation is that it is able to detect the acoustic vibrations produced by the penetrative impact of micrometeoroids with the drum surface.

## 2.4 Plate Set-Up:



Figure 2.5: A diagram showing the layout of target plate set up. The four sensors adhered to the plate are shown as grey rectangles. The central square marked with a cross at its centre is depicted to show the area of most likely highest sensor reception. The corners of the aluminium plate were removed to give clearance for the sensor cables.

The PVDF sensors that were used within this project are Durham Instruments model number 1005935-1. The signals of 3 sensors, per plate, were read out for each shot. Each sensor that was used was tested using a digital multi-meter, and all of the sensors were found to have a capacitance of approximately 1.3μF. The aluminium plates measure 10 inches by 10 inches, minus the corners, and approximately 1.500 mm ± 0.005 mm thick. The aluminium alloy that the target plates were made from is of the type: 6061 T6. Aluminium of this type has a density of approximately 2.7 g cm$^{-3}$, and is tempered to have a high tensile strength of around 290 MPa.
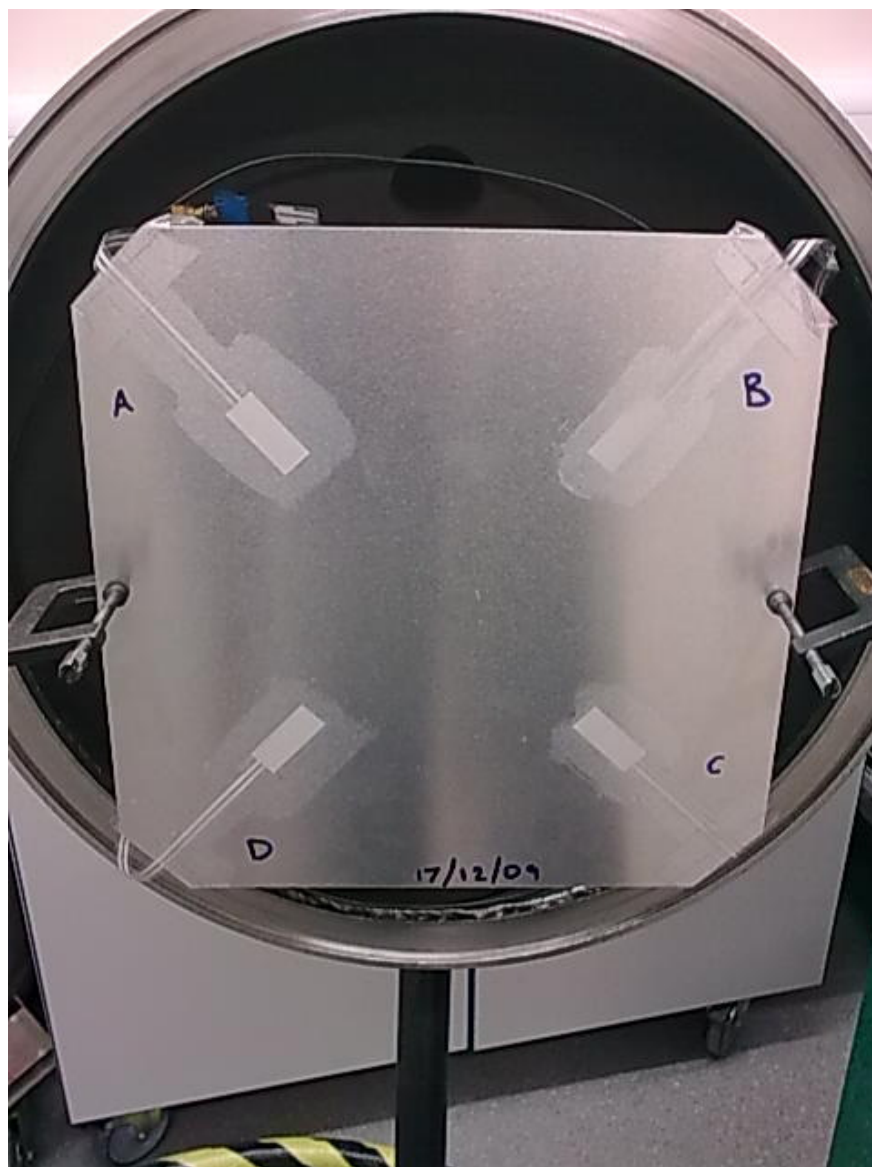


Figure 2.6: This is an image of "Target 1", showing the date of its creation and the sensors clearly marked (A,B,C,D). The target is mounted in the door of the gun.

The aluminium target plates were mounted onto the inside of the target chamber door (fig 2.6). The mounting rig allowed for extra plates to be mounted behind the target plate, to prevent the projectile from reaching and damaging the door to the target chamber. Two rear plates were used (fig 2.7). The closest to the target plate was a 1.5mm thick plate of the same aluminium as the target, and the rearmost plate was double thickness of the aluminium to ensure no accidental penetration occurs. The first rear plate was very rarely penetrated during this project. The distance between the target and the first rear plate was 95mm ± 0.1mm.
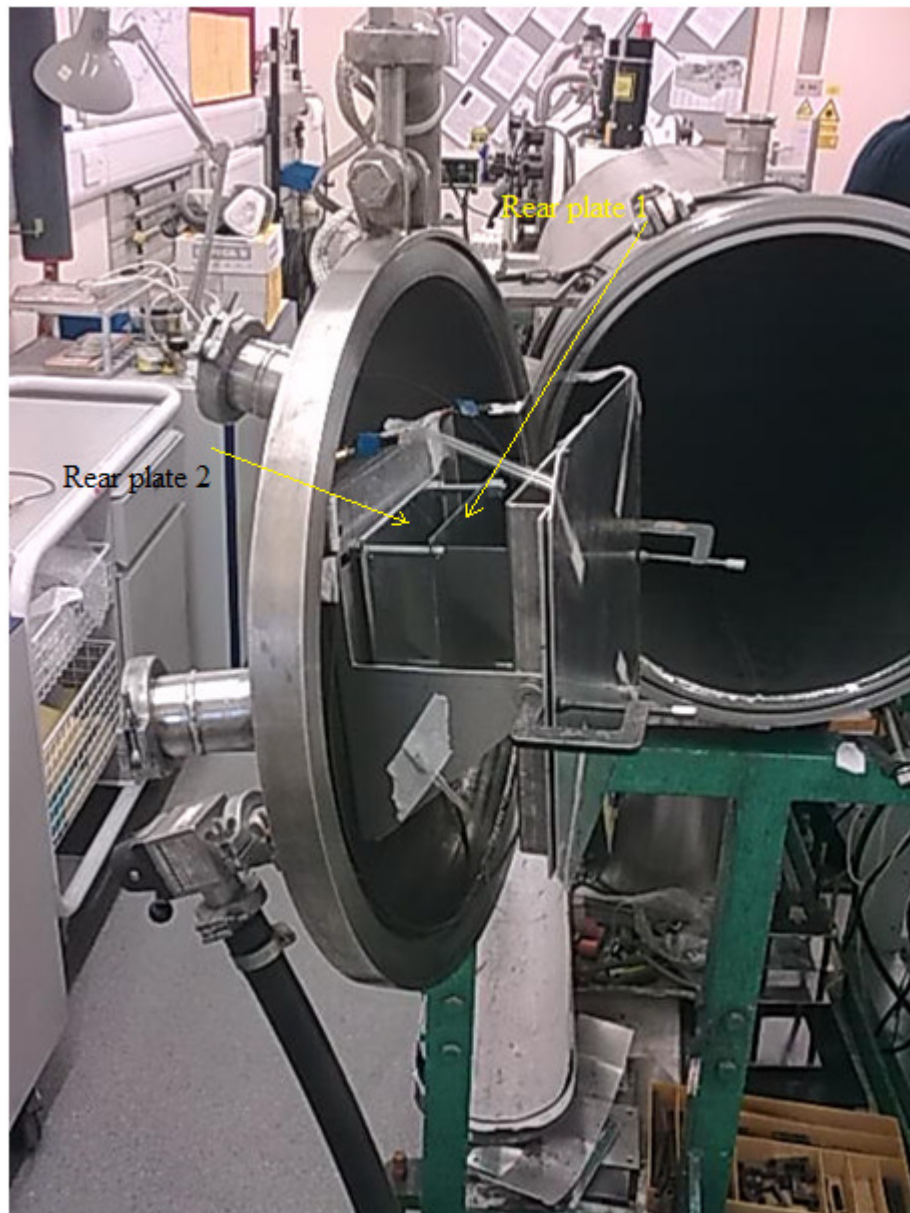


Figure 2.7: This is an image of the target plate mounting from a side view. Here the first rear plate and the rearmost plate can both be seen. The cable from the unused sensor has been secured to the housing to ensure that it does not offer any obstruction.

The target plates were clamped onto the mounting using the small g-clamps shown in fig 2.7. Separating the base of the g-clamp screw from the surface of the target plate was a layer of rubber insulation. On the underside of the plate, separating the target plate from the mounting, were rubber insulation pads. This was done to help to isolate the target plates from the frame. The frame which was used as a mounting for the target plates had the capability of adjustment with regard to the angle at which the plate is held when compared to the axis of the projectiles' motion. During this project, the angle of incidence between the projectile and the target plates was never altered. The surface of the target plate was made normal to the direction of travel of all projectiles used. This configuration is described as 'flat', or as having an angle adjustment of zero (accurate to better than one degree). This was measured at each instance whenever a plate was mounted onto the frame.

The first rear plate, in some cases, was also equipped with a PVDF sensor. In these cases, the thickness of this plate was doubled to approximately 3mm ± 0.005mm. The rear plates were 5 inches by 5 inches in size. The sensor was mounted onto the rear of the plates (fig 2.8), and each of these rear plates were only used to receive one shot each. In these cases, the channel used for the sensor was channel 2, so that the channels in use on the target plate were channel 1 for the sensor in the top left of the plate (A), and channel 3 for the sensor on the bottom right of the plate (C).
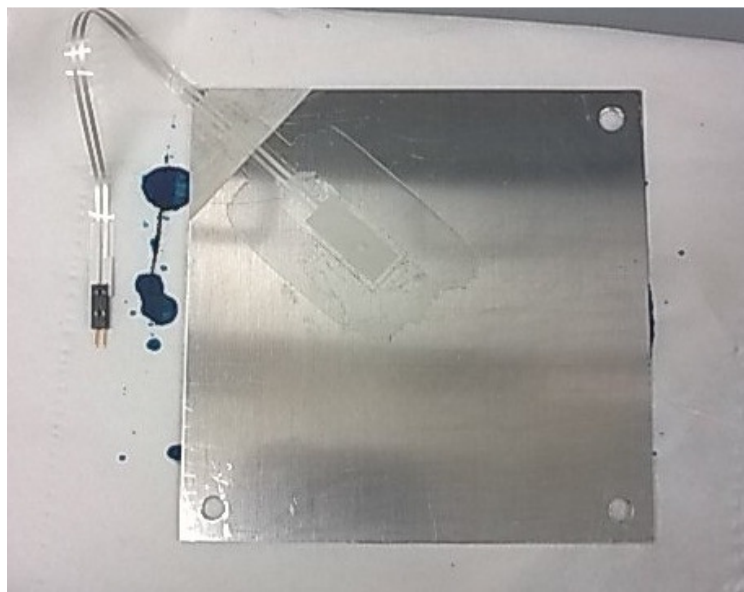


Figure 2.8: This is an image showing the mounting of a PVDF sensor onto the rear of a 3mm rear plate. A thin layer of lacquer has been applied to the aluminium plate before the sensor was glued into place. Masking tape has been added to the plate corner to restrain the sensor cable.

This way, there was sensor reception from two opposing corners of the target plate. In some cases, the first rear plate used for a shot was coloured with blue 'layout' ink (fig 2.9). This was used to give a larger optical contrast between areas of impact damage, and undamaged areas of the plate.
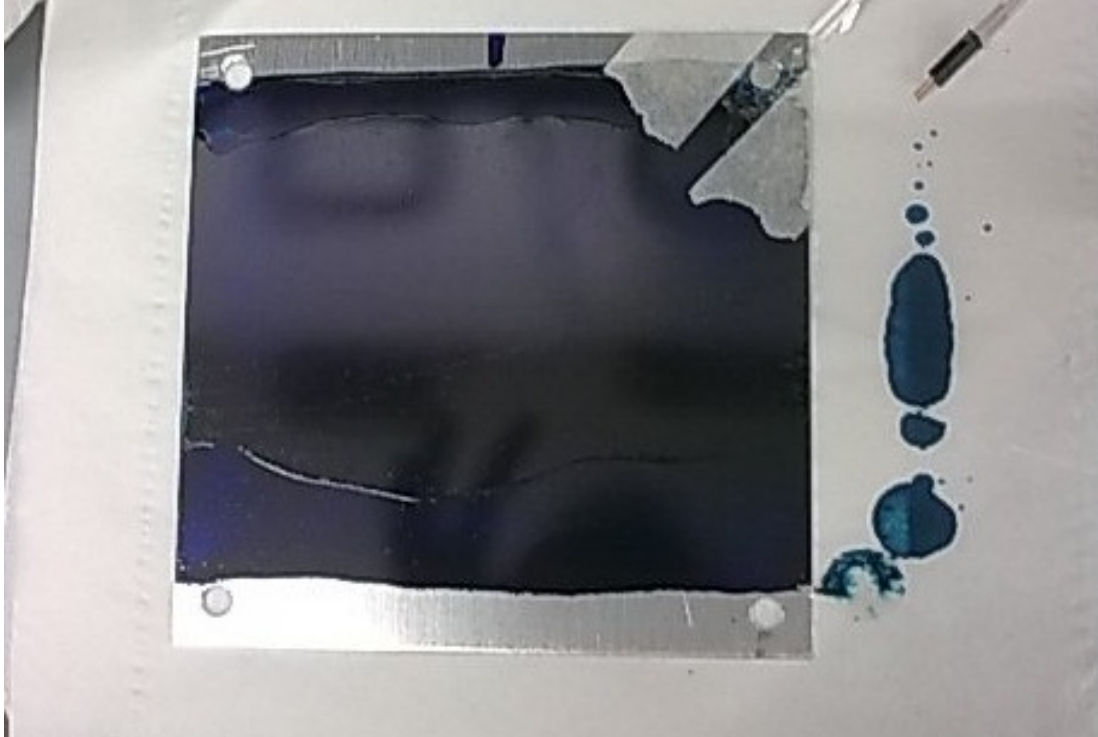


Figure 2.9: This is an image showing the front of a 3mm rear plate after it has been coloured using layout ink.

To protect the sensor mounted upon the rear plate from penetrative debris, a shield was created, covering the region of the plate where the sensor was located (fig 2.1.0). This shield plate was used for all shots that included the use of a rear plate that featured a sensor. This shield obscured an equal portion of the plate for each shot (fig 2.1.5), and assuming that the debris cloud from the initial impact with the target plate would spread circularly in a uniform fashion, per degree, then the shield would prevent an equal fraction of the total debris from each shot from hitting the rear plate. This means that, assuming the amount of debris colliding with the rear plate relates to the output signal amplitude, the shield will not affect the relative magnitudes of signal amplitudes between shots that cause differing amounts of debris to hit the rear plate. The rear plate apparatus was isolated from the mounting frame with the use of rubber dampeners (fig 2.1.1) and insulated threads of the mounting screws. The rear plates, when used when equipped with a sensor, were

mounted at a distance of 83mm ± 0.5mm from the target plate, when measured from the front of the target plate, to the front of the first rear plate. The sensors on the rear plates were mounted 9cm ± 0.5mm away from the top left corner, when viewed from the rear.
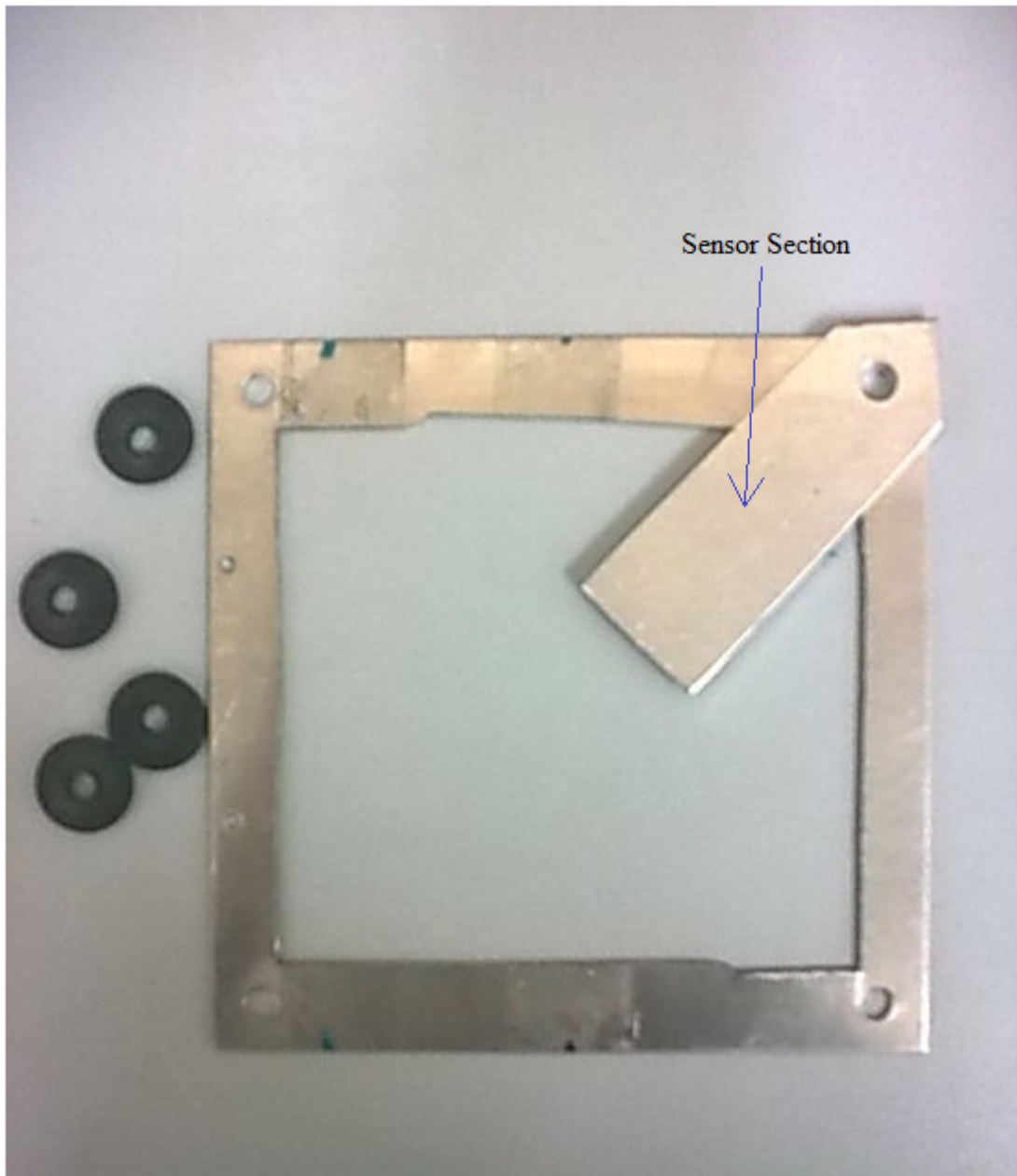


Figure 2.1.0: This shows the mounting frame used to support the sensor 'shield'. This frame was mounted in front of each first rear plate, and isolated from it using the rubber dampers shown in the image.

Figure 2.1.1: This is an image which shows the screws used to mount the rear plates. This image shows the rearmost plate already in position, and at the top of the screws there are one set of dampers in place, and the threads have been insulated. The mounting frame for the target plate can be seen on the right, in front of the mounting screws.

Figure 2.1.2: This image shows the rear plate mounted onto the screws. The second set of dampers have been added to the mounting, isolating the plate.



Figure 2.1.3: This image shows that the excess isolation tape from the mounting threads has been removed.

Figure 2.1.4: This image shows the shield frame mounted in front of the rear plate.
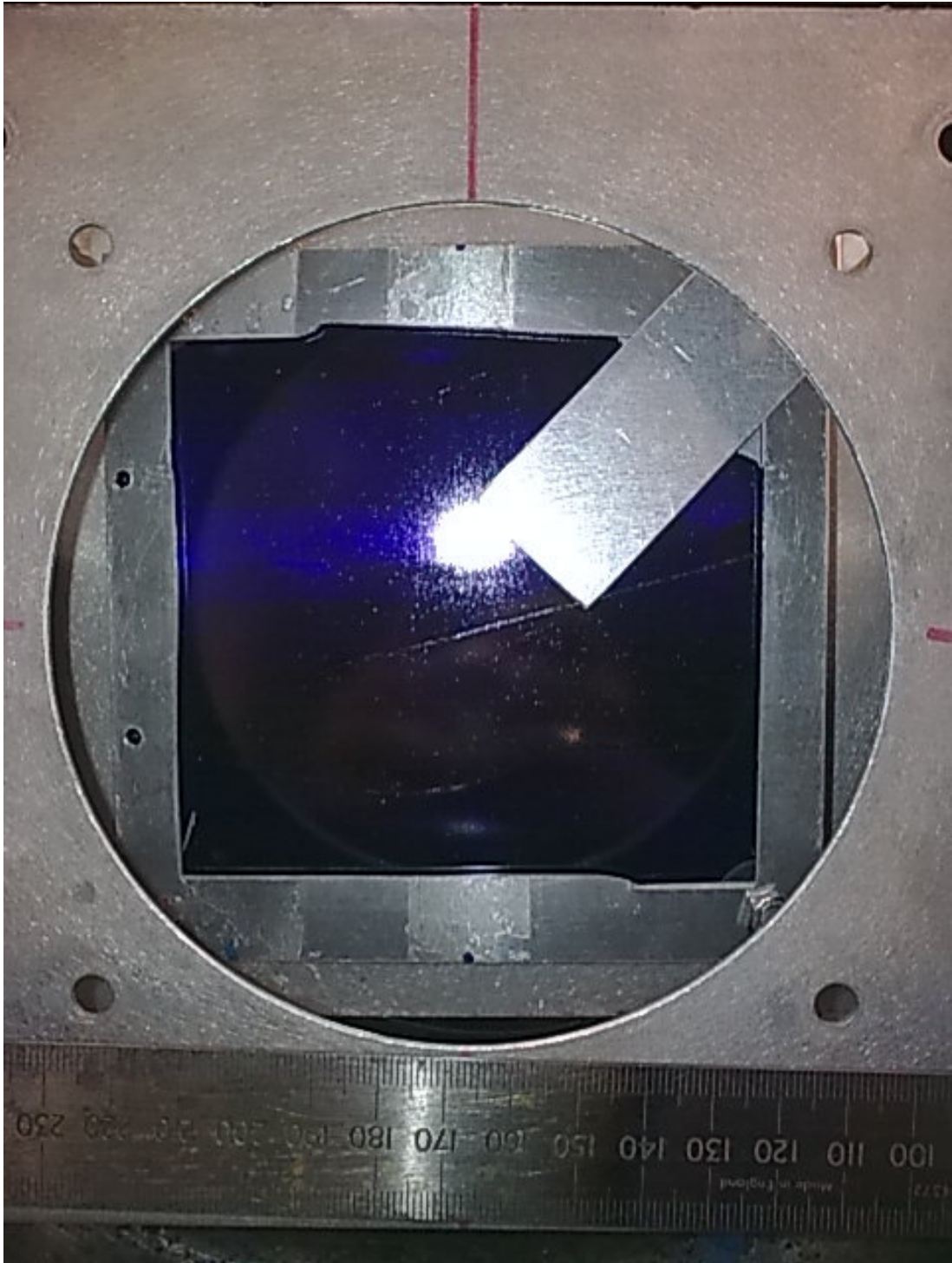
Figure 2.1.5: This image shows the cover given by the shield frame. This view is from directly in front of where the target plate would be positioned. The 'visible' part of the rear plate, shown in blue, is the portion of the rear plate that was left unprotected and left open to the possibility of impacts from debris from the penetration of the target plate.

**Plate Set-Up (cont):**

The purpose of the placement of the PVDF sensors was to measure a voltage signal induced by oscillation of the plate, which caused a deformation of the PVDF film which was adhered to the surface of the plates.
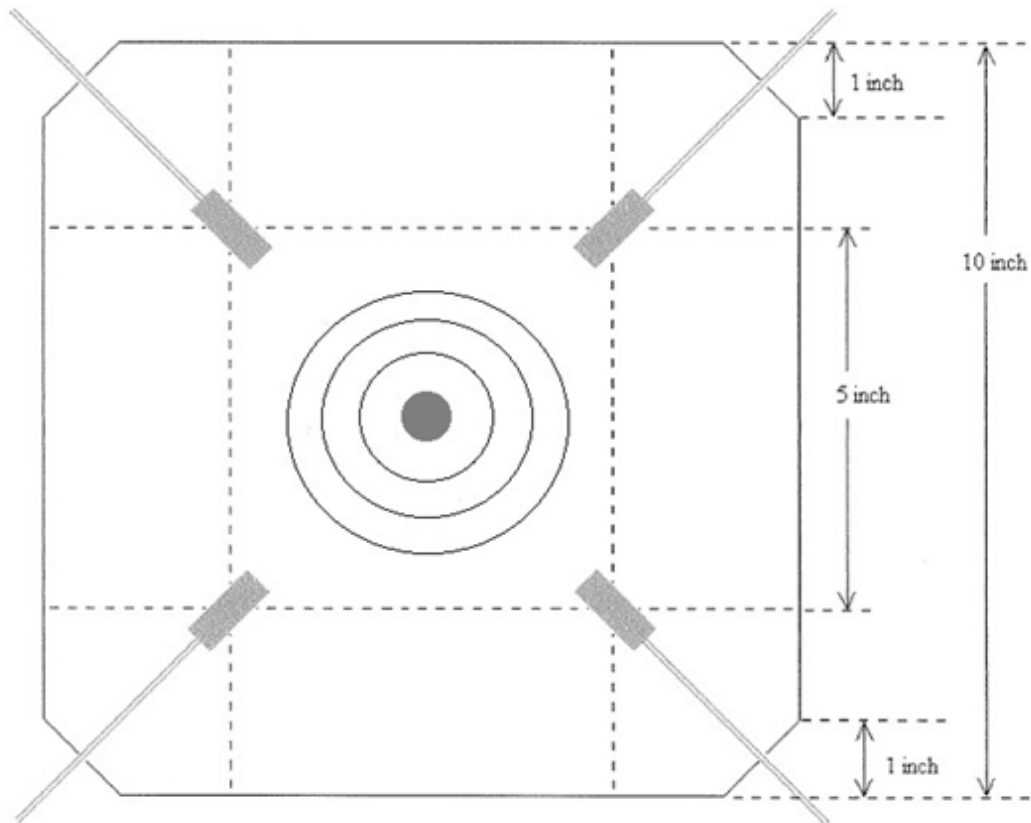


Figure 2.1.6: This diagram shows the manner of acoustic propagation taking place as an impact occurs upon the target plate. The grey circle in the centre represents the impact of an object against the plate. The concentric circles around the centre represent the acoustic wave propagation.

As can be seen in fig 2.1.6, when an object impacts the centre of the plate, the energy is dispersed in a circular fashion (when considered in two dimensions like this), according to the speed of sound through the target material. If we assume that the sensors are all mounted equidistantly from the centre of the plate, and from their respective plate corners, then we may also assume that the acoustic wave propagation should reach all of the sensors simultaneously. However, if the impact was to occur at some other point on the plate, which was somewhere closer to some sensors than others, then this does not remain true. See fig 2.1.7 for an example.

With regard to thin plates, the types of waves that propagate with the highest velocity are longitudinal waves. Due to the fact that perfect longitudinal waves only truly propagate through unbounded solids, it can be assumed that only quasi-longitudinal waves will propagate in a solid that is bounded in one plane (such as a thin plate).

Where the wave propagation speed for an unbounded solid is

$$c_L = \sqrt{\frac{D}{\rho}}, \tag{2.8}$$

and the Bulk Modulus of the material is

$$D = \frac{E(1 - \mu)}{(1 + \mu)(1 - 2\mu)}, \tag{2.9}$$

then it may be assumed that the wave propagation velocity in solids that are bounded in one place, such as a thin plate, is

$$c_{L,I} = \sqrt{\frac{E}{\rho(1 - \mu^2)}}. \tag{2.1.1}$$

where '$E$' is the Young's Modulus, '$\mu$' is the Poisson number, and '$\rho$' is the density of the material. [7]

As shown in the figure 2.1.7, if the impact is not at the centre of the plate, then the distance between the impact epicentre and some sensors will be shorter than the distance between the impact epicentre and the other sensors. For example, in the diagram above, the impact is closer to the sensors on the left of the plate than it is to those on the right, which means that the acoustic waves have a further distance through the material to travel before they reach the sensors on the right side of the plate, compared to the distance the waves will travel before reaching those on the left. In theory, this means that if the speed of sound through the material were known, and the time delay between the impact and the detection of the impact by the sensors was also known, then the distance between the impact and each sensor could be calculated.
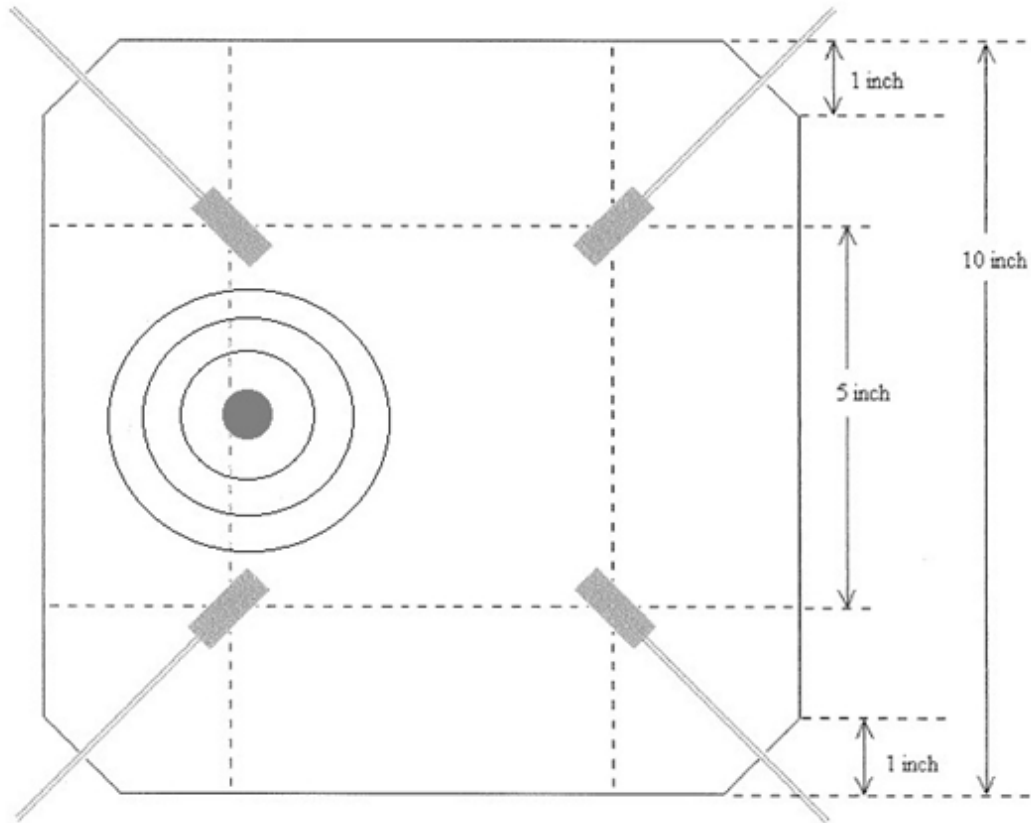
Figure 2.1.7: This diagram shows the target plate being impacted by some object, represented by a grey circle. The impact is not at the centre of the plate.

Given at least three sensors, this means that the actual location of the impact could be calculated – however, such calculation was not part of this project [7, 8, 28].

The PVDF sensors were connected to a PC, and their output was read during each shot. The computer was set to begin the recording of the digitised signal representing the induced voltage, from the deformation of the sensors, at the activation of a trigger source connected to the oscilloscope used to detect the signal intensity given from the two light curtains. At the time when the oscilloscope records this sudden change in intensity, the program, NI LabView signalexpress, begins recording the sensor signal data. The recording was maintained for a period of six milliseconds, with increments of one microsecond. Fig 2.1.8 provides an example of raw data received from one single sensor during an impact, over the recording period. Before analysis, the signal in question was examined for noise and the beginning of the impact event was identified. Data representative of the time before the detection of the impact was considered to be noise, and was ignored.
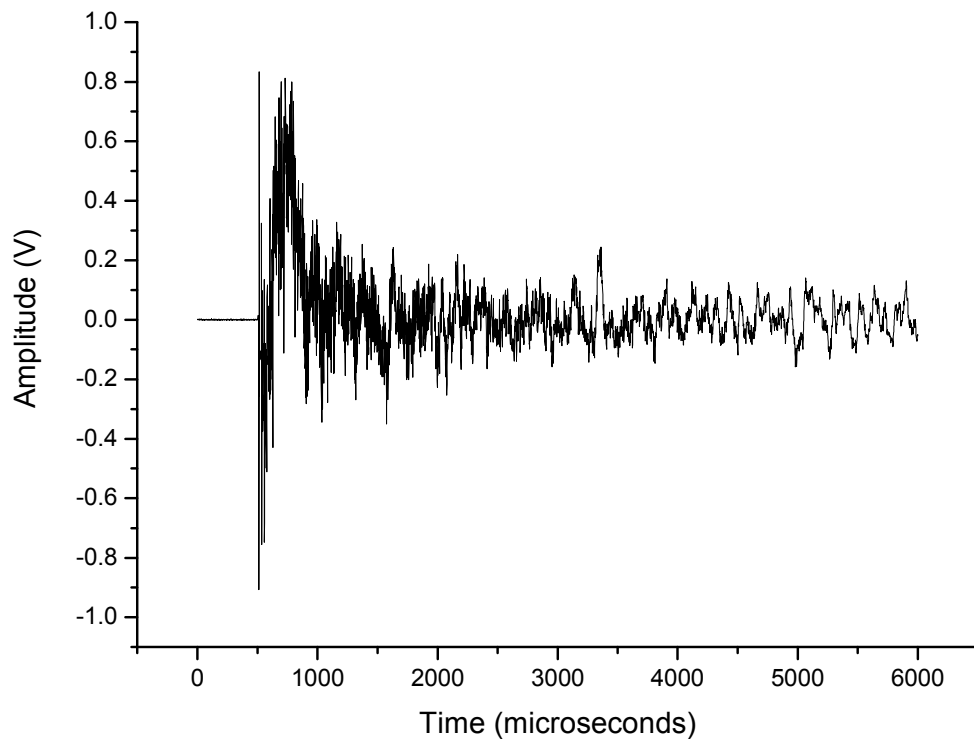
Figure 2.1.8: This is an example of a raw signal trace from a PVDF sensor. The sensor was mounted upon a front plate, and the impact was penetrative, caused by a stainless steel ball bearing, travelling at ~6kms$^{-1}$.

The range of the noise was recorded as typically being between +3.5mV and -2.5mV. This can be seen in the given example, as the flat region prior to the sudden, large, change in voltage. After this, the technique as used by Corsaro et al, 2008, was used to analyse the signal to calculate the 'Decay Time' and the peak amplitude of the signal. The signal data was subjected to data processing within Microsoft Excel, using the AVEDEV function, which is the 'Average Deviation from the Mean' function; each iteration of the calculation included thirty consecutive cells of data, and was continued for the entire data set until reaching the final thirty data cells, where the process was discontinued, so that every iteration was sure to have included thirty cells [29]. The AVEDEV function literally yields a value for the average deviation about the mean, for each 30 data values of the signal, incrementally. This can then be plotted against the original signal, as seen in fig 2.1.9. This can then be used to calculate the decay time and the peak amplitude. The intercept of an exponential decay trend line, fitted to the AVEDEV plot, represents the peak

amplitude of the signal. The decay constant of this trend line represents the decay time.
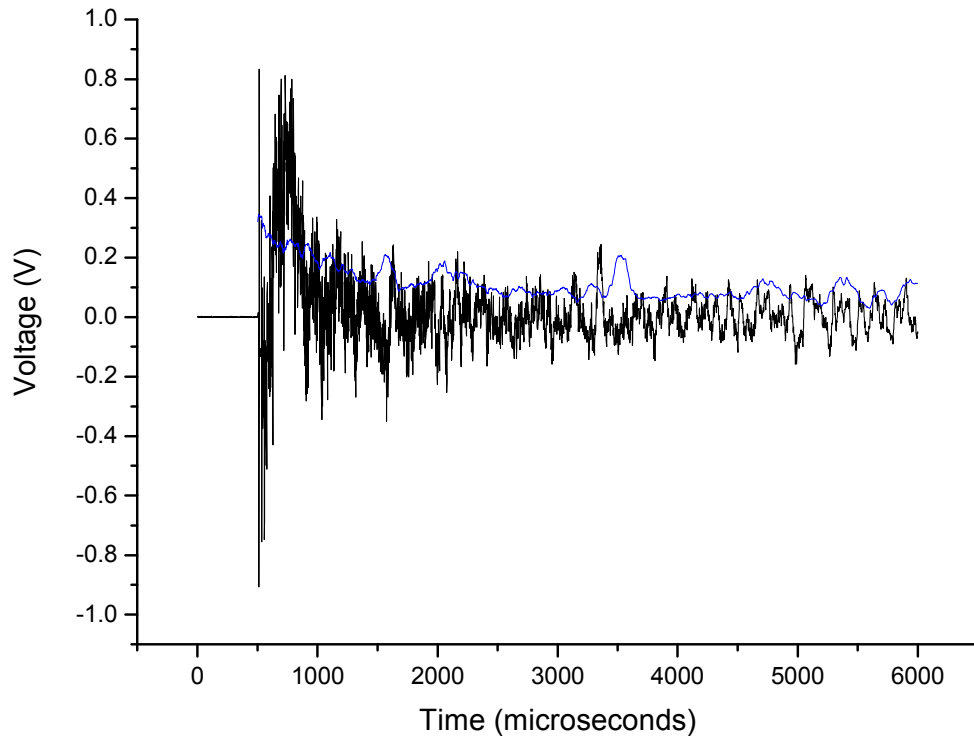


Figure 2.1.9: This is an example of a signal trace taken from a single sensor, the same as fig 2.1.8, except that the envelope (a plot of the AVEDEV function) of the filtered version of the data has been plotted overlapping the original trace.

The traces shown in the figs 2.1.8, and 2.1.9 are raw data, and as such you can observe that the oscillations shown by the sensors feature both high-frequency and low-frequency characteristics. The low frequency characteristics < 30kHz were filtered, and removed from the signal, during data processing.

The decay time of any given signal trace is representative of the 'ringing' of the plate that has been induced by the impact. This ringing occurs due to the finite size of the plate, and is characterised by the plate's dimensions. In this work, the peak signal amplitude has been made the object of interest. While this part of the vibration always occurs early within the recording duration, it is suggested by the author that the initial signal amplitude (i.e., the immediate amplitude produced, after such factors as noise have been compensated for) should also be considered in the future.

**2.5 Bead Drop Testing**

Plate 1: This plate was configured such that three sensors were used for impact detection, and a fourth was not used, despite being mounted onto the plate. The reason for this is that there were only four channels available for digitiser input, and one of those channels was required for use by the light-gas gun oscilloscope as a trigger source. This allowed one sensor mounted on the plate to be treated as a spare, in case one of the other sensors was found to be malfunctioning in some way, or was damaged during experimentation. The fourth channel was used to trigger data recording by the computer. The sensors were fixed to the plate with an adhesive provided by Robert D. Corsaro (United Stated Naval Research Laboratory), which was a cyanoacrylate based glue named "Instant Adhesive 10-128" by "GC Electronics" (fig 2.2.0). Before the sensors were glued into place, a thin layer of lacquer (nitrocellulose based) was applied to the region over which the sensors would lie on the plate. This was to electrically insulate the sensor from the plate.



Figure 2.2.0: An image of the adhesive used in this project.

This plate was then labelled as "Plate 1". It was subjected to bead drop testing in order to calibrate the sensors mounted onto the plate. This involves dropping a ball bearing onto the plate repeatedly, and recording the signal produced by the PVDF sensors. This allows for a relative signal magnitude between the sensors on the plate

to be established, yielding the possibility to calculate absolute signal amplitude values. This is achieved by directly comparing the peak signal amplitude for each sensor, per incidence of impact. For each recorded signal, the peak amplitude was found by locating the maximum half peak-to-peak value for the recorded signal. The PVDF film of which the sensor strips are made, will deform as the plate deforms during oscillation, so it is assumed that the amplitude of oscillation shown by the sensors is the same as that of the plate. It is assumed that the square of the amplitude is directly proportional to the energy of the oscillation of the plate caused by the impact of the ball bearing, i.e., an oscillation is the travel of energy through the plate, and this energy is provided by the impact of the ball bearing. The quantity of energy possessed by this oscillation is proportional to the square of its amplitude, as shown in equation 8 [25].

$$E \propto A^2 .$$
(2.1.2)

The potential energy of the ball bearing at the moment of impact was calculated by performing a simple calculation:

$$E = mgh ,$$
(2.1.3)

where '$m$' is the mass of the ball bearing, '$g$' is the bearing's acceleration due to the force of gravity, and '$h$' is the height of the ball bearing above the target plate.

Therefore, if the mass of the ball bearing is kept constant for all instances at which the bearing was dropped onto the target plate, if the ball bearing is always dropped from the same height, and if we assume that the ball bearing is always allowed to free-fall without influence, then differences in recorded signal amplitude relayed by different sensors must be attributed to the relative sensitivity of the individual sensors. To account for the differences in sensor sensitivity, the average signal amplitude was recorded for all of the sensors used, for a range of impacts. This range of impacts included ten repeats, where the mass of the ball bearing, and the height from which it was dropped were kept constant. The highest average signal amplitude was chosen, arbitrarily, to be the 'baseline' to which all of data recorded from the other sensors would be calibrated. This sensor, and its average signal amplitude, was

chosen because it was the highest, and therefore the most sensitive sensor. Therefore, it was assumed that it was the most efficient. The calibration was achieved by dividing the 'baseline' value (which was the average signal amplitude, from the bead drop testing, for the sensor found to have been the most sensitive) with the average signal amplitude for a sensor in question. This would yield a coefficient by which all signal amplitudes should be multiplied, for those signals given by the sensor in question. For example, if the 'absolute' value of a signal amplitude, for a signal recorded by 'Sensor 1' was desired, then the 'baseline' value should be divided by the average signal amplitude found for 'Sensor 1' during bead drop testing, and this calculated value (the afore mentioned coefficient – or, rather, a coefficient only for 'Sensor 1', in this example) should be multiplied by the signal value from 'Sensor 1' for which the 'absolute' value is desired. Bead drop calibration of this method was carried out for every sensor used within the project, and this includes sensors used on rear plates. The 'baseline' value was calculated, and a sensitivity coefficient was calculated for every other sensor. This assumes that the sensitivity coefficient for the 'baseline' sensor was 1. See section 3.2.

The bead drop testing utilised a fixed arm, fitted with an aperture, to allow precise release of the ball bearing from a consistent height. This arm was a clamp, fixed to a weighted clamp stand, with the aperture mounted within the jaws of the grip. The aperture was a hole drilled within a plastic cylinder. The method for release was to place the ball bearing upon the top of the cylinder, next to the hole, and to force the ball bearing to move horizontally, until it reaches the hole. Upon reaching the hole, the ball bearing will fall freely until it hits the target plate. The top surface of the plastic cylinder is positioned so that it is parallel to the surface of the target plate, which is positioned so that it is parallel to the surface of the ground. The distance between the top surface of the cylinder and the surface of the target plate was measured, so that the drop height of the ball bearing was known. The computer program used to record the sensor signals was set to begin recording sensor signals, for the bead drop tests, upon 'Sensor 1' receiving a signal change corresponding to a rising voltage. 'Sensor 1' was selected arbitrarily, simply due to it being 'number 1'. The ball bearing was made to hit the centre of the plate.

Figure 2.2.5: This is an image showing the target plate equipped with apparatus ready to be used for bead drop testing. The target plate has been mounted upon the same frame that it was mounted upon during testing within the light gas gun, and it has been isolated from it in the same way; the clamps fixing it to the mounting frame have been fitted with rubbed dampers, and rubber padding has been positioned beneath the plate. The weight of the clamp stand has been rested upon the mounting frame, beneath the target plate, to keep the entire apparatus steady. The clamp and aperture cylinder (shown arrowed) have been positioned above the target plate to allow ball bearings to be dropped freely into the centre of the plate. The plate shown in the picture is "Plate 1". Free-fall of the ball bearing began directly from the top of the aperture.

Figure 2.2.6: This is an image showing the use of a rear plate during bead drop testing, during the setting up of the apparatus. Rubber padding was positioned beneath the plate to isolate it.

This set up method was repeated for the second plate, which was labelled "Plate 2".

## 2.6: Summary

This chapter has provided details of the experimental method that will be used throughout this project. This has included descriptions of the apparatus that was used to conduct these experiments. Particular attention has been given to the description of the light gas gun, as it is the main piece of equipment used within this project. Detail has been given to the description of the targets that have been used during these experiments. The next chapter will provide the results of those experiments.

# CHAPTER THREE: RESULTS ANALYSIS

The purpose of this chapter is to provide the data that was acquired through the execution of the previously detailed experimental method, and then to give discussion pertaining to the significance of those results. The experimental method was carried out according to a planned programme, which was devised with the intent to fulfil the objectives of this project. Therefore, this chapter will also include details of the experimental programme, and why the planned experiments are significant with respect to the project and its aims. Of course, as with all of the best laid plans of mice and men, some changes, or additions, to the experimental programme were made during the undertaking of the project. The details of why the decision was taken to amend the experimental programme will also be given within this chapter, along with the aims that those changes were expected to accomplish.

This chapter will be presented in the form of various sub-sections, each detailing results of a different nature. The results will be separated as such, so that the discussion of each may also be confined to the relevant section.

## 3.1 An Overview of Shots Fired into Aluminium Target Plates

Table 3.1: A summary of all light gas gun shots into aluminium target plates. Note: SS = Stainless Steel, Ti = Titanium, WC = Tungsten Carbide, BB = Ball Bearing.

| Shot Number | Date | Projectile | Speed (kms$^{-1}$) | Impact Type | Plate Number |
|---|---|---|---|---|---|
| 1 | 17/12/09 | 1mm SS BB | 5.18 | Hole | 1 |
| 2 | 04/02/10 | 1mm Ti BB | 5.04 | Hole | 1 |
| 3 | 04/02/10 | 1mm Glass | 5.60 | No Impact | 1 |
| 4 | 09/02/10 | 1mm SS BB | 5.07 | Hole | 1 |
| 5 | 09/02/10 | 1mm WC BB | 5.04 | Hole | 1 |
| 6 | 16/02/10 | 1mm Glass | 5.03 | Hole | 1 |
| 7 | 16/02/10 | 1mm WC BB | 4.86 | Hole | 1 |
| 8 | 02/03/10 | 1mm Ti BB | None | No Impact | 1 |
| 9 | 02/03/10 | 1mm Ti BB | 4.99 | Hole | 1 |
| 10 | 12/04/10 | 1mm SS BB | 1.11 | Hole | 2 |
| 11 | 12/04/10 | 1mm SS BB | 7.57 | Hole | 2 |
| 12 | 12/04/10 | 1mm SS BB | 5.18 | Hole | 2 |
| 13 | 13/04/10 | 1mm SS BB | 3.06 | Hole | 2 |
| 14 | 13/04/10 | 1mm SS BB | 3.91 | Hole | 2 |
| 15 | 20/05/10 | 1mm SS BB | 7.65 | Hole | 2 |

Table 3.1 shows all of the shots performed during this project while using aluminium plates as a target. Please note that where a shot has been marked as having a speed of 'None', it is meant that no speed was recorded for the projectile. This is because there was some malfunction, and the shot was unsuccessful, in that it did not hit the target, and the oscilloscope was unable to record a speed. This is most likely to have been because the projectile hit the stop plate. If a shot has been marked as 'No impact' in the 'Impact Type' column, then this means that some malfunction occurred, and that the projectile failed to hit the target. Out of the fifteen shots that were fired, two of them failed to hit the target (it should be noted that even if a speed is recorded for a shot, it can still fail to hit the target). All of the other shots hit the target, yielding an overall shot success rate of approximately 87% for this project,

overall. This shows that the light gas gun has a finite likelihood for malfunction which is not negligible, and therefore it should not be considered as an infallible experimental tool. The majority of projectiles that were fired were made of stainless steel.

Table 3.2: Properties of the projectiles used within this project.

| Projectile Type | Measured Diameter (mm) | Measured Mass (mg) | Calculated Density (kgm$^{-3}$) |
|---|---|---|---|
| Glass | $1.0000 \pm 0.00005$ | $1.3780 \pm 0.00005$ | $2631.8 \pm 0.3$ |
| Titanium (Ti) | $1.0000 \pm 0.00005$ | $2.3940 \pm 0.00005$ | $4572.2 \pm 0.5$ |
| Stainless Steel (SS) | $1.0000 \pm 0.00005$ | $4.0640 \pm 0.00005$ | $7761.7 \pm 0.9$ |
| Tungsten Carbide (WC) | $1.0000 \pm 0.00005$ | $7.7910 \pm 0.00005$ | $14879.7 \pm 1.7$ |

Table 3.2 shows the properties of projectiles fired using the light gas gun during experiments throughout this project. All of the spheres that were used as projectiles were measured before they were used, using a digital micrometer, to verify their diameter. Projectiles were measured in this manner and then selected when they were found to have a diameter of 1.0000mm ± 0.00005mm, according to the digital micrometer. The metal ball bearings that were measured were all found to yield this measurement upon the first measurement of a ball bearing in question. The glass spheres, however, varied in diameter with an approximate range of 0.0015mm ± 0.00005mm, and therefore more spheres of this type were required to be measured before a ball bearing of the correct size could be found. This is most likely due to the differences in the manufacturing processes required to produce metal ball bearings, when compared with glass spheres. After projectiles were selected for shooting, they were measured using a microbalance to obtain their mass. It can be seen in table 3.1 that the two shots which failed to hit the target, within this project, were using a glass projectile, and a titanium projectile, respectively. The most likely reason for this is that those types of projectile were the two that were composed of materials that have the lowest density, and as such, were the two with the lowest mass that were used within this project. The consequence of this is that they are the two kinds of projectile that were used, that had the lowest momentum relative to the other types of projectile, when fired at the same speed. If the projectiles have a lower mass, and

thus by definition, a lower inertia (again, assuming they were travelling at the same speed as the other projectiles), then they were susceptible to being forced away from their original (intended) trajectory by any perturbing forces that may occur during the time of flight of the projectile. One such perturbing force, for example, would be any stiction between the plastic sabot casing during the process of it being discarded, and the projectile. Another possible reason why a projectile may not hit the target as intended is that it may have fragmented during its flight. Typically, this would be because the projectile was composed of a material with a relatively low compressive strength. However, there is no evidence that any smaller impacts occurred due to fragments hitting the target with regard to acoustic data; those shot that are recorded as having no impact were shots where the acoustic data showed no sign of impact, and was thus discarded.

There are small craters upon the plate, situated in very close proximity to impact holes caused by other projectiles; however, it is not known whether or not these are very small fragments of those projectiles which caused the main hole that the small craters are very close to. The lack of evidence in the form of acoustic data would suggest that these small craters were not formed by fragmentation of either of the two shots that are recorded as having no impact, assuming that the impact of a fragment small enough to create such a crater would impart enough energy to the plate for the PVDF sensors to register a change in induced voltage. This discussion of the reliability of projectile impact is not yet representative of the variability in relative reliability between different types of projectile. For instance, glass projectiles are relatively unreliable for use by the method of experimentation, for both of the reasons already discussed (low density and susceptibility to fragmentation), and the 87% shot success rate quoted for this project would be inaccurate if, for example, the majority of shots used a glass ball bearing as the projectile. It is typical for only one in three 1mm glass projectile shots to be successful.

By using a select variety of impact conditions, the effect upon the differences between recorded signals, given by PVDF sensors, would be observed across the range of impacts. For this purpose, shots were fired from the light gas gun with speeds across a range between $1.11kms^{-1}$ and $7.65kms^{-1}$, and a variety of densities, ranging between 2631.8 kg m$^{-3}$ and 14879.7 kg m$^{-3}$.

## 3.2 Bead Drop Analysis

To determine the relative sensitivity of each sensor, testing was conducted so that the most sensitive sensor could be identified. After this was achieved, the sensitivity of all of the other sensors was determined, relative to the most sensitive. This was achieved by measuring the numerical value of the voltage induced by each sensor during the application of a stress. This stress was kept constant for each sensor, and repeated so that the average half peak-to-peak voltage amplitude could be calculated for each sensor, from a set of output signals, induced by the repeatedly applied stress.

Assuming that the stress applied to each sensor was the same, any differences in the magnitude of the induced voltage would be due to differences in sensor efficiency. For a stress that is kept constant, the most efficient sensor is the most sensitive, in that it will produce a relatively higher half peak-to-peak voltage compared to less efficient sensors. The stress that was applied to the sensors, during this experiment, was an oscillation of the aluminium target plate to which the sensors were bonded. This oscillation was caused by a controlled impact, in the form of a ball bearing that was allowed to free fall onto the plate. After the average numerical value of the half peak-to-peak voltage caused by this repeated impact was calculated for each sensor, this value for the highest sensor was divided by this value for each and every other sensor in turn. The result of each of these calculations is the coefficient value of how much more sensitive the most sensitive sensor is, than the sensor in question (i.e., the sensor for which the result is assigned to) (this coefficient is a pure number decimal value). This value can then be used as a coefficient by which all of the recorded values of the peak-to-peak voltage can be multiplied, for the sensor to which the value is assigned. This corrects the recorded voltage, and yields the true, scaled, voltage, that the sensor would induce, should it have had an efficiency equal to that of the most efficient sensor originally discovered.

In this section, these coefficients are calculated for each sensor. This allows all of the recorded half peak-to-peak voltage measurements to be corrected so that the numerical values represent induced voltages from sensors that would theoretically have an equal efficiency, as explained above. The consequence of this is that it allows differences in recorded voltages, for changes in stress, shown by different

sensors, all to be truly proportionate. If the values of recorded peak-to-peak voltage were not corrected, then the differences in those voltages between sensors, for different stresses, would not be proportional to those stresses – as they would be obscured by the differences in efficiency between the sensors. Therefore, this calibration technique was necessary, as an observation of the relationships between sensor voltage output, and applied stress, was desired.

Table 3.3: The bead drop test results for Plate 1.

| Repeat Number | Sensor 1 (mV) | Sensor 2 (mV) | Sensor 3 (mV) |
|:---:|:---:|:---:|:---:|
| 1 | 3.38 | 2.80 | 2.31 |
| 2 | 2.69 | 3.00 | 2.69 |
| 3 | 2.57 | 3.60 | 3.18 |
| 4 | 2.92 | 3.27 | 3.44 |
| 5 | 3.32 | 3.93 | 3.06 |
| 6 | 3.08 | 3.67 | 3.79 |
| 7 | 3.77 | 3.62 | 2.15 |
| 8 | 3.35 | 3.08 | 2.59 |
| 9 | 3.97 | 4.32 | 3.82 |
| 10 | 3.42 | 3.24 | 2.17 |
| Average | 3.247 | 3.453 | 2.92 |
| Standard Deviation | 0.44262 | 0.46253 | 0.633667 |
| Coefficient | $1.0634 \pm 0.2$ | 1 | $1.1825 \pm 0.3$ |

The first plate to receive bead drop testing was Plate 1. The results for this test are shown in table 3.3. The test involved the use of a 3.0000mm ± 0.00005mm ball bearing, being allowed to free fall from a height of 20cm ± 0.01cm, to impact the centre of surface of Plate 1, as described within the methodology section. It can be seen from table 3.3 that 'Sensor 2' was found to be the most efficient, and was thus assigned a voltage coefficient equal to 1. It was also observed that 'Sensor 2' was 1.0634 times more efficient than 'sensor 1', and 1.1825 time more efficient than 'Sensor 3', which both equate to 'Sensor 2' being on average 6.34% and 18.25% more efficient than the other two sensors, respectively, as is evidenced by table 3.3.

These values are well within the spread on the signals from drop to drop. The overall variation in response is enormous. Also, it isn't in the same sense for each repeat number. i.e., each sensor doesn't maintain the ratios of sensitivity from drop test to drop test, so there seems to be some intrinsic variation in the sensor response, and not in the drop condition



Figure 3.1: This is an image of an example of a plate undergoing bead drop testing. The free fall aperture has been positioned at the required height above the plate, and in such a position as to allow the ball bearings to impact the centre of the plate, at a point equidistant from all of the plate's PVDF sensors.

The next plate to be subjected to bead drop testing was Plate 2. Once again, this test involved the use of a 3.0000mm ± 0.00005mm ball bearing, which was allowed to free fall, and impact upon the centre of the target plate, from a height of 20cm ± 0.01cm. The induced voltage caused by the stress of the plate oscillation, after each impact, was recorded. The results of the analysis performed on that recorded data is shown in table 3.4.

Table 3.4: The half peak-to-peak values recorded for the bead drop testing of Plate 2.

| Repeat Number | Sensor 1.2 (mV) | Sensor 2.2 (mV) | Sensor 3.3 (mV) |
|---|---|---|---|
| 1 | 2.41 | 2.33 | 3.00 |
| 2 | 2.33 | 2.61 | 3.48 |
| 3 | 2.87 | 2.62 | 4.42 |
| 4 | 2.61 | 2.61 | 3.95 |
| 5 | 3.08 | 2.55 | 3.55 |
| 6 | 2.85 | 3.33 | 4.12 |
| 7 | 2.42 | 2.75 | 4.17 |
| 8 | 2.26 | 2.38 | 2.47 |
| 9 | 2.43 | 3.00 | 2.65 |
| 10 | 2.77 | 2.35 | 3.22 |
| Average | 2.603 | 2.653 | 3.503 |
| Standard Deviation | 0.274997 | 0.311664 | 0.666401 |
| Coefficient | 1.3265 ± 0.2 | 1.3015 ± 0.2 | 0.9857 ± 0.2 |

Table 3.4 shows the analyzed results of the bead drop testing performed on 'Plate 2'. From here on, the sensors that were used on Plate 2 shall have their name appended to denote their parent plate, and shall therefore be known as 'Sensor X.2', where 'X' is the sensor number, and '2' represents Plate 2. The same will be done for 'Plate 1', using 'X.1'. It was observed that 'Sensor 2.1' was 1.3265 times more efficient than 'Sensor 1.2', 'Sensor 2' was 1.3015 times more sensitive than 'Sensor 2.2', and that 'Sensor 2.1' was 0.9857 times as sensitive as 'Sensor 3.2'. As such, it was observed that 'Sensor 2.1' was 32.65% more efficient than 'Sensor 1.2' and 30.15% more efficient than 'Sensor 2.2'. However, it was observed that 'Sensor 3.2' was 1.43%

more efficient than 'Sensor 2.1'. Since 'Sensor 2.1' had already been discovered as being the most efficient sensor on the previously constructed plate, and that this sensor has already been selected as the sensor to which all of the other sensors would be calibrated, this sensor was allowed to keep its assignment of a voltage coefficient of 1. This was not a problem, as it simply meant that the marginally more efficient sensor, 'Sensor 3.2', was assigned a voltage coefficient that was less than 1, to make the recorded induced voltages given from this sensor, proportional to the other recordings.



Figure 3.2: This graph shows the half peak-to-peak voltage values for each sensor, and for every repeat of the bead drop, for Plate 1.

After bead drop testing had been conducted using both target plates, testing was also conducted using the rear plates that had sensors attached. Each rear plate is identified by the type of projectile that it was used to receive. In total, there were three such plates, which were used as a rear plate for the following shots, respectively: A 1.0000mm ± 0.00005mm tungsten carbide (WC) ball bearing, a 1.0000mm ± 0.00005mm stainless steel (SS) projectile, and a 1.0000mm ± 0.00005mm titanium (Ti) ptojectile.
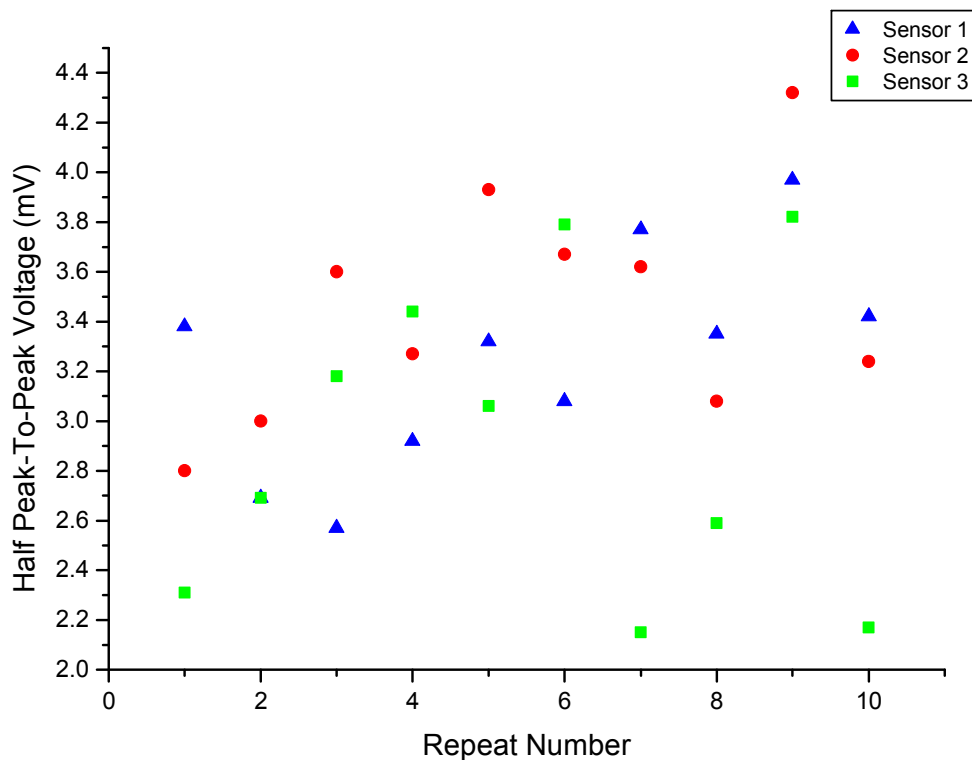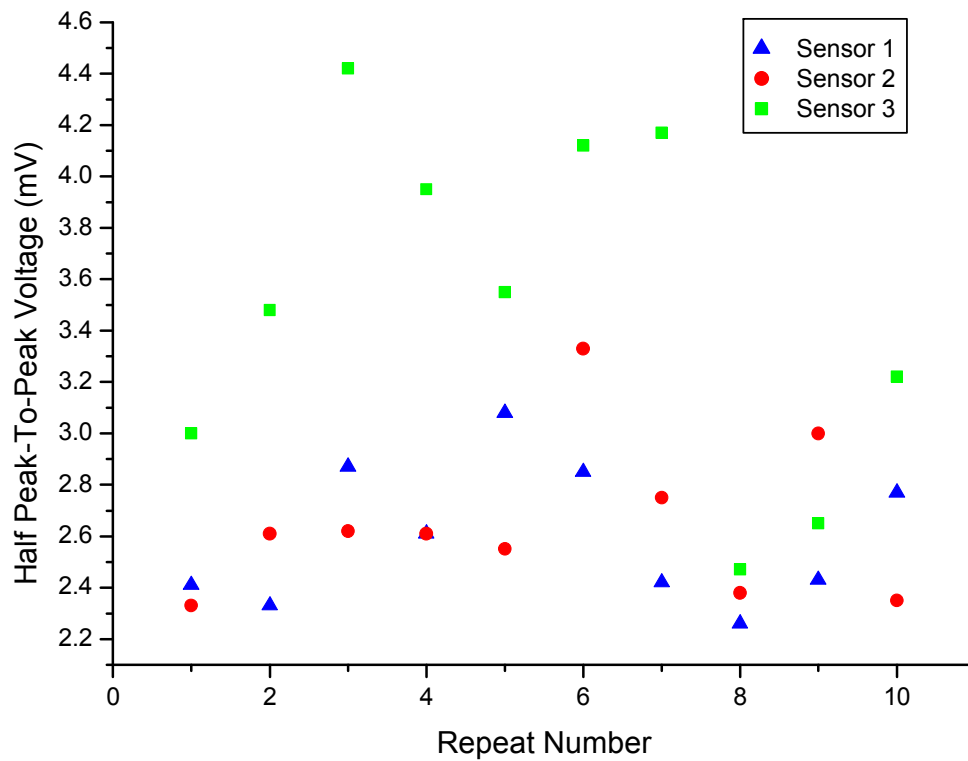
Figure 3.3: This graph shows the half peak-to-peak voltage values for each sensor, and for every repeat of the bead drop, for Plate 2.

It was found later that the half peak-to-peak signal voltages recorded for these plates, during light gas gun shots, were significantly larger in magnitude than those recorded for the target plates, for all impacts. It was for this reason that it was decided that the rear plate sensors would be calibrated separately, despite using the same method, to those of the target plates. All rear plate sensors underwent bead drop testing, and the rear plate sensor with the highest efficiency was identified, ready for calibration. The consequence of this is that the recorded voltages taken from rear plates would be proportional to those of other rear plates, but not to those of target plates. In this sense, they will be regarded as two discreetly calibrated systems, which have not yet been calibrated with each other i.e., the plate sizes are different, so it cannot be certain that the sensor measurements would be the same.

Table 3.5 shows the results of bead-drop-testing upon all of the rear plates used that were equipped with a PVDF sensor. It was found that the plate that was to be

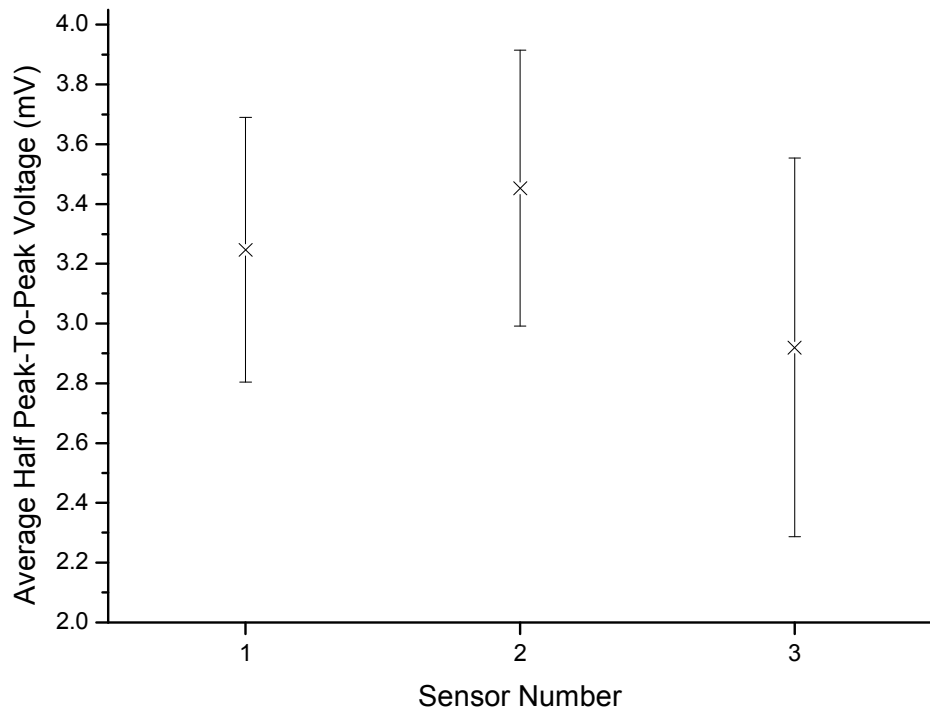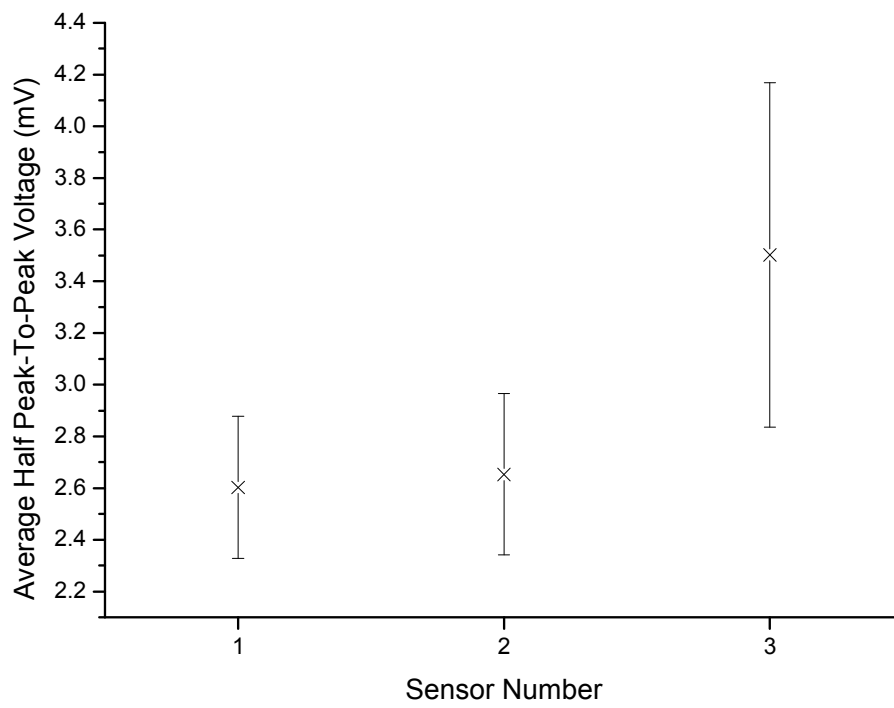Figure 3.4: The average half peak-to-peak voltage for the sensors of Plate 1.



Figure 3.5: The average half peak-to-peak voltages for the three sensors of Plate2.

Table 3.5: The half peak-to-peak values recorded for the bead drop testing of rear plates. (drop parameters were made identical to those of the bead drop testing of target plates.

| Repeat Number | Plate WC (mV) | Plate SS (mV) | Plate Ti (mV) |
|---|---|---|---|
| 1 | 2.03 | 2.15 | 2.05 |
| 2 | 1.92 | 3.02 | 2.09 |
| 3 | 1.43 | 1.92 | 1.64 |
| 4 | 1.13 | 2.61 | 1.64 |
| 5 | 2.63 | 2.90 | 1.66 |
| 6 | 1.48 | 2.21 | 1.52 |
| 7 | 2.21 | 2.84 | 1.54 |
| 8 | 1.78 | 2.41 | 1.66 |
| 9 | 1.64 | 2.41 | 1.44 |
| 10 | 1.90 | 2.43 | 1.96 |
| Average | 1.815 | 2.49 | 1.72 |
| Standard Deviation | 0.427688 | 0.352956 | 0.229541 |
| Coefficient | $1.372 \pm 0.4$ | 1 | $1.448 \pm 0.3$ |

used as a rear shield during a stainless steel light gas gun shot, was the plate equipped with the most efficient sensor. It was observed that the sensor equipped to Plate SS was 1.372 times more efficient than the sensor equipped to Plate WC, and 1.448 times more efficient than the sensor attached to Plate Ti. This equates to the sensor equipped to Plate SS being 37.2% more efficient than Plate WC, and 44.8% more efficient than Plate Ti. It can be seen from figure 3.7 that Plate SS was observed to be equipped with the most efficient sensor, and was thus assigned a voltage coefficient of 1. This allowed for the calculation of coefficients for the other two rear plates that were used, so that their observed half peak-to-peak voltages could be adjusted to find proportional values.

This section has provided details of the bead drop analyses that were performed upon all of the PVDF sensors used within this project. The data acquired during this testing, and the data subsequently presented within this section, shall be used in later sections for the correction of data acquired during light gas gun experiments.
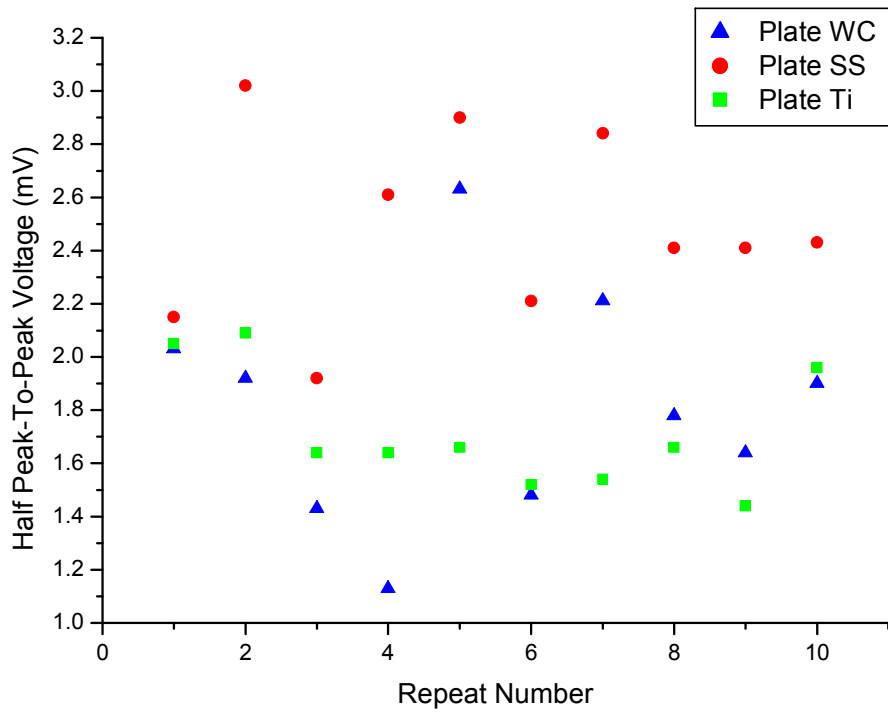
Figure 3.6: The half peak-to-peak voltage values for each sensor, and for every repeat of the bead drop, for all rear plates equipped with a sensor.
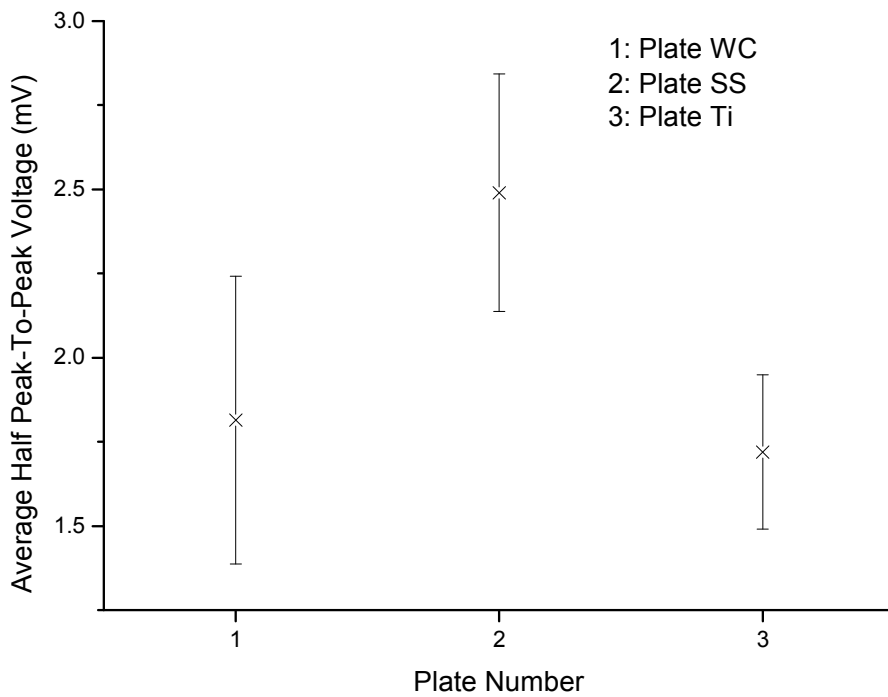


Figure 3.7: The average half peak-to-peak voltages for the three sensors equipped to rear plates.

## 3.3 The Effects of Variation in Projectile Composition

This section will provide an in-depth analysis of the results taken from a shot programme designed to investigate the variations in PVDF sensor output due to changes in projectile density. During this shot programme, a regime of approximately constant speed was maintained for all projectiles that were shot, as was a constant projectile diameter. However, the material composition of the projectile was varied. The aim of this was to increase the mass of the projectile, while maintaining a 1.0000mm ± 0.00005mm projectile diameter. This would enable an observation of the differences in PVDF sensor induced voltage output, relative to a change in projectile momentum. Projectiles were made to hit the centre of the plate. Where the centre of the plate was already penetrated, the plate was moved slightly (~1-2cm) so that the previous impact location was not disrupted.

Table 3.6: Shots from the project that included within the programme which had the objective of investigating effects of variation in projectile composition.

| Shot Number | Date | Projectile | Speed (kms$^{-1}$) | Impact Type | Plate Number |
|---|---|---|---|---|---|
| 1 | 17/12/09 | 1mm SS BB | 5.18 | Hole | 1 |
| 2 | 04/02/10 | 1mm Ti BB | 5.04 | Hole | 1 |
| 5 | 09/02/10 | 1mm WC BB | 5.04 | Hole | 1 |
| 6 | 16/02/10 | 1mm Glass BB | 5.03 | Hole | 1 |

An attempt was made to maintain a regime of constant speed for all of the projectiles used within this programme. The chosen speed was 5 km s$^{-1}$, as this is within the middle of the range of speeds afforded by the light gas gun that was used. This velocity also offered a projectile momentum that would yield reliability in terms of shot success rate. The impact data were analysed in terms of their relative kinetic energy (during flight), and it was intended for projectiles to only have a variation in kinetic energy due to their differences in mass, due to differences in material density. If there were significant differences in projectile speed, then significant differences in projectile kinetic energy (during flight) would not only be attributable to differences in projectile mass (and thus material density). Therefore, if a constant speed is not maintained, then the resultant effects of a change in projectile density

cannot be reliably observed. The variation in projectile speed that was achieved was very good, as evidenced by the results in table 1. The average projectile velocity was 5.07 km s$^{-1}$, with a standard deviation of 0.072 km s$^{-1}$. This equates to the standard deviation in the projectile speed to being 1.42% of the average projectile speed. It was decided that this was an acceptable level of variance.

The kinetic energy shown in table 3.7 was calculated using the values of the recorded speed, and the measured mass of the projectile. As evidenced by table 3.7, the shot with the highest kinetic energy, in this case, has actually resulted in a signal being recorded from Sensor 1 with the lowest half peak-to-peak voltage, relative to all of the signals recorded from the other shots.

The data provided by table 3.7 indicates that, once again, the shot that, theoretically, yielded the highest projectile kinetic energy, actually resulted in a recorded of, relatively, the lowest half peak-to-peak voltage.

Table 3.7 shows, once again, that the projectile that, theoretically, had the largest kinetic energy, yielded what was observed to be, relatively, the lowest recorded half peak-to-peak voltage, induced by the sensor in question.

The values of the recorded half peak-to-peak voltage, shown in tables 2, 3, and 4, are all adjusted values. By this, it is meant that the raw recorded magnitudes have been multiplied by the voltage coefficients found for the sensors in question, and the resultant value has been shown within the tables. This value is a 'true' voltage, which is a name given to distinguish those values from the 'raw' values.

The data shown on the two graphs, figure 3.8, and figure 3.9, are evidence that projectiles possessing varying kinetic energies may yield different induced voltages from poly(vinylidene fluoride) sensors, when they are made to impact a thin aluminium plate to which those sensors are adhered. This statement is made with the assumption that those projectiles do not vary in size or velocity, but vary only in density.

The error margin for each data point shown within the graph, figure 3.9, is not negligible.

Table 3.7: The half peak-to-peak voltage values retrieved for the recordings of the output of Sensors 1, 2, and 3.

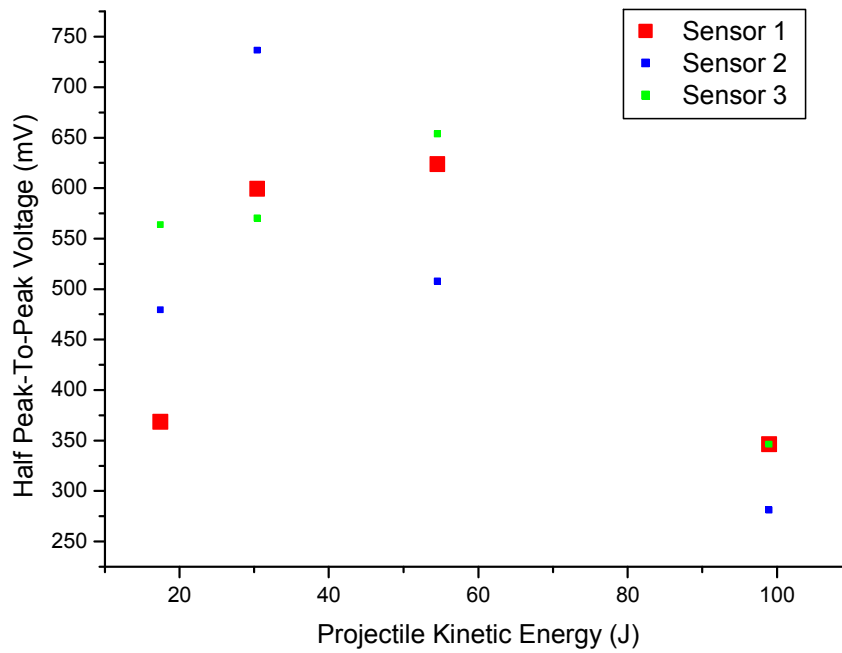| Projectile | Speed | Kinetic Energy | Half Peak-To-Peak Voltage | | |
|---|---|---|---|---|---|
| | (kms⁻¹) | (J) | Sensor 1 (mV) | Sensor 2 (mV) | Sensor 3 (mV) |
| 1mm SS BB | 5.18 | $54.52 \pm 0.74$ | $623.7 \pm 3.5$ | $508.00 \pm 3.5$ | $653.485 \pm 3.5$ |
| 1mm Ti BB | 5.04 | $30.41 \pm 0.43$ | $599.4 \pm 3.5$ | $736.44 \pm 3.5$ | $570.2725 \pm 3.5$ |
| 1mm WC BB | 5.04 | $98.95 \pm 1.39$ | $346.3 \pm 3.5$ | $281.24 \pm 3.5$ | $346.2715 \pm 3.5$ |
| 1mm Glass BB | 5.03 | $17.43 \pm 0.25$ | $368.6 \pm 3.5$ | $479.38 \pm 3.5$ | $563.8042 \pm 3.5$ |

Figure 3.8: The recorded half peak-to-peak voltages for each impact, for each sensor. Note that the data markers for Sensor 1 have been enlarged, to show that one data point overlaps with another. This enlargement allows the position of both points to be identified.
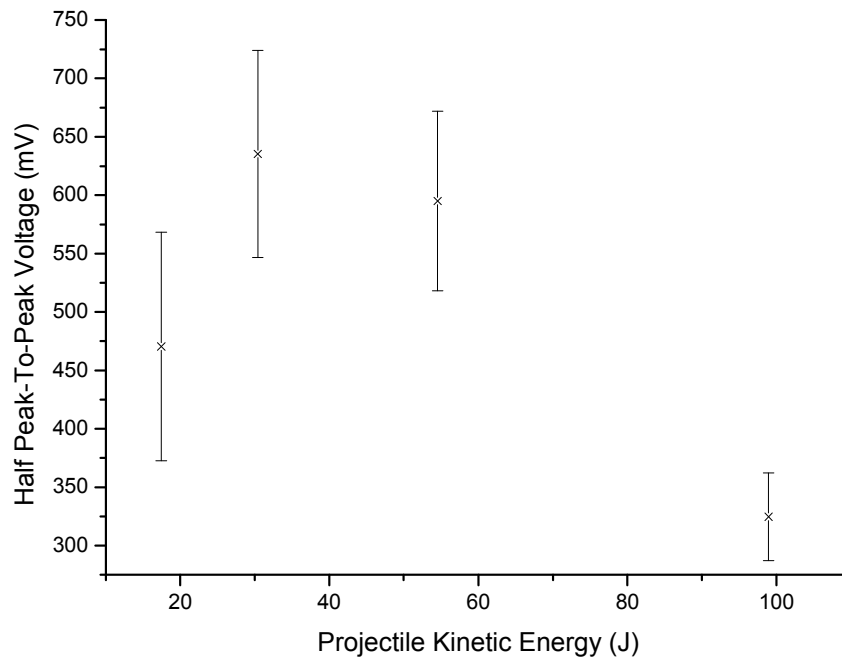


Figure 3.9: The average recorded half peak-to-peak voltage, for each shot, across all three of the sensors that were used.

The graph shows that, despite the error for some data points, the error decreases across the range of points as the kinetic energy of the projectile increases. That is to say: The data point representative of the induced voltage yielded by the projectile with the lowest kinetic energy, had the largest error, and the next point, representative of the induced voltage yielded by the projectile with the next lowest kinetic energy, had the next largest error, and so on. Each data point will be identified by the projectile it represents, and the errors, which are the standard deviation about the mean value of the induced half peak-to-peak voltage, for each shot, are as follows: The Glass shot (shot 6) average had an error of 20.8% of the mean; the Titanium shot (shot 2) average had an error of 14% of the mean; the Stainless Steel shot (shot 1) average had an error of 13% of the mean; the Tungsten Carbide shot (shot 5) average had an error of 12% of the mean. Considering that the method used to execute each of these shots was kept constant, one possible reason for the variation in error across the range of results is that the nature of the strain that is applied to the thin aluminium plate is different for each shot, and this has some effect upon the way that the PVDF sensors would induce a voltage.

The aim of this shot programme was to assess how the induced voltage from PVDF sensors, adhered to a thin aluminium plate, would vary, if at all, according to the stress applied by projectiles of various densities. Considering the results, and that the projectile kinetic energy only varied (excluding some small error) according to the projectile mass, and thus density (as projectiles were all of the same size), it is suitable to state that this objective was achieved. However, the original prediction was that the recorded half peak-to-peak voltage of a shot would increase as the density (and thus kinetic energy) of the projectile was increased. This prediction, during this shot program, has been shown not to be true, as evidenced by the results shown within this section. Despite the relatively large error seen within the results, in particular the first three data points, figure 2 shows that the same half peak-to-peak voltage was not recorded for all shots in this programme. This suggests that the induced voltage caused by a PVDF sensor does indeed vary as the stress applied to a thin aluminium plate, to which the sensor is adhered, is applied by projectiles with varying density. Considering the error, it is possible that the uncertainty in the results is such that the first three data points, in truth, could have yielded the same result. However, the results do not suggest that this is possible for the fourth data point,

representing the Tungsten Carbide shot. This data point clearly holds a lower value than the others, and has a much smaller margin of error. The error within the results shown by the graph, figure 3.9, has been detailed, and its importance has been highlighted. However, to allow for a further discussion of the results, it will be assumed, during the continuation of this speculation, that the results shown in this section are a true reflection of the behaviour of induced voltage by PVDF sensors adhered to a thin aluminium plate, caused by stresses applied by projectiles with varying density.

Making this assumption, it can be seen that the half peak-to-peak voltage induced does not simply increase as the density, and thus kinetic energy, of the projectile increases. In fact, it can been seen to perhaps be constant (within the spread of the data), or initially increase, and then decrease, until reaching its lowest value with the projectile with the highest kinetic energy, the Tungsten Carbide shot. Much like the variation in error shown across these results, one possibility is that the reason for this behaviour is that, despite an increase in the kinetic energy of the projectile, the magnitude of the induced voltage is a feature that is characterized by the nature[†] of the impact-induced oscillation.

Another possibility, following this logic, is that the relatively low average half peak-to-peak voltage produced by the Glass shot is simply due to the fact that this projectile has a relatively low kinetic energy, considering its density, and thus it may only possessed a relatively low amount of energy to impart to the target, when compared to the other projectiles. This may seem contrary to statements in the initial part of the discussion, but it is not.

---

† A note on what is meant by the 'nature' of an oscillation within this discussion: In this project, as described within the methodology section, the oscillation of the plate is measured directly, and recorded as an induced voltage. Due to the strain applied to the PVDF sensors being directly related to the voltage they induce, and the strain being in oscillation, the voltage over the time period of the recording thus also resembles an oscillation, with regard to manner in which its amplitude varies with time. Therefore, it is assumed that the variation of voltage with time is representative of the oscillation of the aluminium plates. Therefore, the nature of the oscillation of the voltage amplitude is assumed to be the same as that of the mechanical oscillation of the plate. The 'nature' of an oscillation, in this case, simply refers to the specific set of characteristics that the oscillation in question possesses, which gives it the form and appearance that it has.

Considering that a mechanical oscillation is a form of displacement of energy, and for this to be established, energy must first be imparted to the oscillating medium before it would begin to oscillate. It is assumed that: The quantity of energy that is imparted, the rate at which this occurs, and the spatial distribution of this energy transfer with regard to the medium, are all factors that would determine the nature of the resultant oscillation across it.

By contrast, the Titanium shot did not, relatively, have a very high kinetic energy (less than one third of that of the Tungsten Carbide shot), and yet it yielded the highest average half peak-to-peak voltage, induced by the sensors. One possibility is that, compared with the other shots, the nature of this oscillation is again, in part, characterized by the amount of kinetic energy imparted by the projectile. In this case, however, rather than some constraint being imposed upon the possible resultant voltage magnitude (due to a maximum possible yield, for any given quantity of kinetic energy – a quantity of energy cannot be transferred from one body to another, if it is a greater quantity than that body possesses), the characterization (relative to the nature of the oscillations caused by the other shots) is due to the amount of kinetic energy absorbed by the aluminium plate, compared to the amount that is transmitted through it, to be carried away (assuming a penetrative impact). This possibility is the same for the Tungsten Carbide shot, and may offer an explanation why this shot, with the largest projectile kinetic energy, would yield the lowest average half peak-to-peak voltage.

It is possible that the projectile penetrates the plate without imparting as much energy as the other shots, characterizing the resultant plate oscillation in such a way as to make its nature one that would yield a relatively low average peak-to-peak voltage. The assumptions made within this speculation have been in reference to penetrative impacts only.

Consider the following mathematical representation of this argument:

$$E = fE_k,$$ (3.1)

Where 'E' is the energy of the plate oscillation, '$E_k$' is the projectile kinetic energy, and 'f' is a decimal fraction, signifying the fraction of the projectile kinetic energy that may be transferred to the plate, during impact.

This subject will be discussed later in subsequent chapters, including the conclusions chapter, where further speculation will be given.

In summary, this section has provided a speculation that there is no direct relationship between a change in projectile kinetic energy (due only to a change in projectile density), and a change in the induced half peak-to-peak voltage. By this, it is meant that instead of a change in density being directly responsible for a change in voltage, it is possible that it could be either unrelated, or related indirectly. An indirect relationship would be one where the magnitude of the induced voltage was directly related to some other variable, which was affected by the magnitude of the projectile's density. If, as speculated, the maximum possible induced voltage that could be yielded from an impact were limited by the amount of energy imparted to the oscillating medium, and thus the amount of energy possessed by the projectile, then there is, at the very least, an indirect relationship between the density of the projectile and the magnitude of the induced voltage, because the projectile's kinetic energy is proportional to its mass.

However, this is not an argument that an increase in projectile kinetic energy would yield a larger maximum possible induced voltage magnitude, but only that the magnitude was limited by it, i.e., assuming that if, after all other variables were considered, a maximum possible inducible voltage were calculated (assuming any quantity of energy were available to be imparted to the plate, during this calculation), then there must be some minimum amount of energy required, to be imparted to the plate, to achieve that induced voltage – for example: If that induced voltage was caused by an oscillation within the medium, that possessed some quantity of energy allowing it to achieve a great enough amplitude to induce the said voltage, then the projectile must impart at least that quantity of energy, which in turn means that the projectile must at least posses that quantity of energy, if not more (the process would not be 100% efficient).

## 3.4 A Discussion of Rear Plate Impact Patterns

Following the discussion given in the previous chapter regarding energy that may be transmitted through a plate, rather than being imparted to it, it was necessary to verify if this were in fact happening. The first place to start with this, logically, was a qualitative assessment of the material that passed through, and from, the plate, to its rear, after the impact. This was done by mounting a plate behind the target plate, and then assessing the impact damage done to this plate, as discussed in the methodology chapter. However, while this was, at first, a plate positioned behind the target plate in an effort to protect the experimental apparatus, it was also later (once the desire for an investigation into the transmitted energy arose) seen as an opportunity to achieve the following: Confirm that material is in fact transmitted through the target plate (and thus conclude that not all of the projectile kinetic energy is transferred to the target plate), the ability to discuss the manner in which the ejecta[†] material was dispersed, and an ability to investigate the relative attenuation of projectile kinetic energy by the target plate for each projectile in comparison with the amount which was transmitted. This section will cover the first two of these aims, by providing an overview of rear plate impacts. The latter of these aims will be covered in a later chapter.

For convenience, the rear plate impact features will be presented in the order of projectile density, beginning with the lowest.

Impact damage is regarded, within this section, as any physical changes that are inflicted upon the rear plate by the light gas gun shot. Most of the rear plates, as stated within the methodology section, were coloured with blue ink. This ink may be abraded from the surface of the rear plate by projectile fragments, and spall from the target plate, as they impact the rear plate. This allows the sites of secondary impacts to be observed, as can be seen in the pictures presented within this section. Comment shall be given towards the distribution of the secondary impacts (those being impacts that occur at the rear plate, as a result of the first, which occurred at the target plate).

---

† The term 'ejecta' in this instance is used to refer to all material, whether originally belonging to the target plate, or the projectile, which is carried from or through the target plate and into the rear area of the plate. Much of this material (although possibly not all) will impact the rear plate.
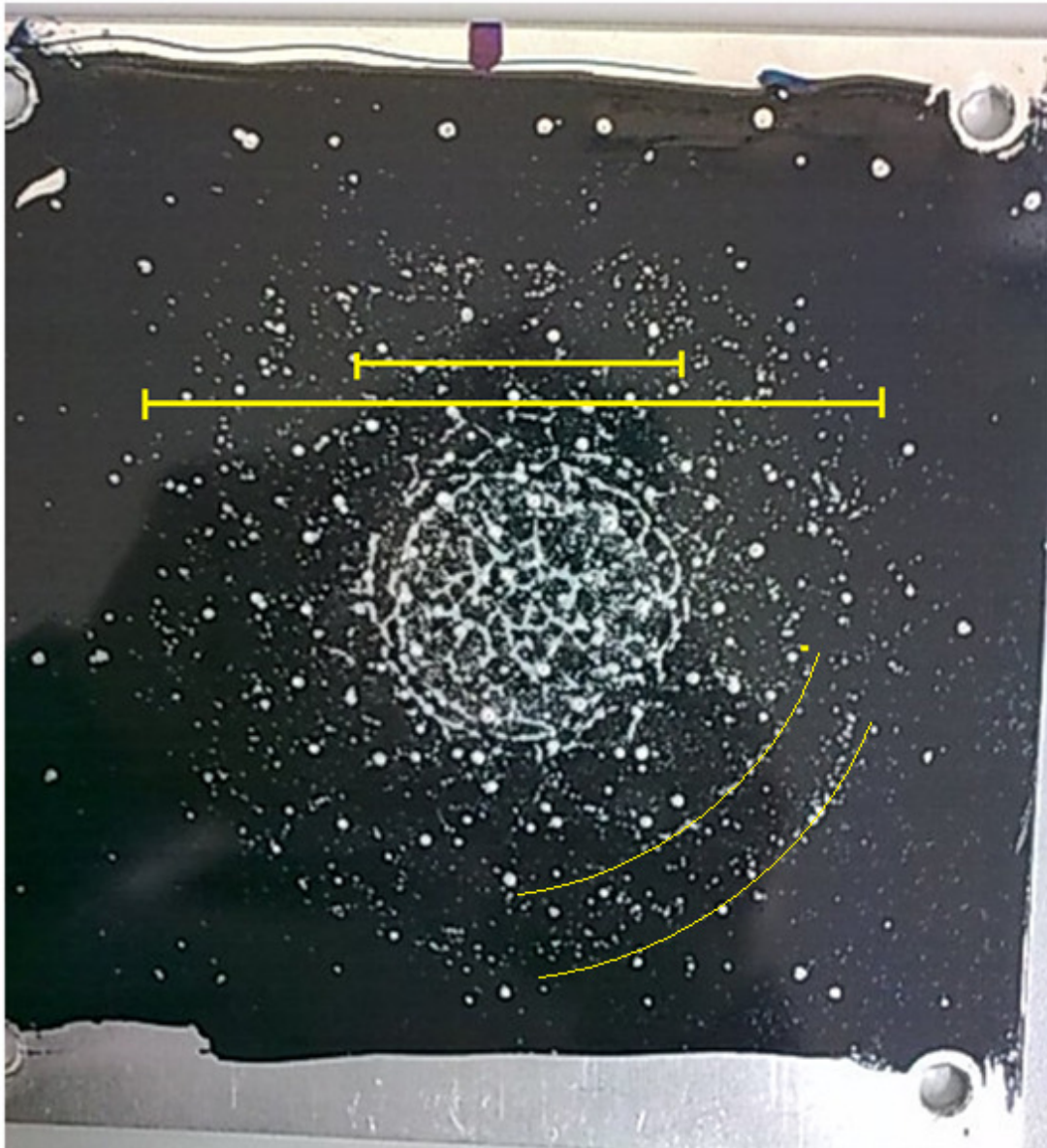
Figure 3.1.0: This image shows the rear plate used to receive a glass shot, during shot 6. The impact damage caused by this shot can be seen; this is caused by both fragments of the projectile and by spall from the target plate. Note an inner region different to the pattern of damage in the outer region.

Figure 3.1.0 shows the impact damage of a rear plate caused by a glass projectile. The spatial distribution of impacts seems to be split into two main groups: An inner circular zone, and an outer ring surrounding the first. Indeed there may be several outer rings. The two different zones are distinguished by their size, and by the character of their constituent impact properties. Those impact features found within the inner zone seem to be, in general, of a larger average size, in appearance, to those of the outer section. The impact features within this zone seem often to be 'linked' or joined, and this gives them the appearance of being not separate, distinct impacts, but

single impacts caused by some debris of irregular shape. It could possibly be described as having the appearance of the 'splash' that one may see from a liquid being projected onto a surface. One possible speculation could be that this may be described as the observation of the debris from the impact of the target plate undergoing 'fluidic' motion, due to the extreme shock that it would receive during impact, before it strikes the rear plate.

There appears to be a sharp definition between the inner and outer region. The second circular region of impact damage, surrounding the first, has the appearance of being roughly twice the diameter, with the first zone being situated at its centre. The impact features within this region appear to, on average, be more 'point like' or circular, and in general much smaller than those in the first zone.

It could be speculated that the damage within the inner zone is comprised mostly of impact features caused by projectile fragments, due to its central location, its smaller size than the second zone, and the dense spatial distribution of the impact features. Following this logic, it could also be speculated that the second zone was comprised mainly of impact features caused by spall from the target plate [34].

The damage from this impact is not limited to these two regions, although the vast majority of the impact features do reside within them, which is why, thus far, they have been all that has been mentioned with regard to the damage on this rear plate. There are some features which reside outside of these regions, as can be seen from figure 3.1.0. These impact features, in general, seem to be relatively large when compared with the majority, and they seem to be sporadically placed.

Figure 3.1.1 shows the impact damage of a rear plate caused by a titanium projectile. In general, the average size of impact features is largest near to the centre of the plate, and gradually decreases as the distance from the centre of the plate increases. There appears to be a 'ring' of particularly large impact craters close to the centre of the plate, which are possibly the result of projectile fragments impacting this plate. The position of impact craters, regardless of their size, seems in general to be quite sporadic. However, it was noticed (as very clearly evidenced by figure 3.1.2) that some rear plate impacts showed patterns within the spatial distribution of their impact features, such as rings or spirals. The rear plate impact shown in figure 3.1.3 could possibly be described as showing such a spiral pattern, beginning with the

roughly circular ring of large craters, at its centre, and comprised of spiral like 'arms' of impacts features, containing craters that decrease in size as their distance from the centre of the plate increases. I suggest that the spiral distribution is caused by the rifling of the launch tube. For a further discussion of this, see chapters 1 and 5.
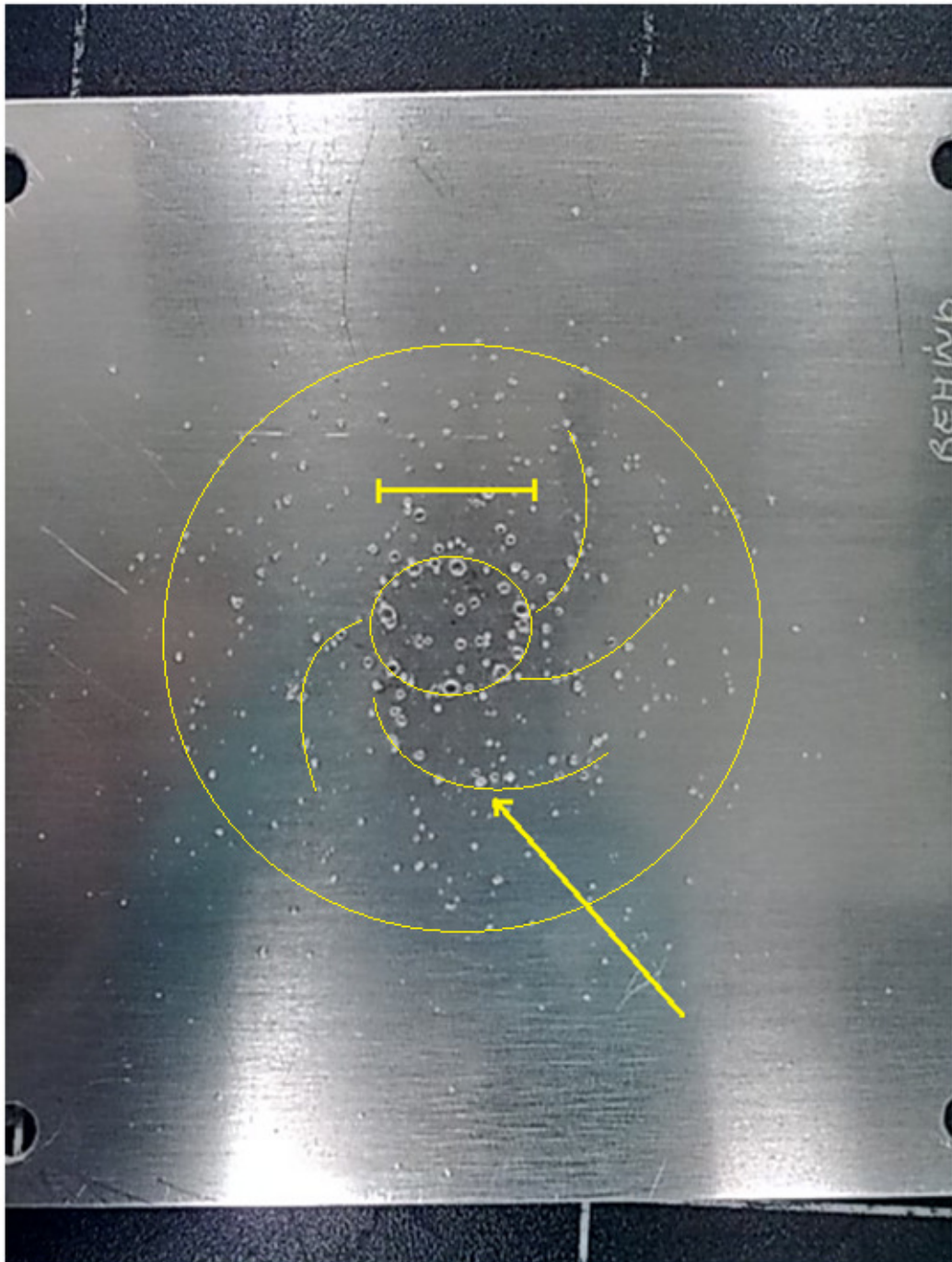


Figure 3.1.1: This image shows the rear plate used to receive a Titanium shot, during shot 2. The impact damage caused by this shot can be seen; it is possible to speculate that this damage is caused by both fragments of the projectile and by spall from the target plate. Note the difference between inner and outer regions.

Figure 3.1.2: This image shows the rear plate used to receive a Stainless Steel shot, during shot 1. The impact damage caused by this shot can be seen; it is possible to speculate that this damage is caused by both fragments of the projectile and by spall from the target plate. Note the sharp difference between inner and outer regions.

This is speculation, as a human observation of what is seen by the eye may be open to subjective interpretation. There may also be two rings.

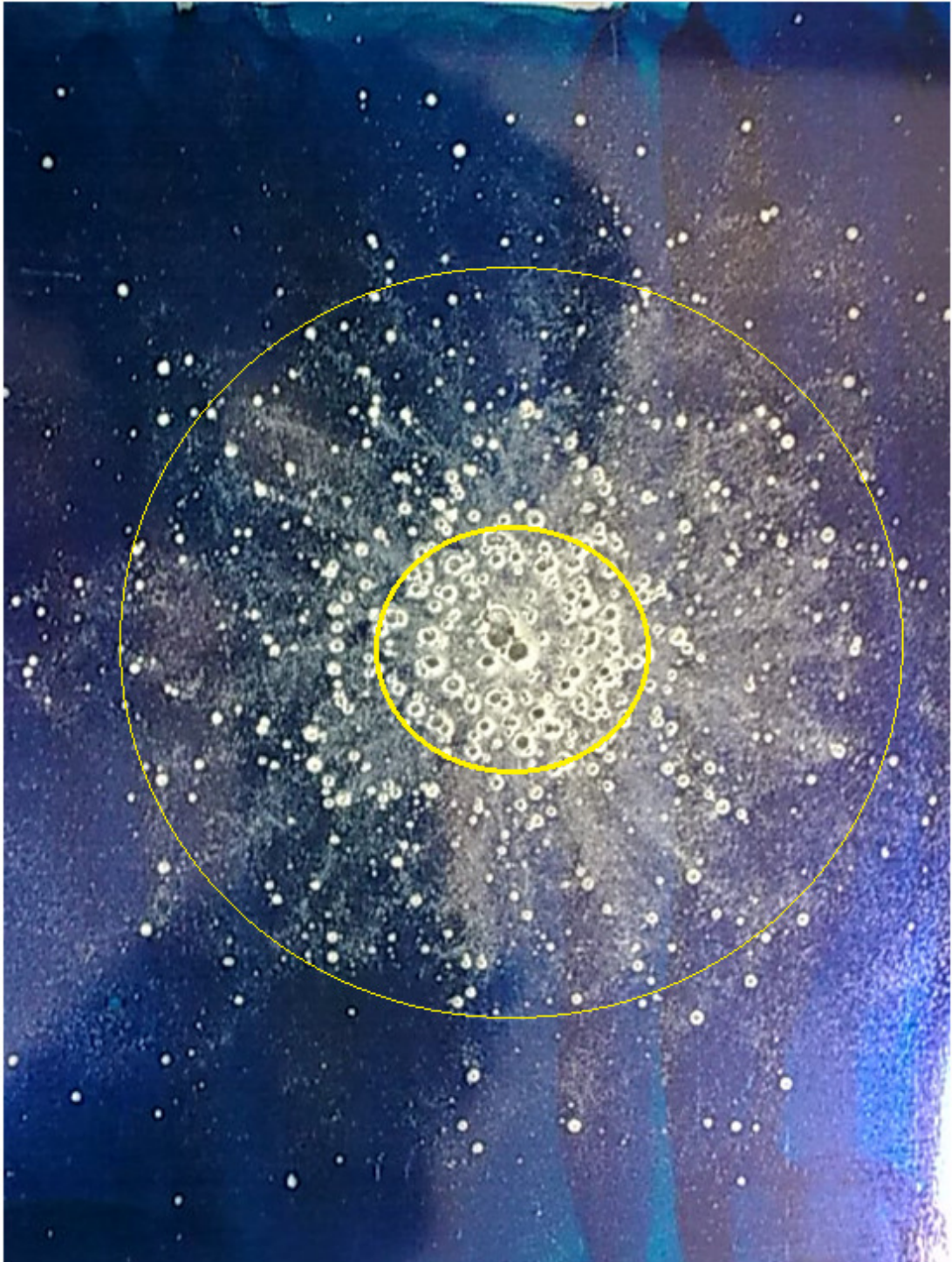Figure 3.1.2 shows the impact damage of a rear plate caused by a stainless steel projectile. In general, the average size of impact features is largest near to the centre of the plate, and gradually decreases as the distance from the centre of the plate increases. Typically, the damage caused to this rear plate seems to be characterized by two different types of impact feature. The first are craters of varying size, caused by either solid fragments of the projectile, or spall fragments from the target plate; the second is an abrasion of the ink from the rear plate surface, in a spray-like manner. This abrasion also seems to have a higher severity at a closer proximity to the centre of the plate. The craters seem to be sporadically placed, other than that they appear to be more densely placed closer to the centre of the plate. It could be speculated that the reason for larger average crater diameter, close to the centre of the plate, is that larger projectile fragments or spall would create a crater of a larger size than debris of a smaller diameter. Those larger debris fragments having more mass would be less affected by any force that would push them away from a flight path towards the centre of the plate – this is something that is particularly relevant to projectile debris fragments, as the original projectile would have been travelling towards the centre before impact, and therefore the only reason for its fragments to deviate from impacting with the rear plate centre, is due to any forces that would cause their flight path to change. This is one possible reason for there being a relatively large pair of craters very near to the centre of the plate, as shown in figure 3.1.2. Another possibility is that the central region of relatively large craters is caused by mainly projectile fragments, and the rest of the impactors are from the plate, and are smaller, and the plate fragments over a wider area as they fly away from the hole.

Figure 3.1.3 shows another rear plate that has been used to stop a stainless steel shot (shot 4). The characteristics of the rear plate damage appear to be the same as those of the previous stainless steel shot, except that the area of the rear plate that was obscured by the sensor shield can clearly be seen to contain no damage. The rectangular area of shield coverage is unmarked, as no debris penetrated the shield. As described within the methodology section, the shielded area was kept constant for each shot that used a rear plate sensor.

Figure 3.1.4 shows the impact damage of a rear plate caused by a tungsten carbide projectile. The damage shown on this plate appears to be characterized by 3 different

regions of damage, some of which overlap. The first is a region covering the centre of the plate, which is a crater-like impact feature. This region is discoloured, and has a white, matte appearance, rather than having the metallic appearance of the aluminium plate; it is possible that this could rule out only a simple abrasion of the surface ink having taken place. This crater-like feature is relatively shallow, compared to its diameter, and its surface is extremely course. This could be caused by very fine fragments which strike the plate, causing one, overlapping, wide, shallow crater.



Figure 3.1.3: This image shows the damage done to a rear plate that has been used to receive a Stainless Steel shot. It has also been shielded with the rear sensor shield apparatus, as described in the methodology section.

This region of the impact damage has possibly been created mostly through the impact of the remains of the projectile, after it collided with the target plate. The relatively large momentum of the projectile (compared to the other projectiles) could account for the relatively large central crater, and the indentation of the plate that is a
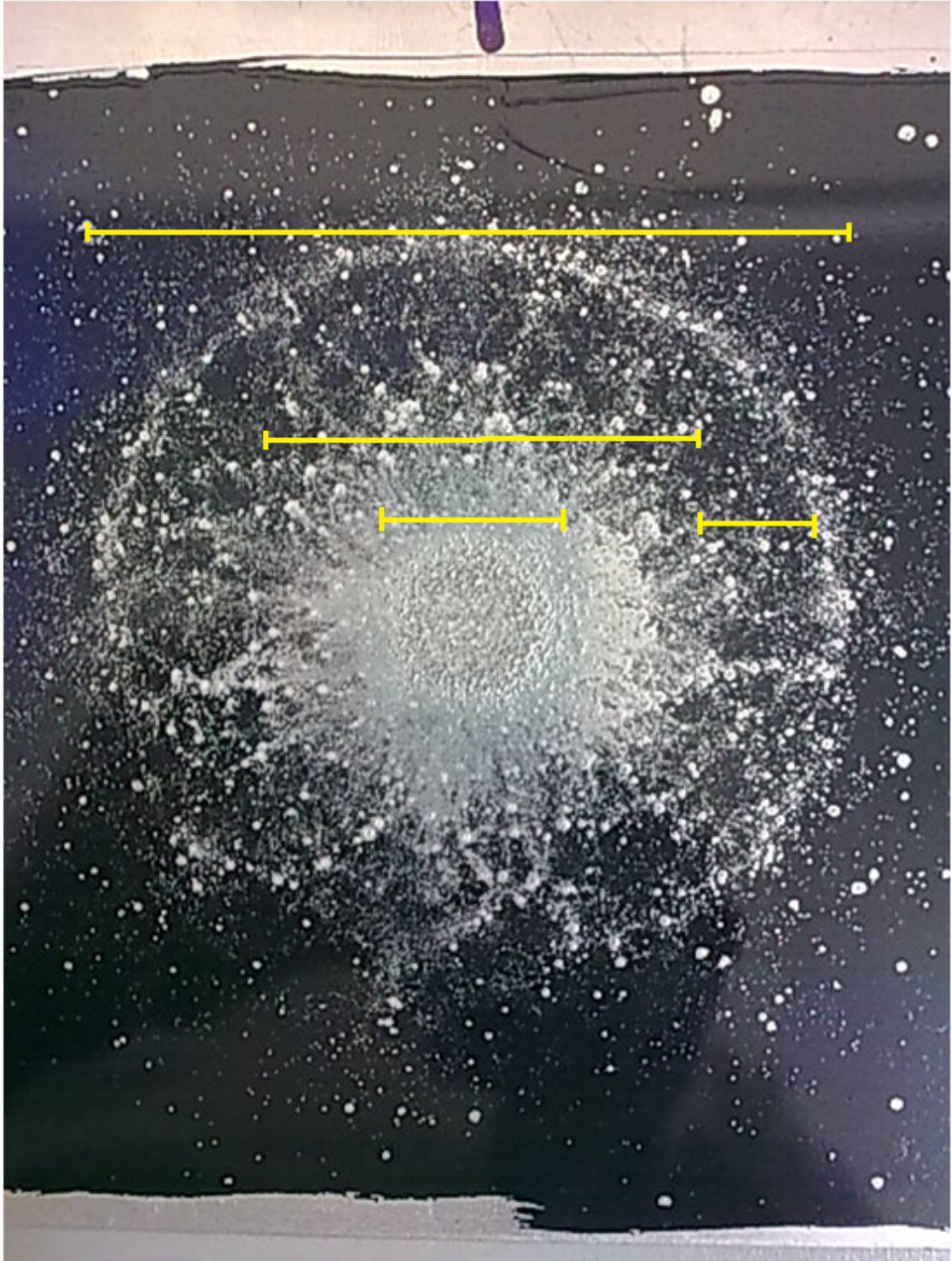


Figure 3.1.4: This image shows the rear plate used to receive a Tungsten Carbide shot, during shot 5. The impact damage caused by this shot can be seen; it is possible to speculate that this damage is caused by both fragments of the projectile and by spall from the target plate.

characteristic of this feature. Impact craters are present upon the surface of the plate, and they are relatively very small in comparison to the central region. These craters, which represent the second type of feature that characterizes the damage done to this plate, are positioned sporadically across the surface of the plate. However, the
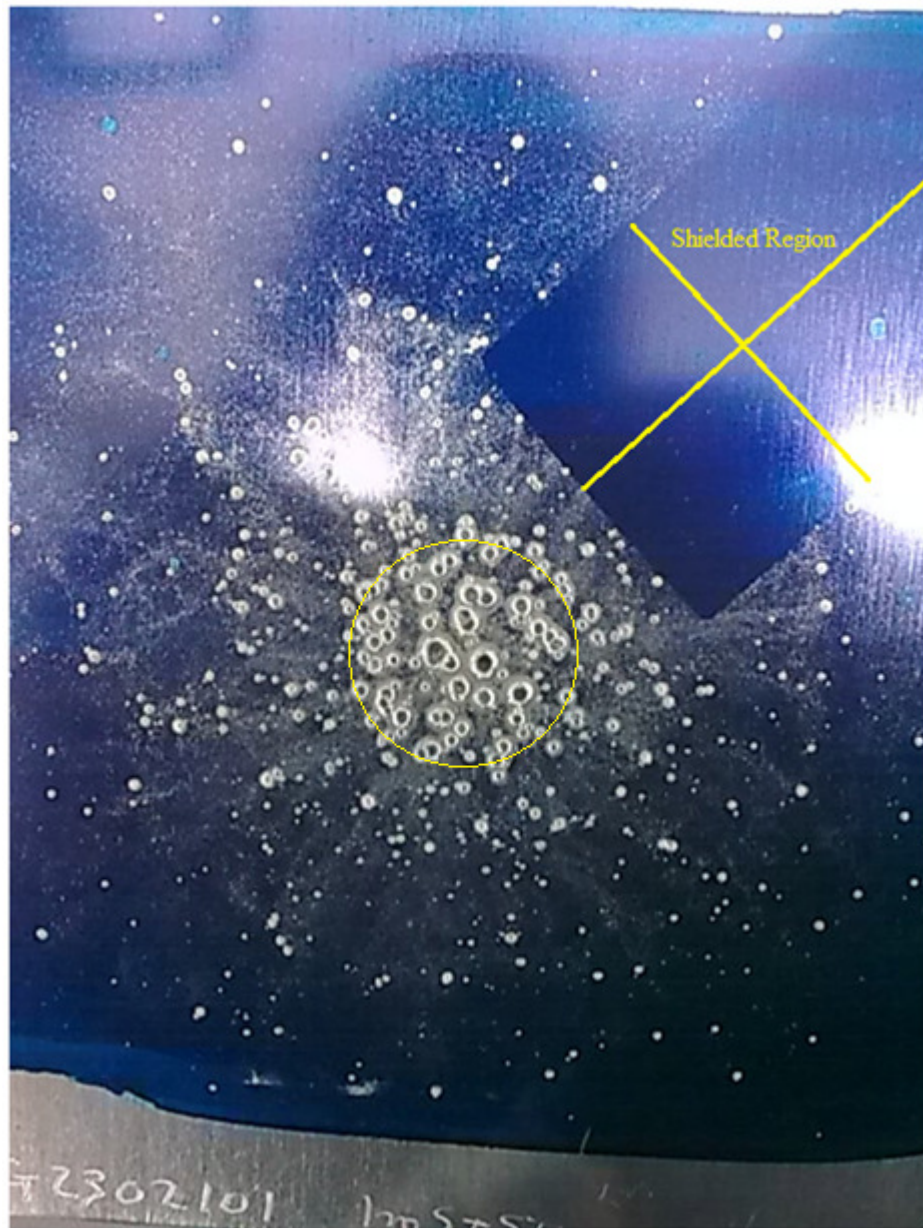


Shielded Region
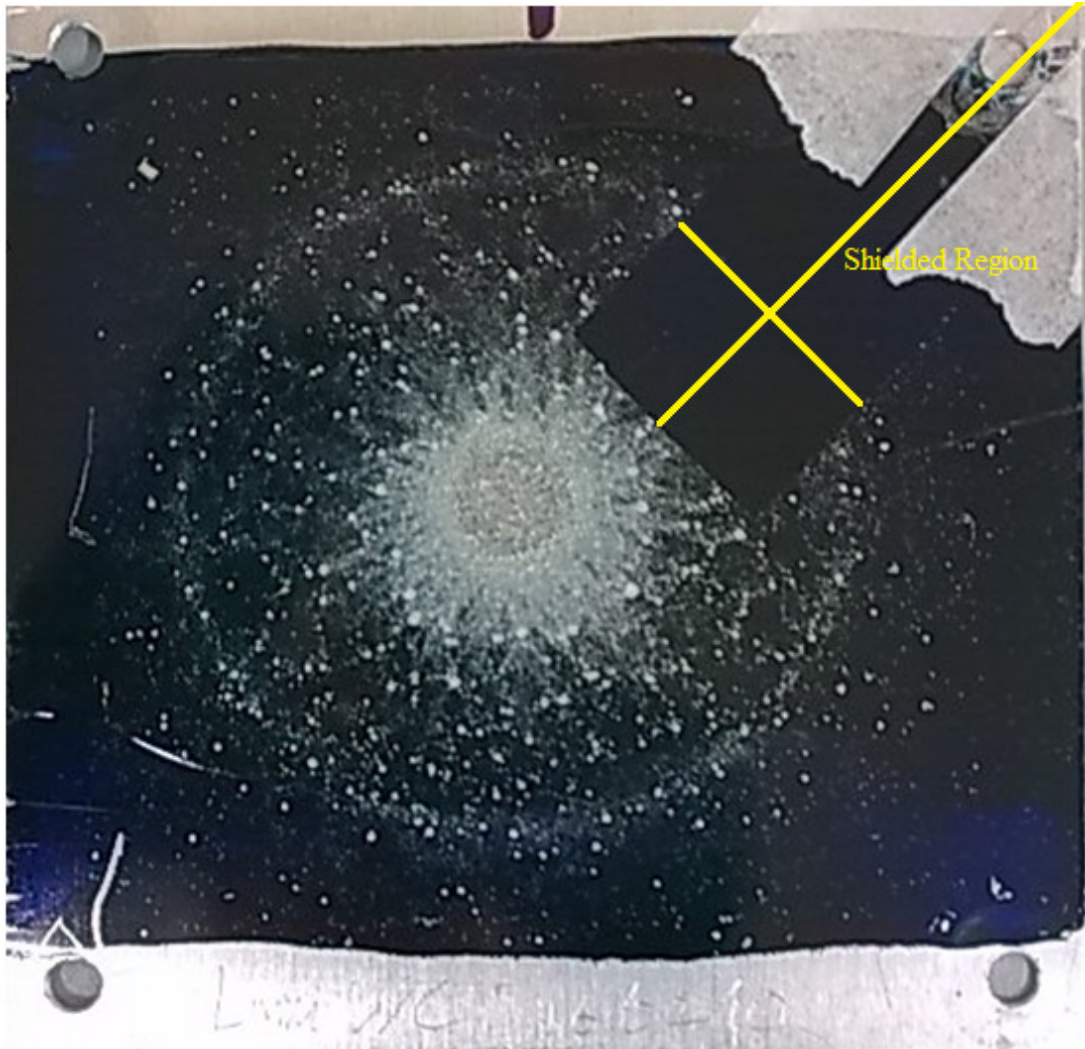
Figure 3.1.5: This image shows the damage done to a rear plate that has been used to receive a Tungsten Carbide shot. It has also been shielded with the rear sensor shield apparatus, as described in the methodology section.

spatial density of occurrence of these craters does not appear to vary much across the surface; there is perhaps a slight decrease in crater density towards the edges of the damaged area. The craters of this type (i.e., normal impact craters, and not the central region) appear to vary in size, and there seems to be, visually, a larger occurrence of relatively larger craters closer to the centre of the plate, than there does nearer to the edges of the damaged area. The third type of impact feature that appears

to characterize the damage caused to this plate is an apparent abrasion of the ink that was applied to its surface. This abrasion appears to have removed the ink from the surface, revealing the shiny metallic appearance of the aluminium from which the plate is made. There appears to be two main regions where this has occurred; the first is in an area immediately surrounding the central crater-like feature described earlier; the second is a circular ring of abrasion, with an interval that seems to be free of this abrasion between the first region, and this circular ring. The ring itself appears to circumvent a circular area with a diameter of approximately three times that of the first, more central, region of abrasion. The severity of abrasion within the first region is greater than that of the second, and reveals clearly the metallic surface of the plate. However, the severity of the abrasion within the ring-region is such that, while the metallic nature of the underlying surface is noticeable, the ink is not completely removed from the region; the ink surface is broken and only sporadically removed from the plate, as though the surface has been sprayed with some abrasive matter.

Figure 3.1.5 shows another rear plate that has been used to receive a tungsten carbide shot, however, this plate has been used in conjunction with the sensor shield apparatus. The coverage area of the shield can clearly been seen, as evidenced by the lack of damage shown within the region. The region contains no impact damage whatsoever, as the shield was not penetrated. This shot shows that the impact pattern shown in fig 3.1.4 was reproducible.

It is possible to determine the chemical composition of secondary impact features by using a scanning electron microscope. It can be seen that, in some cases, secondary impact craters are composed mainly of projectile material. For a discussion of secondary crater composition of witness targets, see [34]. With varying projectile parameters, such as velocity, the 'cone angle' of the resultant debris cloud will also vary. This angle is representative of the amount of spreading that the debris cloud achieves before hitting the next plate, and this describes its final width. The width of the resultant debris cloud is one factor that determines the spatial distribution of secondary impact features upon the next plate. [34]

This section has provided a descriptive overview of the impact damage done to some of the rear plates used within this project. At least one plate used to receive one of each different type of projectile used within the project has been described. The next

section will provide detailed results of the response of sensors that were equipped to rear plates that were used to receive the type of impacts that caused the nature of damage described within this section.

## 3.5 Rear Plate Sensor Results

This section will discuss the results that were observed while using rear plate sensors equipped with PVDF sensors. The purpose of this was to observe the relative magnitude of half peak-to-peak voltage induced on the rear plate sensors when compared to those induced by the sensors equipped to the target plate. This was done with the hope that this method would allow for a discussion of the amount of energy transmitted through the target plate, compared to the amount imparted to it by the projectile.

Table 3.8: The half peak-to-peak voltages observed to have been induced by sensors that were fixed on rear plates.

| Projectile | Speed (kms$^{-1}$) | Kinetic Energy (J) | Half Peak-To-Peak Voltage (mV) |
|---|---|---|---|
| 1mm SS BB | 5.07 | $52.23 \pm 0.73$ | $3415.8 \pm 3.5$ |
| 1mm Ti BB | 4.99 | $29.81 \pm 0.41$ | $1738.3 \pm 3.5$ |
| 1mm WC BB | 4.86 | $92.01 \pm 1.34$ | $5846.0 \pm 3.5$ |

None of the rear plate impacts were penetrative, and this is most likely due to the damage that would have been done to the projectile during its impact with the target plate. It is likely that the shock caused during this initial impact would have caused the projectile to break apart, which is one possible reason why many impact features were observed upon the rear plates. The other contribution to these craters would have been from material removed from the front plate. During the initial impact with the target plate, some of the projectile's kinetic energy would be transferred to that plate, however, this section will show that the majority of the projectile's kinetic energy is actually transmitted through the plate. This energy would be possessed by the fragments of the projectile which pass through the target plate, and debris from the target plate that travels away from the plate. In this experiment, both have been

allowed to impact with a rear plate, and the stress caused by this impact would yield an induced voltage, as described within the methodology section.

From table 3.8, it can be seen that the kinetic energy of the Tungsten Carbide projectile was approximately 3.1 times larger than that of the Titanium projectile, and its impact yielded a half peak-to-peak voltage approximately 3.36 times larger than that of the Titanium impact. The kinetic energy of the Tungsten Carbide projectile was approximately 1.76 times greater than that of the Stainless Steel projectile, and its impact yielded a half peak-to-peak voltage approximately 1.71 times larger than that of the Stainless Steel impact. The kinetic energy of the Stainless Steel projectile was approximately 1.75 times larger than that of the Titanium projectile, and its impact yielded a half peak-to-peak voltage approximately 1.96 times larger than the impact of the Titanium impact.

$$y = -(131.07 \pm 255.65) + (65.46 \pm 3.56) \times X$$
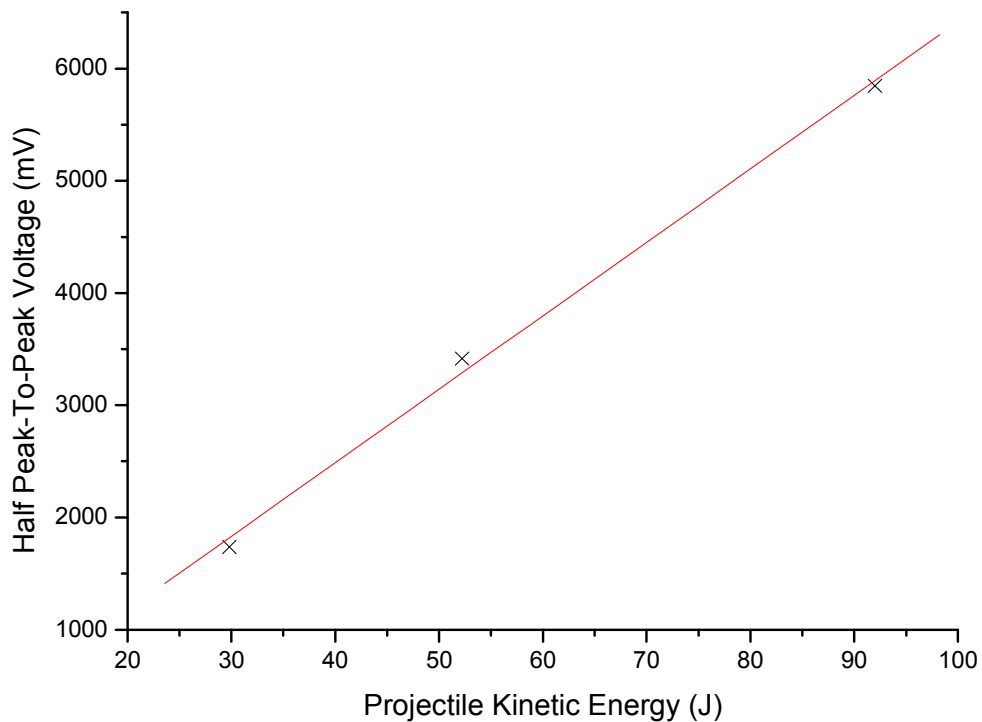
$$R = -0.97$$



Figure 3.1.6: The observed half peak-to-peak voltages induced by sensors equipped to rear plates.

Further, all of the magnitudes of the induced half peak-to-peak voltages are much higher than any of the values observed to have been induced by PVDF sensors that

were equipped to any (front) target plate used within the project. This confirms that within this experiment, it was observed that a significantly larger quantity of kinetic energy, per shot, was transferred to the rear plate, than it was to the target plate. The most likely reason for this is that the rear plate impact was not penetrative, and thus allowed for all of the combined momentum of the projectile fragments, and spall from the target plate, to be transferred to the rear plate upon impact.

Figure 3.1.6 shows that, although the rear plate induced half peak-to-peak voltages were not the same. There was significant variation in voltage as the kinetic energy of the projectile was modified. Unlike the observations taken from target plates, the behaviour of the induces half peak-to-peak voltage followed a well defined trend, and of the three impacts observed, the projectile with the lowest kinetic energy yielded the lowest magnitude of induced half peak-to-peak voltage, and the projectile with the highest kinetic energy yielded the largest magnitude. It should be noted that the type of projectile that yielded the highest voltage magnitude at the target plate, yielded the lowest at the rear plate, and that the type of projectile that yielded the lowest voltage magnitude at the target plate, yielded the highest value at the rear plate; this result supports the speculation given in the previous chapter (that one projectile would impart relatively less kinetic energy to a target plate, during a penetrative impact, compared to another, due to the properties of the projectile material – regardless of the fact that the projectile in question is in possession of a greater amount of kinetic energy) . The observed voltage appears to vary in a linear fashion, suggesting that the induced half peak-to-peak voltage is, in this case, proportional to the kinetic energy of the original projectile. Note that no errors are shown in fig 3.1.6, however, even if the present error was of the same order as those seen on the front plates, this does not explain the apparent trend in the data observed here.

Figure 3.1.7 has been presented with the aim of displaying the difference in trend between the results observed at the target plates, and those observed at the rear plates. It has been observed that, for the types of projectile featured in this section, the induced voltage magnitude decreases as projectile density is increased. Although a linear fit has been applied to the graph, for the data taken from target plate observation, there is insufficient data to support a claim that the relationship, for this case, between induced voltage and projectile density, is indeed a linear one – as data

points seem to deviate from the trend line. More data, for projectiles with density magnitudes somewhere between those of which results have already been observed, would be needed to ascertain an accurate observation of the relationship between those two variables, for this case. In the case of the rear plate impacts, the opposite results has been observed; the magnitude of the induced voltage has been observed to increase as the density of the projectile is increased – and this trend has been observed to fit much more closely to that of a linear relationship, as previously mentioned.

$$y = (-131.07 \pm 255.65) + (65.46 \pm 3.56) \times X$$

$$y = (820.30 \pm 82.35) - (5.20 \pm 1.30) \times X$$
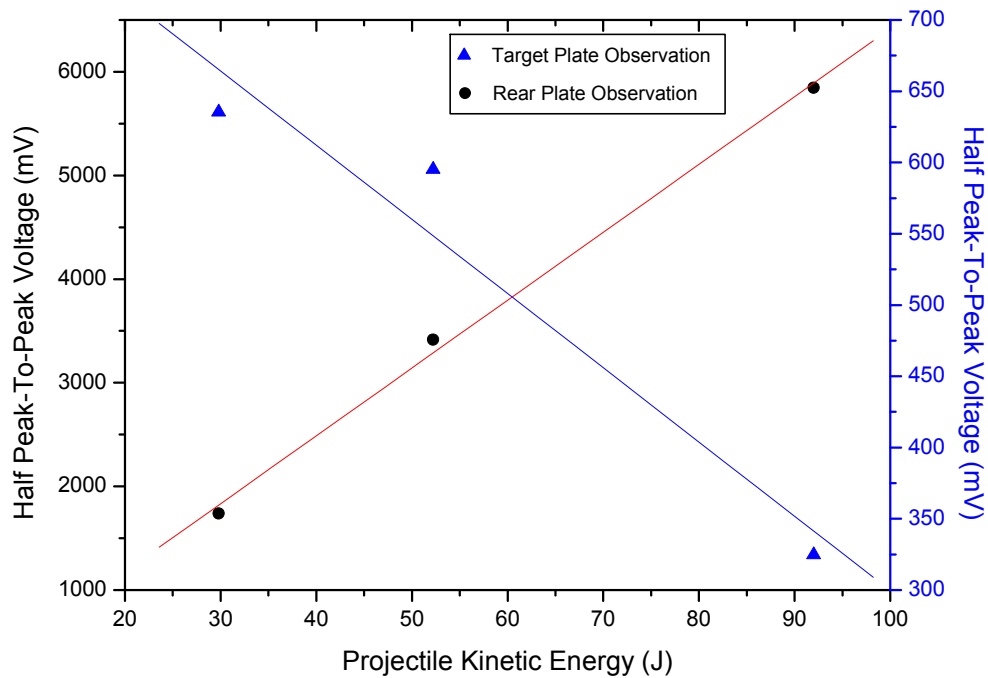


Figure 3.1.7: The observed half peak-to-peak voltages observed for the rear plates (left hand axis), in comparison to the average values of those induced on the target plates (right hand axis), in the same shots.

The purpose of this section was to provide data that would investigate how energy is imparted to a thin aluminium plate, during a penetrative impact, with respect to projectile composition. It has succeeded in showing that a projectile with a relatively high kinetic energy can impart less kinetic energy to a thin aluminium target plate

during a penetrative impact than another similarly sized projectile, with same impact speed, with a lower density, and hence lower energy, and yet allow far more energy to be retained by its daughter fragments and target debris (both are considered, as both may be transmitted through a target plate), than the other projectile in question.

## 3.6 The Effects of Variation in Projectile Speed

This section will provide the results that were observed from impacts upon target plate 2. The purpose of this shot program was to investigate the relationship between projectile kinetic energy and voltage induced by PVDF sensors at the target plate, in some way other than by varying the projectile density as a method of varying their kinetic energy. This was done by instead varying the projectile velocity, and, as such, all projectiles used within this shot program were of the same size, density, and mass. The projectiles used were all 1.0000mm ± 0.00005mm stainless steel ball bearings. This shot programme was conducted so that the observations taken from section 3.3 for comparison, so that they could possibly be verified as being either representative of a change in projectile density, or a change in projectile kinetic energy.

Table 3.9: Shots investigating the effects of variation in projectile speed. SS = Stainless Steel, BB = Ball Bearing.

| Shot Number | Date | Projectile | Speed (Km/s) | Impact Type | Plate Number |
|---|---|---|---|---|---|
| 10 | 12/04/10 | 1mm SS BB | 1.11 | Hole | 2 |
| 13 | 13/04/10 | 1mm SS BB | 3.06 | Hole | 2 |
| 14 | 13/04/10 | 1mm SS BB | 3.91 | Hole | 2 |
| 12 | 12/04/10 | 1mm SS BB | 5.18 | Hole | 2 |
| 11 | 12/04/10 | 1mm SS BB | 7.57 | Hole | 2 |
| 15 | 20/05/10 | 1mm SS BB | 7.65 | Hole | 2 |

As it can be seen from table 3.9, six projectiles were fired at plate 2, for the second shot programme. The projectile velocities were varied over a range between 1.11 km s$^{-1}$ and 7.65 km s$^{-1}$. The shot with the highest speed was repeated, due to an unexpected result on the first shot. However, this result was observed for a second

time, during the repeat, and will be discussed later in this section. None of the shots that were fired during this programme were misfires. All of the shots fired during this programme resulted in penetrative impacts with the target plate. Sensors 1, 2, and 3 were used to monitor the vibration of the plate.

The kinetic energy shown in table 3.1.0 was calculated using the values of the recorded speed, and the measured mass of the projectile.

Table 3.1.0: The half peak-to-peak voltage values retrieved for the recordings of the output of Sensors 1, 2 and 3.

| Shot Number | Speed | Kinetic Energy | Half Peak-To-Peak Voltage | | |
|---|---|---|---|---|---|
| | $(kms^{-1})$ | (J) | Sensor 1 (mV) | Sensor 2 (mV) | Sensor 3 (mV) |
| 10 | 1.11 | $2.50 \pm 0.16$ | $569.26 \pm 3.5$ | $553.33 \pm 3.5$ | $457.57 \pm 3.5$ |
| 13 | 3.06 | $19.01 \pm 0.44$ | $274.00 \pm 3.5$ | $263.14 \pm 3.5$ | $214.70 \pm 3.5$ |
| 14 | 3.91 | $31.04 \pm 0.56$ | $375.88 \pm 3.5$ | $324.92 \pm 3.5$ | $378.06 \pm 3.5$ |
| 12 | 5.18 | $54.52 \pm 0.74$ | $627.70 \pm 3.5$ | $241.92 \pm 3.5$ | $331.64 \pm 3.5$ |
| 11 | 7.57 | $116.33 \pm 1.09$ | $1008.25 \pm 3.5$ | $1058.51 \pm 3.5$ | $826.00 \pm 3.5$ |
| 15 | 7.65 | $118.80 \pm 1.10$ | $782.10 \pm 3.5$ | $629.91 \pm 3.5$ | $387.53 \pm 3.5$ |

Generally speaking, other than for the shot with the lowest speed, the induced voltage magnitudes given by sensor 1, and shown in table 3.1.0, were as expected; the larger the kinetic energy of the projectile, the larger the induced. The shot with the highest kinetic energy (shot 15) did not yield the largest induced voltage magnitude, but it did yield the second largest.

By contrast, the results shown for sensor 2 in table 3.1.0 do not agree with the initial prediction of what the results would be. The induced voltage does not appear to simply increase as the kinetic energy of the projectile is increased.

Similarly, the results from sensor 3 did not meet expectations.

The values of the recorded half peak-to-peak voltage, shown in table 3.1.0, are all adjusted values. By this, it is meant that the raw recorded magnitudes have been multiplied by the voltage coefficients found for the sensors in question, and the resultant value has been shown within the tables. This value is a 'true' voltage, which is a name given to distinguish those values from the 'raw' values.

The results shown in figures 3.1.8, and 3.1.9, suggest in general that half peak-to-peak voltages induced by PVDF sensors adhered to a thin aluminium target plate, will vary with the projectile kinetic energy of the projectile used to impact the plate, and which caused the stress to which the sensors respond piezoelectrically. However, the results provided within this programme remain somewhat unclear, mainly because some data points representative of average values have significant error, and the lowest speed (hence lowest energy impact) does not follow the general trend. Henceforth, within this section, shots will be identified by their shot number. Shot number 10 yielded an average half peak-to-peak voltage magnitude greater than those of shots 11, 12, and 13, despite those shots featuring projectiles with a greater kinetic energy than the projectile used in shot 10. The reason for this is not known. This average value possesses a relatively small error when compared with some of the other average results from this programme. In general, the error with the average results can be seen as such: The first three shots, shots 10, 11, and 12, all possess a relatively small error, whereas the latter three shots, shots 13, 14, and 15, all possess relatively large errors.
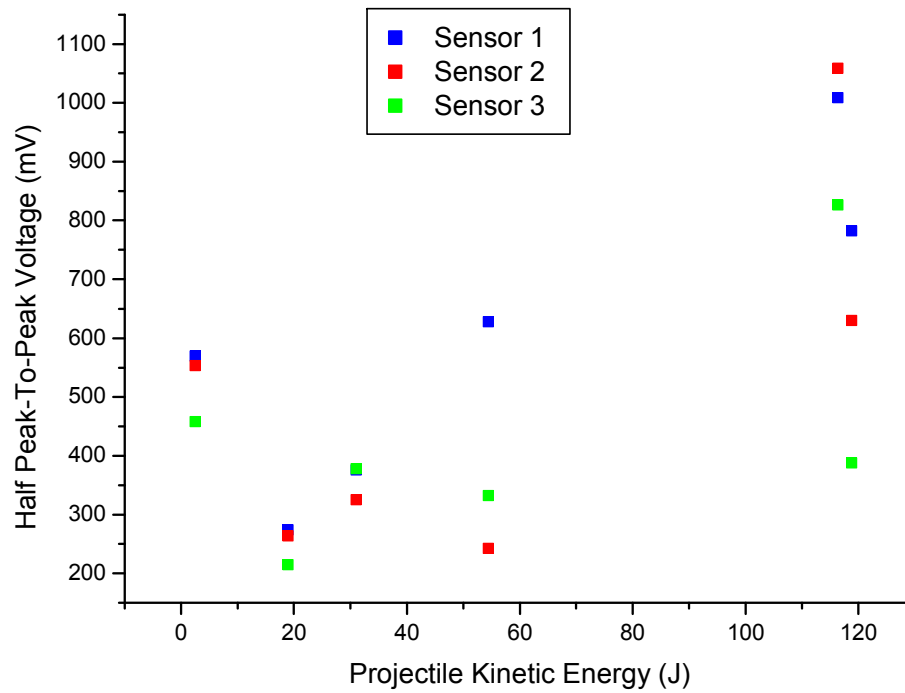
Figure 3.1.8: The recorded half peak-to-peak voltages for each impact, for each sensor.

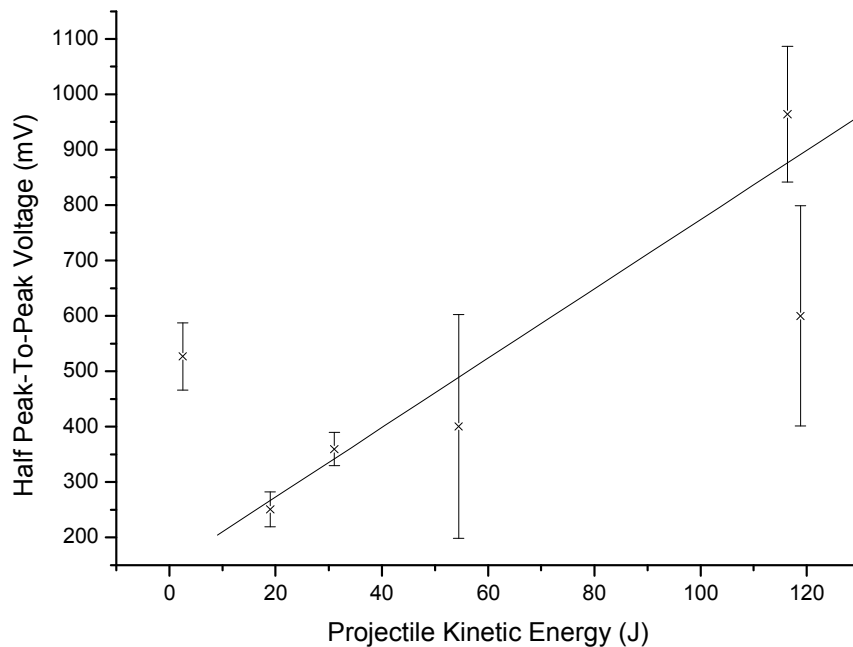$$y = (147.58 \pm 38.58) + (6.26 \pm 1.10) \times X \qquad R = 0.95$$



Figure 3.1.9: The average recorded half peak-to-peak voltage, for each shot, across all three of the sensors that were used. The value for the lowest speed was not included in the linear fit.

The errors were as follows: The average value for shot 10 possessed an error (which was the calculated standard deviation) of 11.5% of the mean result, for shot 11 there was an error of 12.7% of the mean, for shot 12 there was an error of 50.4% of the man, for shot 13 there was an error of 12.6% of the mean, for shot 14 there was an error of 8.4% of the mean, and for shot 15 there was an error of 33.2% of the mean.

The reason for the relatively high magnitude of the average value observed for shot 10 could be speculated upon. For example, if an assumption were made that each shot has some 'rate' at which energy were imparted to the target plate, from the projectile, then a guess could be made that shot 10, due to the projectile having a relatively low velocity, was able to transfer relatively more kinetic energy to the plate than some others that were originally in possession of more kinetic energy, because the projectile interacted with the target plate for some longer time period. IE: it is speculated that some kind of 'coupling' effect exists between the projectile, and the target plate, during impact, and that this can be lengthened or magnified if the projectile possesses a low enough velocity. This, simply put, would be some characteristic of how quickly the projectile manages to penetrate the full thickness of the plate, and thus a thicker plate would yield a larger or longer coupling between the target and the projectile. This would be, only in part, supported by the results seen in section 3.5, where rear plates were used that were of a greater thickness than target plates, disallowing a complete penetration, and yielding relatively very large induced voltages.

Another possibility is that the projectile used within shot 10 did not have sufficient velocity to fully penetrate the target plate, and only caused a partial penetration (despite leaving a clean hole through the plate). For this to be confirmed, an inspection of the impact site would have to be conducted, and the size of the hole would have to be measured. If it was found that only a partial penetration had occurred, then it is possible that little energy was able to be transmitted through the target plate (to eventually impact with the rear plate), and that much of the energy originally possessed by the projectile would have been imparted to the target plate.

Other shots within this program yielded average results that varied, in general, as expected. That is to say that from shot 11, to shot 14, the magnitude of the induced half peak-to-peak voltage increased when the kinetic energy of the projectile was

increased. Shot 15 featured a projectile that was in possession of a kinetic energy greater than the rest, and did not yield the highest value. However, the value for the average voltage magnitude for this shot possessed a relatively very large error.
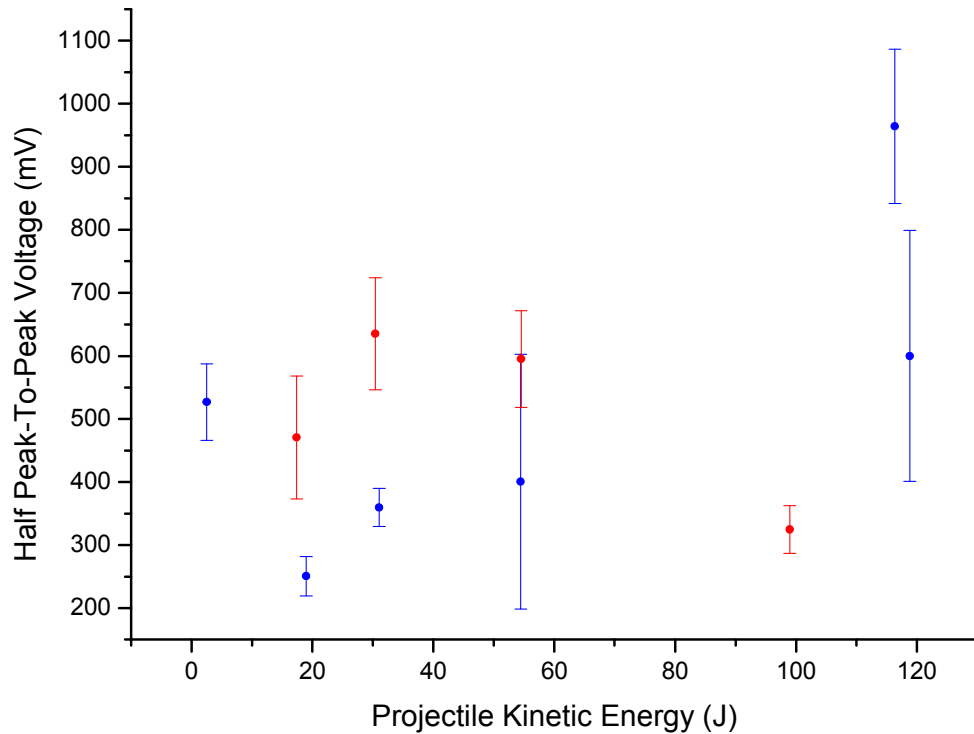


Figure 3.2.0: The average shot results taken from programme 1, compared with those of programme 2. The data from shot programme 1 are shown in red, and the data from shot programme 2 are shown in blue.

A comparison of the results from this programme with those of the previous programme is interesting, see fig 3.2.0. The two shot programmes had several pairs of shots of similar energy, and these shots were: 6 and 13, 2 and 14, and 1 and 12. The calculated kinetic energies of those projectiles were as follows, respectively: 17.4J and 19.0J for shots 6 and 13, 30.4J and 31.0J for shots 2 and 14, and 54.5J and 54.5J for shots 1 and 12. However, despite these projectiles having similar kinetic energies, the impact did not yield induced voltages that were similar. Specifically, shot 6 and 13 did not result in similar induced voltages, despite them having a very similar energy. The exact same thing can be said for shots 2 and 14, also. However, while the observed results did differ, as with the two previous cases, for shots 1 and

12, the error possessed by the average result for shot 12 was very large, and, as shown by figure 3, overlaps significantly with that of shot 1.

To demonstrate the magnitude in difference between the results from programmes 1 and 2, the percentage difference between the two projectile kinetic energies, for each pair of shots listed above, is as follows: The projectile featured in shot 6 had 9% less kinetic energy than the projectile featured in shot 13, and yielded a mean induced voltage 88% higher than that yielded by shot 13. The projectile featured in shot 2 had 2% less kinetic energy than the projectile featured in shot 14, and yielded a mean induced voltage 77% higher than that yielded by shot 14. The projectile featured in shot 1 had 0.01% more kinetic energy than the projectile featured in shot 12, and yielded a mean induced voltage 49% higher than that yielded by shot 12. Shot 6 was a glass sphere with a speed of 5.03 km s$^{-1}$, and shot 13 was a stainless steel ball bearing with a speed of 3.06 km s$^{-1}$. Shot 2 was a titanium ball bearing with a speed of 5.04 km s$^{-1}$, and shot 14 was a stainless steel ball bearing with a speed of 3.91 km s$^{-1}$. Shots 1 and 12 were both stainless steel ball bearings with a speed of 5.18 km s$^{-1}$.

One odd result is, as mentioned within a previous section, the result produced by shot number 5. It has a significantly larger kinetic energy than all shots, other than 11 and 15, and yet has resulted in a magnitude of induced voltage that is smaller than any shot, other than shot 13. This would lend evidence towards the speculation made with regard to the discussion of this shot, made in an earlier section. It is the densest projectile featured in both shot programmes, and has yielded almost the lowest induced voltage. However, it should be noted that the projectile featured in shot 5 had 521% of the kinetic energy of the projectile featured in shot 13, and shot 5 yielded a mean induced voltage that was only 10% greater than that of 13.

### 3.7 A Discussion of the Observed Decay Times within Shot Programmes 1 and 2

Previous chapters have been concerned with the peak voltage amplitudes induced by PVDF sensors, and caused by impacts onto the aluminium target plates. However, this chapter will be concerned with the 'Decay Time' of the signals observed to be induced by the sensors used within this project. The decay time is defined as the amount time that is taken for the original signal amplitude to have become reduced by a factor of $e^{-1}$. A decay time will be given for each shot that took place, and for each sensor used during each of these shots. These results will then be compared.

Table 3.1.1: The decay time values retrieved for the recordings of the output of Sensors 1, 2, and 3.

| Projectile | Speed | Kinetic Energy | | Decay Time | | |
| | (kms⁻¹) | (J) | Sensor 1 (ms) | Sensor 2 (ms) | Sensor 3 (ms) |
|---|---|---|---|---|---|
| 1mm SS BB | 5.18 | $54.52 \pm 0.74$ | 3.53 | 2.63 | 2.45 |
| 1mm Ti BB | 5.04 | $30.41 \pm 0.43$ | 2.6 | 2.35 | 2.23 |
| 1mm WC BB | 5.04 | $98.95 \pm 1.39$ | 3.28 | 4.65 | 4.06 |
| 1mm Glass BB | 5.03 | $17.43 \pm 0.25$ | 2.36 | 2.55 | 2.06 |

The prediction was made that decay times would not vary with some change in projectile, because this property was thought to be a characteristic of the target. However, as evidenced by the results shown in table 3.1.1, this was not observed to be the case. The results for all shots were not the same.

In general, it can be observed that the decay time increased when the density of the projectile was increased. However, at this point it is not possible to say whether this is due to a change in mass of the projectile (as the diameter of the projectile was not varied), or due to a change in kinetic energy of the projectile. There appears to be a single anomalous result that does not fit with the trend shown by the other results, and that is the result for tungsten carbide shot undertaken in programme 1 (shot 5), retrieved from sensor 1.
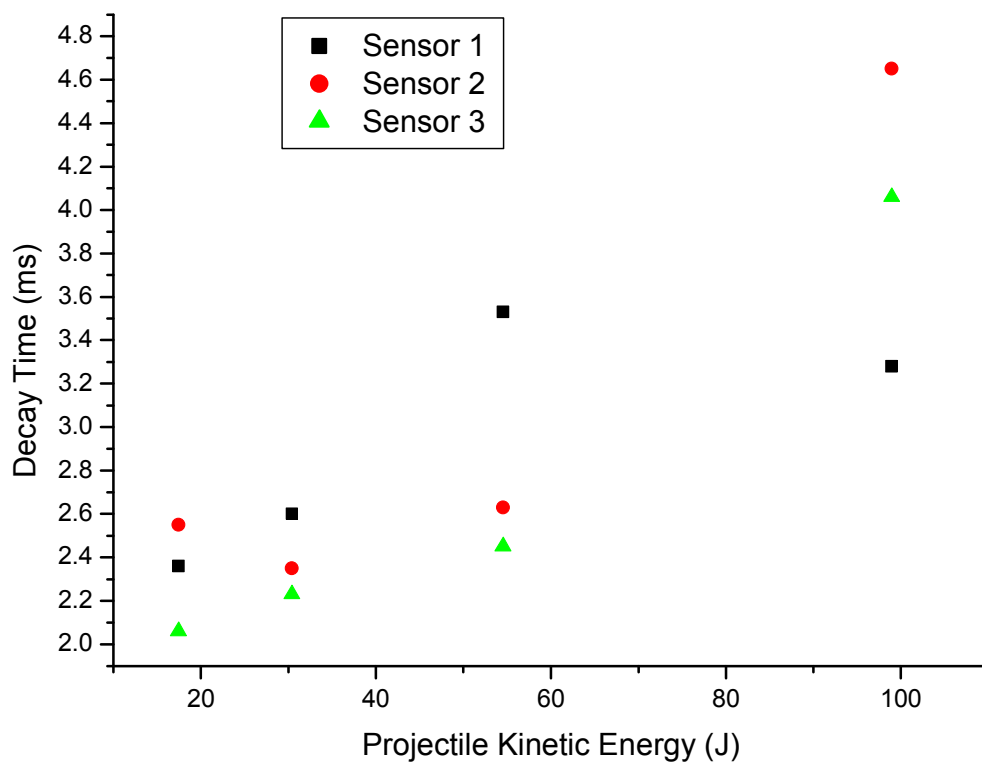


Figure 3.2.1: The decay times for each impact, for each sensor, vs kinetic energy.
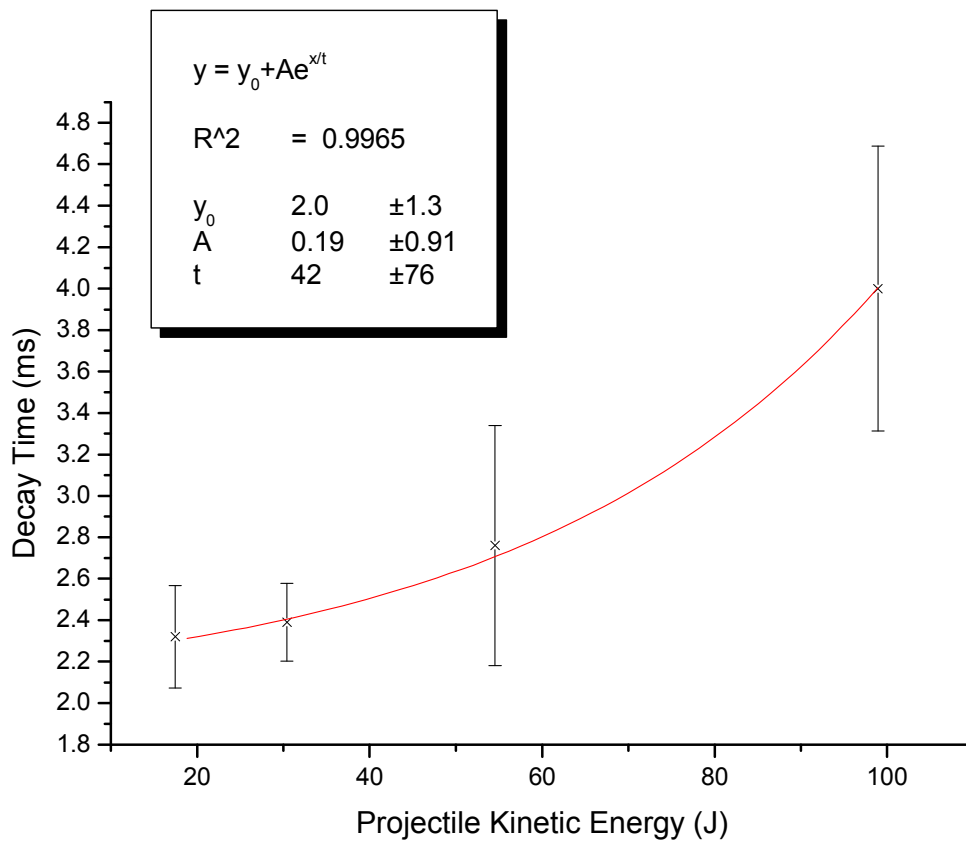
Figure 3.2.2: The average decay time, for each shot, across all three of the sensors that were used, vs kinetic energy.

Figure 3.2.2 shows the average results observed during shot programme 1. A trend line has been added, which follows the following relationship:

$$y = y_0 + Ae^{xt^{-1}}, \tag{3.2}$$

where '$A$' is the initial amplitude, and '$y$' is the decay time. There is, as can be seen in figure 3.2.2, a significant possible error in the results, which is as follows: 9% of the mean for the glass projectile, 8% of the mean for the titanium projectile, 12% of the mean for the stainless steel projectile, and 27% of the mean for the tungsten carbide projectile. The trend shows that the decay time appears to be increasing with an increase in kinetic energy.

The same analysis was performed for the second shot programme.

Table 3.1.2: The decay time values retrieved for the recordings of the output of Sensors 1, 2, and 3, for shot programme 2.

| Shot Number | Speed | Kinetic Energy | Decay Time | | |
| --- | --- | --- | --- | --- | --- |
| | (Km/s) | (J) | Sensor 1 (ms) | Sensor 2 (ms) | Sensor 3 (ms) |
| 10 | 1.11 | $2.50 \pm 0.16$ | 2.44 | 3.21 | 2.5 |
| 13 | 3.06 | $19.01 \pm 0.44$ | 2.05 | 3.52 | 3.25 |
| 14 | 3.91 | $31.04 \pm 0.56$ | 2.17 | 2.87 | 2.8 |
| 12 | 5.18 | $54.52 \pm 0.74$ | 2.11 | 2.57 | 3.61 |
| 11 | 7.57 | $116.33 \pm 1.09$ | 4.52 | 3.34 | 8.08 |
| 15 | 7.65 | $118.80 \pm 1.10$ | 7.01 | -69.52 | 2.5 |

Table 3.1.2 shows that, as the projectile kinetic energy varies, the decay time does not remain constant. While the two shots with the highest kinetic energy did yield the longest decay times, there appears to be no other trend within the results. Shot 15 produced an anomalous result, due to an unpredicted sensor output during the impact of this relatively high velocity projectile. This result was excluded, and regarded as an anomaly.
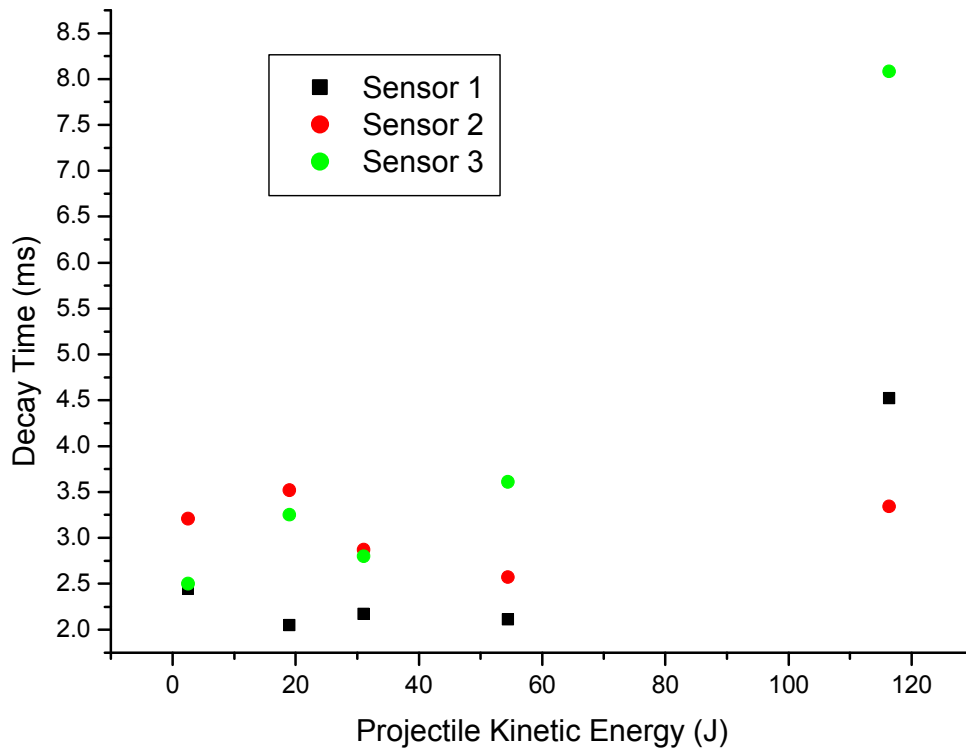


Figure 3.2.3: This graph shows the decay times for each impact, for each sensor, for shot programme 2, vs kinetic energy.

The results shown in figure 3.2.3 shows that for the four shots with the lowest kinetic energies, the decay times only vary by 0.33ms, which is less than the error for any result shown in figure 3.2.4. However, shot 11 was observed to have an average peak amplitude much higher than the other shots, but also possessed a much larger error. The error possessed by this value is large enough that the range of uncertainty to fall within the range over which the values of the other four shots reside. Therefore, it could be speculated that the decay time with respect to the velocity of the projectile may not actually vary (as suspected).

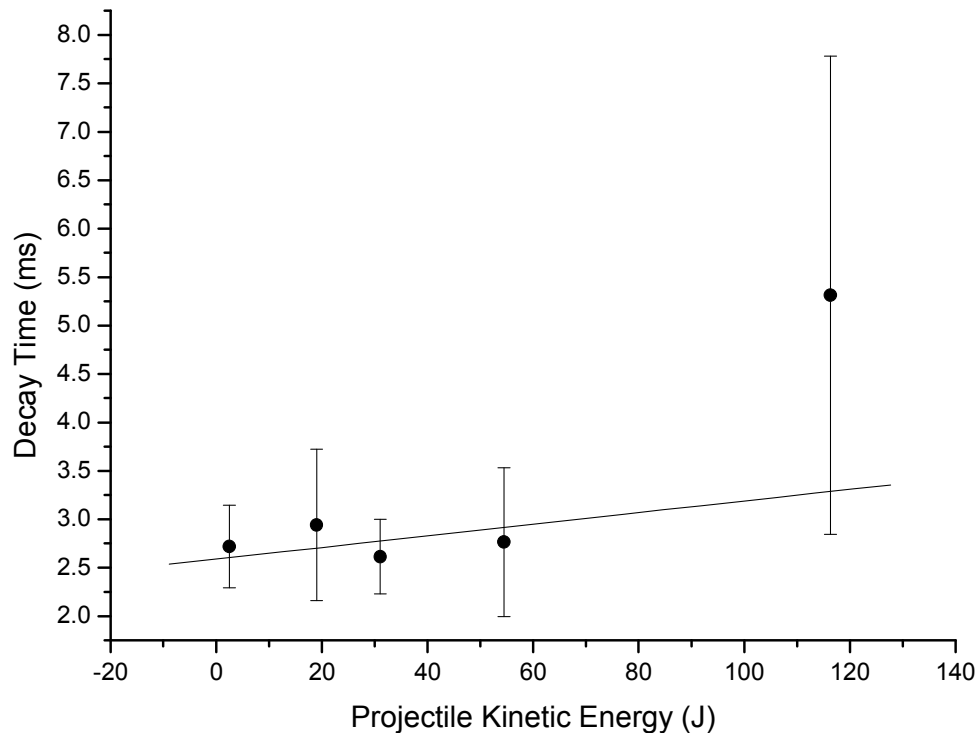$$y = (2.59 \pm 0.4) + (0.006 \pm 0.013) * X \qquad R = 0.41$$



Figure 3.2.4: This graph shows the average decay time, for each shot, across all three of the sensors that were used, for shot programme 2, vs kinetic energy.

However, as shown in figures 3.2.3 and figures 3.2.4, the decay times only appeared not to vary with an increase in kinetic energy until it surpassed 60 J; after this, the decay time did increase. This is supported by the linear fit; the 'R' value was not high, indicating that the fit was not very close, and the gradient was within 10μs of zero. It is possible that below 60 J, any variation of decay time due to changing kinetic energy is less than that variation attributable to method of reproducibility, but that only above 60 J does a significant effect occur. Shots with a kinetic energy of 70 J and 80 J would help to clarify this.

This section has provided the decay times observed to have been characteristic of the target plate oscillations induced during this project. A discussion has been given with regard to those observations and their significance, and the next chapter will provide the conclusions that can be drawn from the findings within this project.

# CHAPTER FOUR:

# F.O.M.I.S

## 4.1 Evaluation of the data produced from using the FOMIS drum as a target

The FOMIS drum was used as a target for a single 0.8 mm stainless steel ball-bearing, which was shot at a velocity of approximately 5 km s$^{-1}$. The drum skin that was used was a 1 mm thick reflective mylar film. Two fibre optic sensors were applied to the drum surface. The fibre optic sensor tips were set at a distance of 2.0 cm $\pm$ 0.05 cm from the edge of the drum surface, and each sensor set at opposite sides of the drum (180º separation). The PVDF sensor was positioned on the very edge of the drum surface, see fig 4.1.

It can be seen from figure 4.2 that, after the time of impact, the signal amplitude rose rapidly, and to such a large magnitude, that saturation was achieved (due to the pre-amplification and digitizer equipment used). In figure 4.3 it can be seen that the rising edge of the first peak of the signal amplitude is not a smooth ascent.
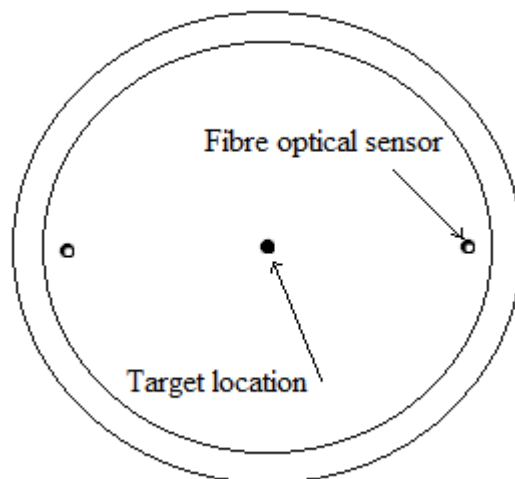
Figure 4.1: The locations of the sensors used by the FOMIS apparatus.



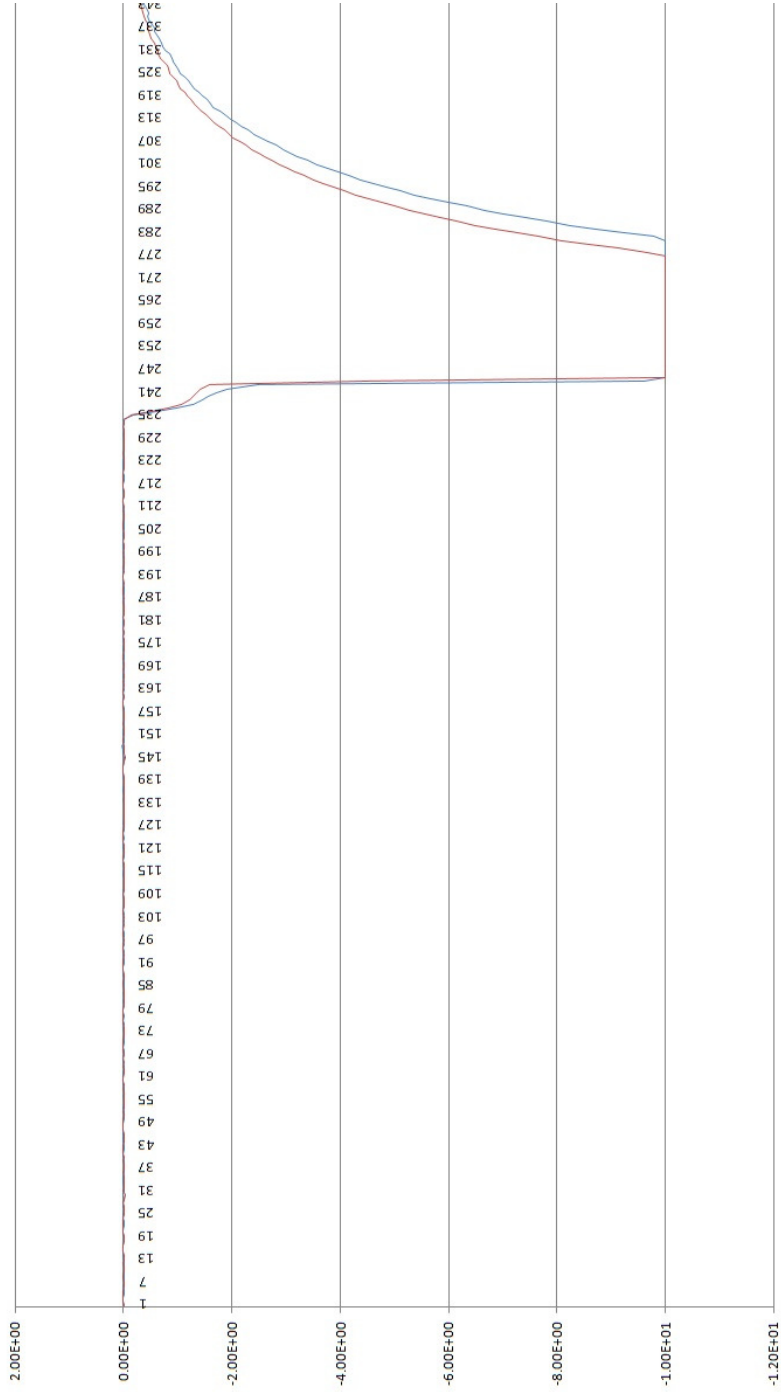Figure 4.2: The FOMIS apparatus mounted within the door of the gun.

Figure 4.2: The initial portion of the signal data, recorded by the pair of fibre optic sensors that were used. This shows the signal data from the time at 0 to 343μs. 0μs is the trigger time.
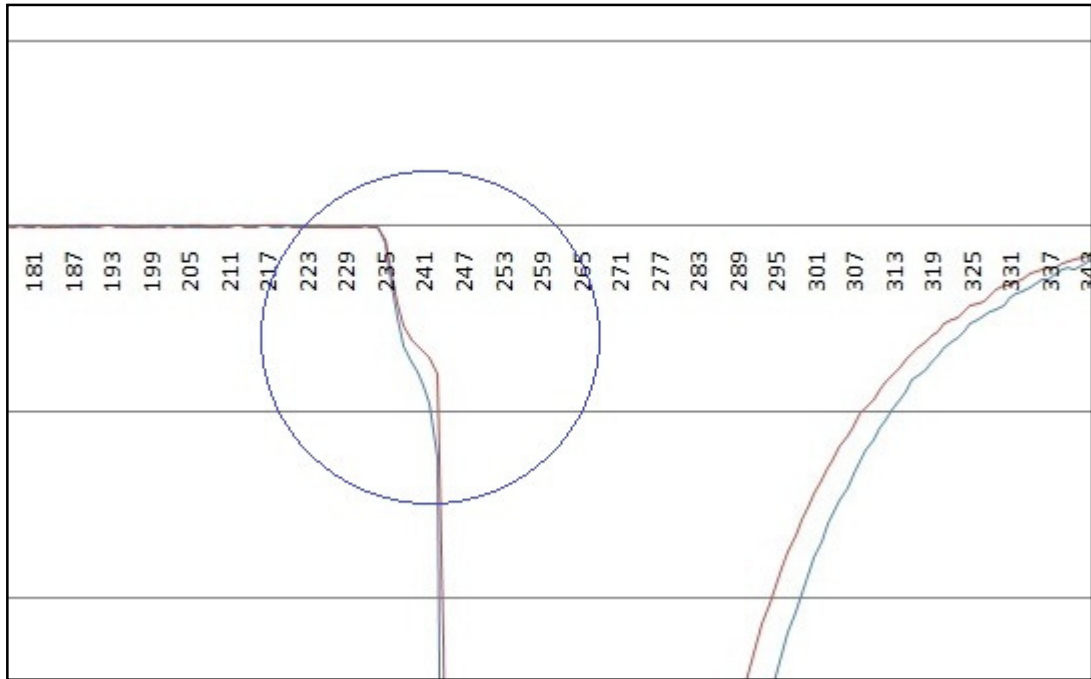
Figure 4.3: A portion of the signal region pictured in figure 4.2. The area of interest in this case is the recorded signal amplitude during the times between 229μs and 247μs. The particular signal feature has been circled in blue.

There is an apparent initial rise, before a shallower region, followed by the signal returning to a steep gradient once more. One possible speculation is that the reason for this is that this first region is actually representative of the impact of gas released by the firing of the light gas gun, which would most likely have been travelling at a greater velocity than the projectile. The signal then has a shallower gradient for a short time (~5 μs) (as can be seen in both data sets, and shown in extended scale in fig 4.3), before returning to a steeper gradient. One possible suggestion could be that the area of shallower gradient is representative of the delay between when the gas jet from the ignition of the light gas gun hits the drum surface, and when the projectile hits the drum surface. Following this, it could also be possible that the sharp rise in signal amplitude gradient, immediately after this point, represents the moment of impact by the projectile.

This data has shown that the FOMIS apparatus has successfully been used to detect the hypervelocity impact of an object. If the same shot procedure were repeated, without the use of a projectile, it could show whether or not the FOMIS apparatus was indeed able to detect the gas jet from the firing of the gun.

# CHAPTER FIVE: CONCLUSIONS

This chapter will provide conclusions that can be drawn from the observations and discussion that has taken place within this project.

The purpose of the experimentation within this project was to investigate the piezoelectric responses of poly(vinylidene fluoride) films, when the strain that they are given is caused by the acoustic vibration of thin aluminium plates, after they have been subjected to hypervelocity impacts. This was to discern whether or not characteristics possessed by an impactor could be distinguished by scrutinizing and analyzing the observed acoustic wave created by the impact.

The initial conclusion of this project is that it is possible to observe that hypervelocity projectiles with different densities will yield acoustic vibrations (of the target) with different peak amplitudes, upon penetrative impact with a thin aluminium plate. However, a simple mathematical relationship between the variation of projectile density, and peak amplitude of the induced oscillation, was not observed, and a wider range of projectile densities would need to be used, in

conjunction with repeat testing, to confirm whether or not a relationship could be established. It was found, for fixed size and spread, that projectiles with a high density, despite possessing a relatively high kinetic energy, will impart less kinetic energy to the target plate. To confirm this, rear plates were fitted with sensor films, to allow for the observation of the peak amplitudes of oscillations induced in these plates by material transmitted through the target plate, caused by non-penetrative impact (material composed of either the remnants of the projectile, or of debris from the target plate). This method proved to be successful, in that an observation was made of a relatively dense projectile yielding a relatively high peak amplitude of oscillation of a rear plate, compared to a relatively low peak amplitude of oscillation of a target (front) plate. It could be that one possible reason for this effect is that the compressive strength of the projectile, in the case of tungsten carbide, would allow it to penetrate the target plate efficiently, and prevent extensive coupling between the projectile and the target plate (and thus prevent transference of a relatively large quantity of the projectile's kinetic energy).

During the experimentation using rear plate sensors, a relationship between the induced peak amplitude and the kinetic energy of the projectile, was observed. This variation of kinetic energy was moderated by an alteration of projectile density (i.e., the projectile velocity and diameter were kept constant). The relationship observed between kinetic energy, and the observed peak amplitude of oscillation, was linear, with a slope of $65 \pm 4$, i.e., there is a strong dependence on the initial impact kinetic energy.

The second result is that the response of sensor films with a variation in projectile speed was observed. However, it was concluded that a wider range of velocities would be required, combined with repeat testing of all velocities used, to be able to establish the details of the relationship between projectile velocity, and peak amplitude of oscillation, existed. This experiment was conducted so that the response of the sensor films could be observed, as the kinetic energy of the projectile was varied using a form of moderation other than projectile density. The reason for this is that, if the result would be observed to be the same as those observed when the projectile kinetic energy was moderated by varying the projectile density, then the results for that experiment could be attributed to the variation in kinetic energy, rather than the change in projectile density. It can be concluded that the results

produced by moderating density, and moderating velocity, were not the same, and as a result, it can be speculated that the observations produced by each method are characteristics of the variation of each of those controlled variables. It can be concluded that for some of the projectiles used, that were provided with an amount of kinetic energy very similar to another projectile composed of a different material, produced different peak amplitudes of oscillation. The particular examples are: Glass and stainless steel, and titanium and stainless steel. i.e., those projectiles that were less dense, and yet were in possession of an amount of kinetic energy very similar to another projectile composed of a denser material, yielded peak amplitudes that were clearly larger than those produced by the second projectile mentioned (where the diameter of the projectiles was a constant).

The third main conclusion of this project is based upon the observations of decay times of the acoustic vibrations that were induced during the experimentation. It was observed that the decay time of the acoustic vibration of the plate varied exponentially as the density of the impactor was varied. This was observed by varying the kinetic energy of the projectile through variation of the projectile density, while keeping both velocity, and diameter, constant. The relationship was observed to conform to:

$$y = 2.0 \pm 1.3 + 0.19 \pm 0.91 \times e^{x(41.8 \pm 75.6)^{-1}}, \tag{4.1}$$

where 'y' is the decay time, and 'x' is the kinetic energy of the projectile.

Whether there was a change in decay time according to a change in projectile velocity was unclear. Most values of the observed decay time were very similar, as though no change was present for the range of velocities used, except for one shot – the fastest projectile. This projectile was calculated to have possessed approximately double the amount of kinetic energy of the next-fastest projectile, and it was observed to have yielded a decay time higher than the rest (which were all very similar). However, the uncertainty of the value of the decay time for the shot in question was large enough to implicate the possibility that a projectile with that velocity could yield a decay time with a value very similar to the rest (the error of the value lies within the range of the rest of the values), and thus it cannot be

concluded that an observation of changing decay time, with speed, was truly established.

**4.1 Further Possible Research**

Shot programme 1 could be improved by performing more shots in the future. If a range of projectiles was used that included materials with densities that have not been included so far, then it may be easier to discern a relationship between a change in kinetic energy with varying density, and voltage amplitude. Particularly, this inclusion could reveal the induced voltage amplitudes caused by projectiles composed of densities that have values somewhere in between those of glass and titanium, and stainless steel and tungsten carbide. This could, in the first instance, reveal which material density would yield the relatively largest peak voltage amplitude, and at the same time it could reveal how rapidly the voltage amplitude would rise, from the amplitude yielded by a projectile with the density of glass, to the amplitude yielded by a projectile with either the density of titanium, or to some other peak (depending on whether or not the peak were afforded by a projectile with a higher, or lower density than titanium). In the second instance, this could perhaps reveal the rate at which the peak voltage amplitude yielded by a projectile with the density of stainless steel would decrease to the amplitude yielded by a projectile with the density of tungsten carbide. Thus filling in the gaps, currently missing due to projectiles with relevant densities so far having not been used, would allow for a more detailed data set to be shown graphically.

The formulation of a new shot programme, where the projectile density, velocity, and diameter were all kept constant, and the strength of the material of which the projectile is composed were a controlled variable, would be beneficial. This could perhaps allow for the clarification of whether the variation in amplitude as the projectile composition was changed, was due to a change in projectile density, or a change in projectile strength. However, this comparison between projectiles should not be performed based upon the 'static' strength of the materials of which those projectiles are made, unless that strength is independent of the rate at which the strain is applied to the projectile. This is because during a hypervelocity impact, the rate at which the strain would be applied to the projectile would be very high ($10^6$ or $10^8$, even), and the strength of the material during this condition may be different

from the strength of the material when the strain is applied very slowly [31]. The equation of strain rate is as follows [32]:

$$\dot{\varepsilon} = \frac{1}{l_0} \frac{dl_0}{dt},$$

(4.2)

where '$l_0$' is the original strength of the material, and '$\varepsilon$' is the strain rate. Knowledge of the strain rate behaviour of different materials would be useful.

Further investigation into the debris patterns of rear plates could perhaps yield a benefit. If indeed it was discovered that spiral formations existed, as suggested in chapter 3, then the reason for this could be suggested. It could be speculated that the rotational motion of the projectile, caused by the rifling of the launch tube of the light gas gun, would cause either material from the projectile or target, that has been sheared away from the original body to which is belonged, to travel tangentially to the rotation of the projectile, as it also travels towards the rear plate. The following is a suggestion, posed by the author, of a method for the investigation of the rotational velocity of an impactor: First, the rear plate should be imaged, and the craters should be identified using a thresholding technique. Once the image has been contrasted to show the position of the craters, the relative location of the centre of the hole caused by impact with the target plate, should be identified upon the image of the rear plate. This location will be the 'origin'. The identified craters should be considered, from this point on, as data points, which may be plotted graphically, where the 'origin', as previously mentioned, is the relative location of the centre of the hole made through the target plate by the projectile, superimposed onto the rear plate. After this has been done, some computerised method of spiral identification should be employed [33]. This would involve using a computer program to determine whether or not the spatial distribution of the data points conforms to that of a spiral. If this has been shown to be the case (a spiral has been identified), then the closest fit of the observed spiral to a mathematical description of that distribution should be calculated. To give a simplistic example, the spiral could conform to an Archimedean type of spiral [34], where the radius from the origin, $r(t)$, is proportional to the angle, $t$, which lies between the radius and the positive x-axis, where its vertex is the origin, such that:

$$r(t) = at, \tag{4.3}$$

where '*a*' is a constant. However, this equation may include other terms, such as:

$$r(t) = \frac{1}{t}, \quad r(t) = \frac{1}{\sqrt{t}}, \quad \text{or } r(t) = lnt, \tag{4.4 - 4.6}$$

among many other possible terms, which would yield different spirals. If the closest fit of an equation to the spiral were given, then the spatial distribution of data points over $2\pi$ radians about the origin would be known. This distribution (about $2\pi$ radians) would correspond to one full revolution of the projectile (as it was able to spin once fully, to provide the distribution of debris over the rear plate in such a spiral formation). Assuming that the distance between the target plate and the rear plate is known, then by calculating the number of spiral revolutions that are present on the plate (i.e., how many sets of craters there are over a period of $2\pi$ radians, as the radius from the origin is increased), it could be speculated that this was close to the number of revolutions that the projectile would have made during the time it would take for it to travel across the equivalent distance (between the target plate and the rear plate). For example, it is speculated that if there were $3\pi$ radians of data points distributed in a spiral formation, over an increasing radius, then this would correspond to one and a half revolutions of the projectile. The relevance of this is that if such a rear plate could be returned from space, then a systematic speculation could made with regard to the rate of spin that objects had, before they impacted with the spacecraft. In the laboratory, this could be tested by using a smooth bore launch tube and a sabot-stripping technique, with a small hole in the stop plate. This would allow the projectile to be fired without providing spin to it. After shots had been conducted in this manner, the rear plate debris patterns could be inspected as previously discussed.

Overall, this project has successfully shown that the response of PVDF sensors varies with projectile composition, and with projectile speed. This has been shown to be true for the induced peak voltage amplitude, and for the decay time of the recorded signal. It has been shown that, during a penetrative impact, some fraction of the projectile kinetic energy is transferred to the target plate, and some is transferred to the rear plate (the remainder).

# REFERENCES

[1] Spacecraft Systems Engineering 3rd Edition, eds. P.Fortescue, J.Stark and G.Swinard. Pub. Wiley 2005, ISBN: 001293827.

[2]  V.Dikarev and E.Grün et al. 2005, *Modeling the Sporadic Meteoroid Background Cloud,* Earth Moon and Planets **95**, 109-122

[3] V.Dikarev et al. 2005, *The New ESA Meteoroid Model,* Advances in Space Research **35**, 1282–1289.

[4] H.Sdunnus et al. 2004, *Comparison of Debris Flux Models,* Advances in Space Research **34**, 1000-1005.

 [5] J.A.M.McDonnell et al. 1997, *Microparticle Populations at LEO Altitudes: Recent Spacecraft Measurements,* Icarus **127**, 55-64.

[6] Technical Report on Space Debris 1999, United Nations.

[7] F.Schäfer and R.Janovsky 2007, *Impact sensor network for detection of hypervelocity impacts on spacecraft,* Acta Astronautica **61**, 901-911.

[8] S.Fukushige et al. 2006, *Development of perforation hole detection system for space debris impact,* International Journal of Impact Engineering **33**, 273-284.

[9] A Dictionary of Astronomy 1997, Oxford University Press.

[10] D.J.Gardner et al. 2006, *Hole Growth Characterisation for Hypervelocity Impacts in Thin Targets,* International Journal of Impact Engineering Vol.**19**, No.7, 589-602.

[11] F.Hörz et al. 1995, *Hypervelocity penetration in aluminium 6061 and 1100 alloys,* Proceedings to the 1995 International Conference on Metallurgical and Materials Applications of Shock-Wave and High-Strain-Rate Phenomena, 273-283.

[12] Satellites*,* eds. Joseph A. Burns and Mildred Shapley Matthews, Pub. The University of Arizona Press 1986, ISBN : 0816509832.

[13] J.L.Ortiz et al. 2006, *Detection of sporadic impact flashes on the Moon Implications for the luminous efficiency of hypervelocity impacts and derived terrestrial impact rates,* Icarus Vol. **184**, 319-326.

[14] B.M.Cudnik et al. 2003, *Ground-Based Observations of Lunar Meteoritic Phenomena,* Earth Moon and Plants **83**, 145-161.

[15] M.J.Burchell et al. 2009, *The SMART-1 Lunar Impact* Icarus Vol. **207**, No. 1, 28-38.

[16] B.H.Foing 1996, *The Moon as a Platform for Astronomy and Space Science,* Advances in Space Research Vol. **18**, No. 11, 1117-1123.

[17] The Moon : Resources, Future Development and Colonization, eds. David Schrunk, Burton Sharpe, Bonnie Cooper and Madhu Thangavelu, Pub. Praxis 1999, ISBN : 0471976350.

[18] G.Horneck et al. 2003, *HUMEX, A Study on the Survivability and Adaptation of Humans to Long-Duration Exploratory missions, Part 1: Lunar Missions,* Advances in Space Research, Vol. **31**, No. 11, 2389-2401.

[19] M.Lambert 1997, *Hypervelocity Impacts and Damage Laws,* Advances in Space Research, COSPAR Vol. **19**, No. 2, p. 369-378.

[20] F.KSchäfer et al. 2008, *Ballistic limit equation for equipment placed behind satellite structure walls,* International Journal of Impact Engineering **35**, 1784-1791.

[21] R.Corsaro et al. 2010, *Micrometeoroid and Lunar Secondary Ejecta Flux Measurement: Comparison of Three Acoustic Systems,* 41st Lunar and Planetary Science Conference.

[22] Whitehouse Scientific, http://www.whitehousescientific.com, Accessed 15th August 2010.

[23] Crozier and Hume 1954, *High-Velocity, Light-Gas Gun,* Journal of Applied, Physics **28**, 892-894.

[24] M.J.Burchell et al. 1998, *Hypervelocity impact studies using the 2 MV Van de Graaff accelerator and two-stage light gas gun of the University of Kent at Canterbury,* Measurement Science and Technology **10**, 41-50, 1999.

[25] Physics for Scientists and Engineers 5th Edition, eds. G.Tipler and F.Mosca, Pub. Freeman 2004, ISBN : 0716743892.

[26] Solid State Physics 2nd Edition, eds. Hook and Hall, Pub. Wiley-Blackwell 1991, ISBN: 0471928054.

[27] Ferroelectric Polymers: Chemistry, Physics and Applications, eds. Hari Singh Nalwa, Pub. Marcel Dekker 1995, ISBN: 0824794680.

[28] S.Standen 2009, MSc Thesis, The University of Kent.

[29]  R.Corsaro 2009, *Processing of Acoustic Signals from Impacts on Plates,* United States Naval Research Laboratory.

[31] Zhuo-Cheng Ou 2009, *Analytical Approach to the Strain Rate Effect on the Dynamic Tensile Strength of Brittle Materials,* International Journal of Impact Engineering **37**, 942-945.

[30] S.R.V. Barnes 2004, MSc Thesis, The University of Kent, *The Effects of Highly Oblique Hypervelocity Impacts on Spacecraft Shielding*.

[32] Wolfram Research, <http://scienceworld.wolfram.com/physics/StrainRate.html>, Accessed 21st July 2010.

[33] H.Singh 1997, *2D Spiral Recognition with Possibilistic Measures,* Pattern Recognition Letters **19**, 141-147.

[34] Mathematische Basteleien, < http://www.mathematische-basteleien.de/spiral.htm>, Accessed 18th June 2010.